Universidade Federal Do Rio Grande Do Sul
Escola de Engenharia
Programa de Pós-Graduação em Engenharia Civil: Construção e Infraestrutura

Micael Rubens Cardoso da Silva

Effects of kaolinite and montmorillonite calcined clays on the sulfate balance, early hydration and artificial pore solution of limestone calcined clay cements

Porto Alegre
2022

MICAEL RUBENS CARDOSO DA SILVA

EFFECTS OF KAOLINITE AND MONTMORILLONITE CALCINED CLAYS ON THE SULFATE BALANCE, EARLY HYDRATION AND ARTIFICIAL PORE SOLUTION OF LIMESTONE CALCINED CLAY CEMENTS

Master's dissertation presented to the Postgraduate Program in Civil Engineering: Construction and Infrastructure at the Universidade Federal do Rio Grande do Sul as part of the requirements for obtaining the title of Master's in Civil Engineering.

Prof. Ana Paula Kirchheim
Dr., Universidade Federal do Rio Grande do Sul, Brazil
Supervisor

Prof. Brant Walkley
Dr., The University of Sheffield, United Kingdom
Co-supervisor

Porto Alegre
2022

MICAEL RUBENS CARDOSO DA SILVA

EFFECTS OF KAOLINITE AND MONTMORILLONITE CALCINED CLAYS ON THE SULFATE BALANCE, EARLY HYDRATION AND ARTIFICIAL PORE SOLUTION OF LIMESTONE CALCINED CLAY CEMENTS

Prof. Ana Paula Kirchheim
Dr., Universidade Federal do Rio Grande do Sul, Brazil
Supervisor

Prof. Brant Walkley
Dr., University of Sheffield, United Kingdom
Co-supervisor

Prof. Ângela de Moura Ferreira Danilevicz
Coordinator PPGCI/UFRGS

EXAMINERS

Prof. Antônio Carlos Vieira Coelho (USP)
Dr., Université Catholique de Louvain, UCL, Bélgica

Prof. Paulo Ricardo de Matos (UFSM)
Dr., Universidade Federal de Santa Catarina, Brazil

Prof. Saulo Roca Bragança (UFRGS)
Dr, Universidade Federal do Rio Grande do Sul

ACKNOWLEDGMENTS

To my mother for all her love, encouragement, care, and for always believing in me. We have been through so much. It is impossible to describe how proud I am of you and how happy I am to have you in my life! This victory is ours.

To my supervisors. Prof. Ana Paula is an incredible person and a competent and inspiring professional who always motivates her 'children' to go beyond! Proud to be her student. To Dr. Brant, thank you for accepting our invitation and being attentive throughout this process. I am sure I will be in good hands in the Ph.D.

To my boyfriend Everton, thank you for being fundamental in this stage. He showed me that life is balance, support, and love, that we are human, and that happiness is about the journey, not the arrival.

To everyone at LINCE! Especially to José, Matheus, Muriel, Roger, Paula, Rayara, and Py for their partnership during this stage. A space in the heart to my friend Camila Malacarne for the affection and for always being sure I could count on her! To Marlon, thank you for his calm and for teaching us that this walk should be light. To Laura for her time at LINCE as a post-doc. To the fellows at LINCE, like Andreza and Marina, who were fundamental in this process, they were friends and companions and greatly helped! I root for you all!

To LAMTAC/NORIE. To the technicians Airton and Ari who were always attentive and helpful whenever I needed them. Max and Iago for the company of many trips to the "R.U" during the pandemic. Carol Giordani for her attention and willingness to help whenever anyone needs it. To Lucia for the countless laughs, conversations and company of our afternoons, one of the people I loved most to meet! To Professor Angela Masuero, thank you for the LAMTAC space and her affection and dedication to making each of us feel welcome at NORIE.

To my old friends who supported me when I needed them most, such as Maurilio, who always supported me, to my housemates, and to the new friends I made during these more than two years in Porto Alegre.

To Intercement for the fundamental partnership with the public University through LINCE.

To UFRGS for the infrastructure and quality teaching, and to its laboratories, which were great partners, such as LACOR, LTM, LACER, LAMTAC, etc.

To the PPGCI for the quality teaching and to all the professors who contributed to my professional development.

To the panel members, thank you for accepting our invitation and contributing to the quality of my work.

To my friends, teachers and all the dozens of people helping me in the campaign to get my Ph.D. at the University of Sheffield!

AGRADECIMENTOS

À minha mãe por todo o seu amor, incentivo, cuidado e por sempre acreditar em mim. Passamos por tanta coisa. É impossível descrever o quanto eu tenho orgulho de você e sou feliz em tê-la em minha vida! Essa vitória é nossa.

Aos meus orientadores. Prof. Ana Paula, uma pessoa incrível e uma profissional competente e inspiradora, que motiva os filhotes a irem sempre além! Orgulho de ser seu aluno. Ao Dr. Brant por aceitar o nosso convite e por ter sido uma pessoa tão atenciosa em todo esse processo. Tenho certeza que estarei em boas mãos no PhD.

Ao meu namorado Everton por ser fundamental nesta etapa. Mostrou que a vida é equilíbrio, apoio e amor, que somos humanos e que a felicidade se trata da jornada e não da chegada.

A todos do LINCE! Em especial ao José, Matheus, Muriel, Roger, Paula, Rayara e Py pela parceria nessa etapa. Um espaço no coração para minha amiga Camila Malacarne pelo carinho e por sempre ter a certeza que poderia contar com ela! Ao Marlon pela calma e por nos ensinar que esta caminhada pode e deve ser leve. À Laura pela passagem tão querida no LINCE como Pós-doc. Aos bolsistas do LINCE, como a Andreza e a Marina, que foram fundamentais nesse processo, foram amigas, companhias e ajudaram muito! Torço muito por vocês!

Ao LAMTAC/NORIE. Aos técnicos Airton e Ari que foram sempre atenciosos e prestativos sempre que precisei. Max e Iago pela companhia de muitas idas ao R.U durante a pandemia. Carol Giordani pela atenção e disposição em ajudar sempre que alguém precisa. À Lucia pelas inúmeras gargalhadas, conversas e companhia das nossas tardes, uma das pessoas que mais amei conhecer! À professora Angela Masuero, pelo espaço do LAMTAC e por seu carinho e dedicação em fazer que cada um de nós se sentisse acolhido no NORIE.

As meus amigos antigos que apoiaram em momentos que muito precisei, como o Maurílio que sempre me apoiou, aos colegas de apartamento e aos novos amigos que fiz nesses mais de dois anos em Porto Alegre.

A Intercement pela parceria fundamental com a Universidade Pública através do LINCE.

A UFRGS pela infraesrutura e um ensino de qualidade. Aos seus laboratórios que foram grandes parceiros, como o LACOR, LTM, LACER, LAMTAC, etc.

Ao PPGCI pelo ensino de qualidade e para os todos os professores que contribuíram para o meu desenvolvimento profissional.

Aos membros da banca por aceitarem nosso convite e pela contribuição que enriqueceu a qualidade do meu trabalho.

Aos meus amigos, professores e a todas as dezenas de pessoas que estão me ajudando na campanha para chegar ao meu PhD na Universidade de Sheffield!

“No one is too small to make a difference.”

(Greta Thunberg)

ABSTRACT

SILVA, M. R. C. **Effects of different kaolinite and montmorillonite calcined clays on the sulfate balance, early hydration and pore solution of limestone calcined clay cements.** 2021. Master's dissertation in Civil Engineering - Postgraduate Program in Civil Engineering: Construction and Infrastructure, Engineering School, Universidade Federal do Rio Grande do Sul, Porto Alegre, 2021.

Combining clinker with limestone and calcined clay has been one of the main strategies to reduce CO_2 emissions in the cement production industry. Calcium sulfate is mainly used to control setting times. Compared to ordinary Portland cement, these blended cements exhibit accelerated sulfate depletion during hydration. This is highly influenced by the calcined clays' physical and chemical effects and methods for determining the appropriate sulfate content require further investigation. There is no unique or best method to ensure sulfate balancing, nor what effects different clay minerals (kaolinite vs. montmorillonite) have on this adjustment. Thus, this study aimed to assess methods for the optimum sulfate content determination, in terms of SO_{3total}, of ternary cements composed of both calcined clays. In addition, their physical and chemical effects on the sulfate balance, early-age hydration, and artificial pore solution chemistry were evaluated. The impacts of the clays were compared with an inert material (quartz powder) in a reference cement. The experimental program was divided into two phases. In phase 1, sulfate optimization was carried out using isothermal calorimetry, compressive strength, thermogravimetric (TG) analysis, and chemical shrinkage (CS) analysis at different ages. In phase 2, the impact of fineness, dissolution, and possible adsorption capacity of the calcined clay minerals were evaluated by isothermal calorimetry, ICP-OES and zeta potential, respectively. Phase 1 demonstrated that there is no single best technique to predict sulfate optimization, especially for LC³s, but combining several techniques can assist in more coherent decision-making. A careful combination of calorimetry results with compressive strength can be useful at early ages. TG results do not relate well to the other techniques but are useful for comparative reactivity between cements. As well as CS, since it is not sensitive to detect changes between total SO_3 contents but indicates the reactivity of cement pastes as a function of reduction of volume paste. Also, due to chemical and physical effects, the use of kaolinite clay should be more careful, as there was the highest increase in sulfate demand in all analyses. Phase 2 emphasized the physical and chemical effects of calcined clays in LC³ and alkaline solutions on the sulfate balance. The results suggested that during hydration, sulfate depletion kinetics tend to be similar between kaolinite and montmorillonite clays with fineness, but, due to the availability of Al ions for dissolution, the sulfate demand was higher for the cements with kaolinite clay. On the other hand, the physicochemical characteristics of calcined montmorillonite clays (such as availability of Si and Al ions, zeta potential) had little impact on sulfate demand even with increasing fineness.

Keywords: Kaolinite. Montmorillonite. Hydration. Sulfate balance. LC³.

1 INTRODUCTION

This chapter presents the context and justification of the proposed theme, gaps of knowledge, research objectives, delimitations, and master thesis structure.

1.1 CONTEXT

Despite the economic disruptions owing to the COVID-19 pandemic, cement is still one of the world's most manufactured materials. In 2020, the cement sector produced around 4.1 Gigatons (Gt) of Portland cement and had 3.7 Gt clinker capacity (USGS, 2021). The environmental impacts caused by its production have gained attention as one of the challenges to climate-carbon targets. The sector accounts for approximately 8-9% of global anthropogenic carbon dioxide (CO_2) emissions to the atmosphere (MONTEIRO; MILLER; HORVATH, 2017) and it is also the third-largest industrial energy consumer, responsible for 7% of the global industrial energy consumed (IEA, 2018). Such impacts can be even higher considering the predicted population growth in the coming decades (UNITED NATIONS, 2021), increasing the concrete demand, especially in developing countries.

There exists no single solution to overcome such a situation. However, reducing the clinker factor has been a well-established way to lower the CO_2 footprint and move towards sustainable production of concrete and cement industries (UN ENVIRONMENT, 2017). This practice is well consolidated within the cement industries worldwide. In Brazil, the clinker factor changed from 80% in 1990 to 67% in 2014, promoting one of the lowest CO_2 emissions in the world, with only 0.564 tons of CO_2 into the atmosphere per ton of cement produced (SNIC, 2019). The increasing incorporation of supplementary cementitious materials (SCMs) as partial replacement of clinker or as partial replacement of Portland cement in concrete mixtures can be the main responsible for such achievement (JUENGER; SNELLINGS; BERNAL, 2019).

SCMs are usually siliceous, aluminous, or calcium aluminosilicate materials that typically have either hydraulic or pozzolanic properties and rarely only a filler contribution (JUENGER; SNELLINGS; BERNAL, 2019). In another case, there are the carbonate materials, such as limestone, that the cement industry has widely used. Typically, the SCMs

are waste products, natural pozzolans, or activated minerals (SKIBSTED; SNELLINGS, 2019). The first group includes industrial by-products such as fly ash, blast furnace slag, and silica fume. Second, they are naturally pozzolanic materials due to chemical composition and reactivity in an alkaline solution such as pumice-type (NAJAFI KANI; ALLAHVERDI; PROVIS, 2012) or diatomaceous earth (SIERRA *et al.*, 2010). At the same time, other SCMs (e.g., natural clays) can have their chemical reactivity increased through calcination, chemical processes (FLEGAR *et al.*, 2019), or even mechanochemical activation (TOLE; HABERMEHL-CWIRZEN; CWIRZEN, 2019).

Over the last decades, fly ash, blast furnace slag and limestone have been the most common SCMs used as clinker substitutes, according to the CSI WBCSD report (MÜLLER; HARNISCH; MESGUEN, 2008). However, the investigation promoted by the United Nations Environmental Program (UN ENVIRONMENT, 2017) shows the limited slag and fly ash supplies, making CO_2 emission reduction targets based on these cements also limited in the not-so-distant future. According to this report, only two materials can meet the yearly demand in cement production: limestone and calcined clays. In this context, stands out a recent and promising technology for low-carbon cement production called Limestone Calcined Clay Cements (LC^3) which can provide high clinker replacement levels.

The cement (clinker + gypsum) substitution by limestone and calcined clay was for the first time deeply investigated by Antoni et al. (2012a). The results showed the potential of cement substitution up to 45% by both SCMs, providing better mechanical performance at 7 and 28 days than the OPC. LC^3 has shown satisfactory performance and durability under such mixed proportion. At least a range of 40-60% of metakaolin content in the calcined clay used is enough to comparable strength of OPC (AVET; SCRIVENER, 2018a), having less effect on the rheological behavior (SCRIVENER *et al.*, 2019), which could decrease the chemical admixtures demand and purchasing costs when comparing with high-grade kaolinitic clays. In terms of durability, the LC^3 cements have resistance to chloride transport (MARAGHECHI *et al.*, 2018), protection reinforcement, ASR reaction mitigation, and carbonation behavior similar to other pozzolanic cements, as mentioned by Scrivener et al. (2018).

The technology has already shown success in industrial trials since it uses lower calcination temperature (in the case of calcined clays) and same processes involved in OPC production. In 2014, an LC^3 pilot production was carried out using available technologies in India. The results indicated this product's good strength properties and economic viability (BISHNOI *et*

al., 2014). In 2015, an industrial trial was conducted in Cuba to produce 130 tonnes of the LC³. The material was suitable for making hollow concrete blocks and precast concrete following Cuban standards and provided 30% CO_2 savings on the cement manufactured (VIZCAÍNO-ANDRÉS *et al.*, 2015). In 2016, another trial was conducted in India, using locally available raw materials. The results showed that these cements could be produced in existing plants without modifying conventional production technology. In addition, cement's strength was comparable to OPC and superior to the Pozzolanic Portland Cement (PPC) analyzed (EMMANUEL *et al.*, 2016). In 2020, a Colombian company, Argos S.A, announced an investment in commercial LC³ production, called "Green Cement", in Rio Claro Plant. Motivated by the predicted increase in cement consumption in the country, such cement industry elected this technology as an alternative in cement production with costs compatible with the market and lower environmental impact. The results pointed out reducing up to 38% less CO_2 emissions and up to 30% energy consumption (ARGOS S.A., 2021).

Industrial trials of LC³ production have not yet been done in Brazil. However, using SCMs is a common practice in the country (SNIC, 2019). The Brazilian Portland cement standard (ABNT, 2018) already allows high substitutions of clinker by SCMs such as blast furnace slag (35-75%), pozzolans (fly ash, calcined clays, natural pozzolans) (15-50%) and limestone (6-25%). However, calcined clay and limestone combined under a high level of clinker substitution in LC³ will need standardization. In the case of calcined kaolinitic clays, or commercially called metakaolin, there are standards to be used such SCM as additions in concrete, mortar and pastes (ABNT, 2010a) and can also be used in small amounts (6-14%) in Portland cement composed of pozzolanic material, such as CP II Z, or higher doses (15-50%) in CP-IV (ABNT, 2018). In this context, aligned with the global trend of LC³ production, new adaptations facing the combined use of metakaolin with limestone in high clinker substitution may be addressed in the cement production market in Brazil and the rest of the world.

1.2 JUSTIFICATION

The prominent use of calcined clays as SCM is justified for several reasons, such as their reactivity, the territorial distribution, and the high availability of reserves in the earth's crust. The topsoil of the northern hemisphere consists mainly of illite/mica clay minerals and kaolinite, while the subsoil has extensive reserves of montmorillonite (smectite group) and

illite/mica. In the southern hemisphere, kaolinite is the predominant clay mineral at both depths (ITO; WAGAI, 2017), followed by minor illite/mica and montmorillonite reserves, respectively.

Clays are materials composed of different minerals and can be used in various fields, but their applicability in cement industry is one of the most common approaches. The illite, kaolinite, and montmorillonite clay minerals have a structural disorder known as dehydroxylation after thermal treatment, which gives them sufficient reactivity to react with products of reaction from Portland cement hydration (FLEGAR *et al.*, 2019) and promotes high levels of clinker substitution. It is known that the kaolinite clay mineral has the most increased reactivity in the cement matrix among the clay minerals aforementioned (FERNANDEZ; MARTIRENA; SCRIVENER, 2011b). However, concerns about transportation distances or shortages of raw materials may encourage other clay types to produce low carbon cements to increase CO_2 savings further. For instance, bentonite (a clay-rich in montmorillonite) in Denmark to develop limestone calcined clay blended cements have become a suitable alternative since the kaolin reserves are locally scarce (CEMENTIR HOLDING, 2020).

SCMs interact with blended cement mainly through their physical and chemical effects (JUENGER; SNELLINGS; BERNAL, 2019). Studies with fresh pastes suggest that calcined clays increase the water demand (da SILVA et al., 2021) and the requirement for chemical admixtures (SCRIVENER *et al.*, 2019) for a specific rheological behavior, mainly due to their high fineness, specific surface area (SSA_{BET}) and mineralogical structure (FAVIER et al., 2018; SCRIVENER et al., 2019; da SILVA et al., 2021). The effects of such features on the hydration of blended cements is still a matter of debate, especially related to their impact on the sulfate balance of blended cements. The studies on LC^3 have indicated a faster sulfate depletion than OPC (ZUNINO; SCRIVENER, 2019). In this sense, the adjustment of the gypsum (calcium sulfate) content has been made by an extra addition to that used in the cement under criteria based on isothermal calorimetry results (ANTONI *et al.*, 2012b; AVET; SCRIVENER, 2018b, 2020), which in practice has several limitations. Therefore, it is necessary to determine the optimum sulfate content using several techniques (ANDRADE NETO; DE LA TORRE; KIRCHHEIM, 2021) and pay attention to the peculiarities of the materials used, such as different calcined clays.

Studies report that clays are the materials most responsible for accelerating sulfate depletion in LC^3 cements. The mechanisms justifying this behavior are still under discussion, but the filler effect (fineness), ion dissolution and possible sulfate ion adsorption on the clay surface

are the main arguments raised about the effects of calcined clays (MAIER *et al.*, 2021; ZUNINO; SCRIVENER, 2019). The complexity of these interactions is even more remarkable considering different clay minerals other than kaolinite, such as montmorillonite, which can be incorporated in the production of these blended cements with limestone and calcined clay, known as LC^3. Further investigations are needed into the impact and reactivity of different calcined clays to provide new insights to academia and the cement industry.

1.3 KNOWLEDGE GAP

There is no consensus on the most appropriate techniques for determining sulfate content in blended cements with limestone and calcined clays and on which factor determines their accelerated sulfate depletion. Most literature reported is based on calcined kaolinite clays' behavior in this phenomenon. Thus, the effect of montmorillonite clay has never been reported.

Therefore, are the usual techniques suitable for determining the optimum sulfate content of these cements? Will the optimum sulfate content be the same in cements using most common techniques? What impacts the accelerated sulfate depletion more, the chemical or physical effects of the calcined clays? Does the different dissolution of these clays have a bearing on sulfate depletion? How does the concentration of ions occur in alkaline solutions that simulate pore solution over time? What is the zeta potential of these calcined clay in artificial pore solution? These questions drive this research's experimental design to solve knowledge gaps on this subject that needs further investigation.

1.4 RESEARCH OBJECTIVES

The general objective of this study is:

To evaluate the possibility of determining the optimum sulfate content, in terms of total SO_3, in LC^3 with kaolinite and montmorillonite calcined clays, using the main existing techniques. Also, investigate those calcined clays' physical and chemical effects and also the sulfate balance, early-age hydration and artificial pore solution chemistry of the mixtures.

The specifics objectives are:

- To perform a critical analysis of existing techniques to determinate optimum sulfate content ($SO_{3optimum}$) in LC³ with different calcined clays and their effects on the results;

- To evaluate the impact of filler effect (fineness) from calcined clays on the sulfate depletion kinetics of LC³;

- To relate the ions dissolution and the zeta potential of gypsum and calcined clays in artificial pore solution to the differences observed in the sulfate balance and hydration of LC³.

1.5 DELIMITATIONS

- **Calcined clays:** the research evaluate two clays as sources of kaolinite and montmorillonite clay minerals. A natural kaolinite clay and commercial sodium bentonite, respectively;

- **Cements mix proportions** were done by weight % (wt%), despite the different specific gravity of the evaluated clays. This may also affect the number of particles in the final cement;

- **Clinker and gypsum:** all procedures were performed using one type of industrial clinker and mineral gypsum ($CaSO_4.2H_2O$).

2 PART 1: LITERATURE REVIEW

This chapter brings a review of the general research topic. This section provides brief information about kaolinite and montmorillonite clay minerals, essential aspects related to calcined clays such as the role of calcination, methods to evaluate pozzolanic reactivity, their dissolution and surface charge characteristics. Recent research on sulfate balance, hydration, and pore solution chemistry in LC³ are reviewed to better understand the effects of calcined clays in such properties.

2.1 CLAY AND CLAY MINERALS

2.1.1 Definition and classification

Clays have been used by human-being since antiquity. Nowadays, clays are still a widely applied material. For instance, it can be used to manufacture bricks, porcelain tiles, refractory materials, cement production, as a constituent of paint, plastics and paper, or even the cosmetic industry. The scientific study of clays is relatively recent, dating back to the mid-1930s; it has been carried out by people from many different backgrounds, such as geologists, archaeologists, chemists, civil engineers, etc. (BERGAYA; LAGALY, 2013). There are several concepts of "clays" or "clay minerals" in the literature, so it is possible that there is not the most correct concept of all.

The attempts to define these materials are old. The first definition of "clay" was appointed by Georgius Agricola (1494-1555), a German scholar (GUGGENHEIM *et al.*, 1995). Centuries later, the Joint Nomenclature Committees (JNC) of the Association Internationale pour l'Etude des Argiles (AIPEA) and the Clay Minerals Society (CMS) started to work together on the clay (minerals) definitions. As a result, "clay" was defined as "[…] a naturally occurring material composed primarily of fine-grained minerals, which is generally plastic at appropriate water contents and will harden when dried or fired"; and "clay mineral" as "[…] phyllosilicate minerals and minerals which impart plasticity to clay and which harden upon drying or firing" (GUGGENHEIM *et al.*, 1995). Thus, the term "clay minerals" can include some coarse and/or synthetic materials as opposed to its considered in terms of "clays".

Some authors define "clays" as fine-grained material that consists of a hydrated silicate of aluminum with impurities, and plasticity when wet and can be used in the manufacture of bricks, cement, ceramics, etc. (HASHIR, 2018). The Brazilian standard also defined "clay" and "clay minerals". Clay is defined as "fine-grained soil composed of particles with dimensions smaller than 0.002 mm, presenting cohesion and plasticity," while clay minerals would be "hydraulic silicates of aluminum with varying amounts of iron, magnesium, potassium, sodium, lithium, etc. […] formed by SiO_4 tetrahedrons and octahedrons of $Al(OH)_6$ lamellas, with variable crystallinity" (ABNT, 1995). Note that the term "fined-grained" is quantified in Brazilian standard. However, JNC and CMS pointed out that it is not the most suitable approach since a specific particle size classification is not equal to all disciplines.

The JNC/AIPEA and CMS describe plasticity as the distinctive characteristics of the clay (GUGGENHEIM *et al.*, 1995). However, no criteria for reliable plasticity are provided. Recently, a new definition of clay-based on plasticity index (PI) and liquid limit (LL) was proposed by (MORENO-MAROTO; ALONSO-AZCÁRATE, 2018), suggesting "clays" when PI>LL/2. The method presented is an effort to update soil classification methods for engineering purposes through plasticity and simple sieving as a more straightforward approach than conventional methods.

There are other ways to classify clays, e.g., in the industrial context, they can be distinguished into four types: (i) bentonites with montmorillonite as the main clay mineral; (ii) kaolins containing kaolinite; (iii) palygorskite and sepiolite; and (iv) 'common clays' which contain mixed-layer minerals such as illite–smectite (BERGAYA; LAGALY, 2013). Such authors presented a detailed classification considering the origin and main clay mineral constituents (Table 1).

The arrangement of T and O layers is a usual parameter to clay's classification into 1:1 (TO), 2:1 (TOT), or mixed-layer minerals (GARG, 2015). Therefore, clay minerals consisting of alternate layers of Si tetrahedra and Al octahedra define the 1:1 group, while clay minerals with an extra Si layer overlying the Al layer define the 2:1 clay mineral group. A more detailed classification considers their net charge layer and octahedral character (BERGAYA; LAGALY, 2013).

Table 1 - Current name of clays

Current name of clays	Origin	Main clay mineral constituents
Ball clay	Sedimentary	Kaolinite
Bentonite	Volcanic rock alteration of authigenic	Montmorillonite
Bleaching earth	Acid-activated bentonite	Decomposed montmorillonite
Common clay	Sedimentary or by weathering	Various, often illite/smectite mixed-layer minerals
China Clay	Hydrothermal	Kaolinite
Fire Clay	Sedimentary	Kaolinite
Flint clay	Sedimentary with subsequent diagenesis	Kaolinite
Fuller's earth	Sedimentary, residual, or hydrothermal	Montmorillonite, sometimes palygorskite, sepiolite
Primary kaolin	Residual or hydrothermal alteration	Kaolinite
Secondary clay	Authigenic sedimentary	Kaolinite
Refractory Clay	Authigenic sedimentary	Kaolinite
Laponite	Synthetic	Hectorite-type smectite
Nanoclay	-	Mostly montmorillonite

Source: Adapted from (BERGAYA; LAGALY, 2013)

Table *2* shows an adapted classification of the clay minerals, bringing the net-layer charge (ζ), groups and constituent minerals (GARG, 2015).

Table 2 – Classification of clays minerals (BERGAYA; LAGALY, 2013)

Interlayer material	Group	Idealized Formulae	Minerals
1:1 Clay Minerals			
None or only H_2O	Serpentine	$Si_2Mg_3O_5(OH)_4$	Amesite, berthierine, brindleyite, cronstedtite, fraipontite, kellyite, lizardite, nepouite
	Kaolin	$Si_2Al_2O_5(OH)_4$	Dickite, **kaolinite,** nacrite
2:1 Clay Minerals			
None, ζ ~ 0	Talc	$Si_4Mg_3O_{10}(OH)_2$	Kerolite, pimelite, talc, willemsite
	Pyrophyllite	$Si_4Al_2O_{10}(OH)_2$	Ferripyrophyllite, pyrophyllite
Hydrated exchangeable cations, ζ ~ 0.2-0.6	Smectite	$Si_4(Mg_{3-y}Li_y)O_{10}(OH)_2$ $_yM^+.{}_nH_2O$	Hectorite, saponite, sauconite, stevensite, swinefordite
		$Si_4(Al_{2-y}Mg_y)O_{10}(OH)_2$ $_yM^+.{}_nH_2O$	Beidellite, **montmorillonite,** nontronite, volkonskoite
Hydrated exchangeable cations, ζ ~ 0.6-0.9	Vermiculite	$(Si_{4-x}Al_x)(Al_{2-y}\ Mg_y)$ $O_{10}(OH)_2\ (x+y)M^+$	Trioctahedral Vermiculite
		$(Si_{4-x}Alx)(Mg^{3-}$ $_yM_y^{3+})O_{10}(OH)_2(x-y)/2\ Mg^{2+}$	Dioctahedral Vermiculite
Non-hydrated monovalent cations, ζ ~ 0.6-1.0	True (flexible) mica	$(Si_{4-x}Al_x)(Mg_{3-y}Li_y)\ O_{10}(OH)_2$ $(x+y)K^+$	Biotite, lepidolite, phlogopite
		$(Si_{4-x}Al^x)(Al_{2-y}Mgy)$ $O_{10}(OH)_2,(x+y)K^+$	Celadonite, illite, glauconite, muscovite, paragonite
Non-hydrated divalent cations, ζ ~ 1.8-2.0	Brittle mica	$(SiAl_3)(Mg_2Al)O_{10}(OH)_2,Ca^{2+}$	Anandite, bityite, clintonite, kinoshitalite
		$(Si_2Al_2)(Al_2)O_{10}(OH)_2,Ca^{2+}$	Margarite
Hydroxide sheet, ζ ~ variable	Chlorite	$(Mg,Fe)_3(Si,Al)_4O_{10}(OH)_2$ $(Mg,Fe)_3(OH)_6$	Baileychlore, chamosite, clinochlore, nimite, pennantite/ Donbassite/ Cookeite, sudoite
Regularly interstratified clay minerals			
ζ ~ variable		Trioctahedral	Aliettite, corrensite, hydrobiotite, kulkeite
		Dioctahedral	Rectorire, tosudite
Non-planar hydrous phyllosilicates			
1:1 Minerals with modulated structures	Strips	$(Mg,Fe^{2+})_3Si_2O_4O_5(OH)_4$	Antigorite, Bemenitite
	Islands	$(Mn^{2+},Mg)_3Si_2O_5(OH)_4$	Caryopilite, nelenite, etc.
2:1 Minerals with modulated structures	Strips	$Mg_4Si_6O_{15}\ (OH).6H_2O$	Palygorskite, sepiolite
	Islands	$(K(Fe^{2+},Mg,Mn)_{13}$ $(AlSi_{17}O_{42})(OH)_{14})$	Zussmanite

1:1 Minerals with rolled/spheroidal structures	$Mg_3(Si_2O_5)(OH)_4$	Chrysolite, percoraite
	$Al_2Si_2O_5(OH)_4$	Halloysite

Source:(BERGAYA; LAGALY, 2013; GARG, 2015)

The clay(s) (minerals) used in this study is presented in Figure 1.

Figure 1 - Structure of the clay(s) (minerals) used in this study: kaolin (kaolinite) and bentonite (montmorillonite)

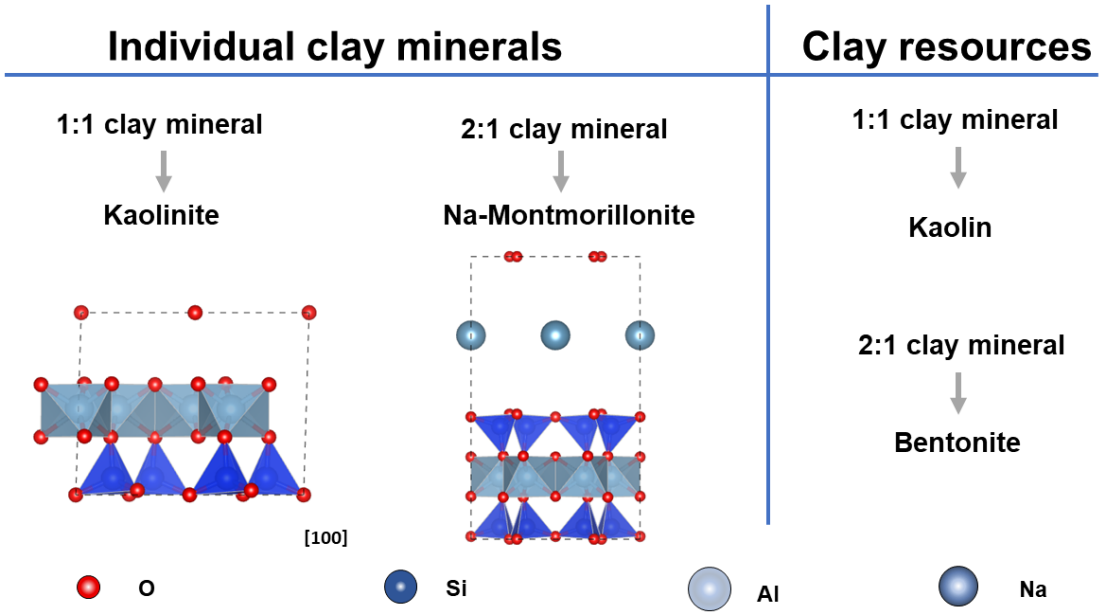

Source: Author using VESTA (MOMMA; IZUMI, 2011)

2.1.2 Kaolinite and montmorillonite clay minerals

There are several types of clay minerals in the earth's crust. Kaolinite, montmorillonite and illite/mica are the most available (ITO; WAGAI, 2017). The first one, is a typical TO-type (or 1:1) clay mineral of the kaolin group with chemical formula $Si_2Al_2O_5(OH)_4$ (Table *2*). Kaolinite has common unit cell structural features of the 1:1 clay mineral group, such as tetrahedral Si and octahedral Al layers joined by bonds of oxygen atoms, as shown in Figure 2. It can be seen that oxygen atoms can be distinctly arranged in the unit cell structure (*red balls*). The tetrahedral Si layer consists of oxygen atoms located in a basal surface (Ob), while the octahedral Al has apical oxygen atoms (Oa) and octahedral oxygen anions (Oo) mainly in the form of OH groups (BRIGATTI; GALÁN; THENG, 2013). Also, TO sheets are linked by common atoms of oxygen (SCHOONHEYDT; JOHNSTON; BERGAYA, 2018).

Kaolinite unit cell has two OH groups. The inner OH group is located where TO sheets are linked. Thus, there is a bond between the Al layer and the hydroxyls OH (Al-OH) in the oxygen atoms' common plane that joins the O and T sheets. The second is located on the outer surface of the Al layer. The H atoms are bonded with oxygen atoms from the O sheets

(SCHOONHEYDT; JOHNSTON; BERGAYA, 2018). These strong bonds are one of the reasons that give the kaolinite a small interlayer space, low expansion coefficient and high chemical stability (MIRANDA-TREVINO; COLES, 2003).

Figure 2 - Crystal structure of kaolinite, 1:1 structure showing a tetrahedral Si layer (T) with octahedral Al layer (O), interlayer space, Oa apical oxygen atoms, Oo octahedral anions (COD, 9009230)

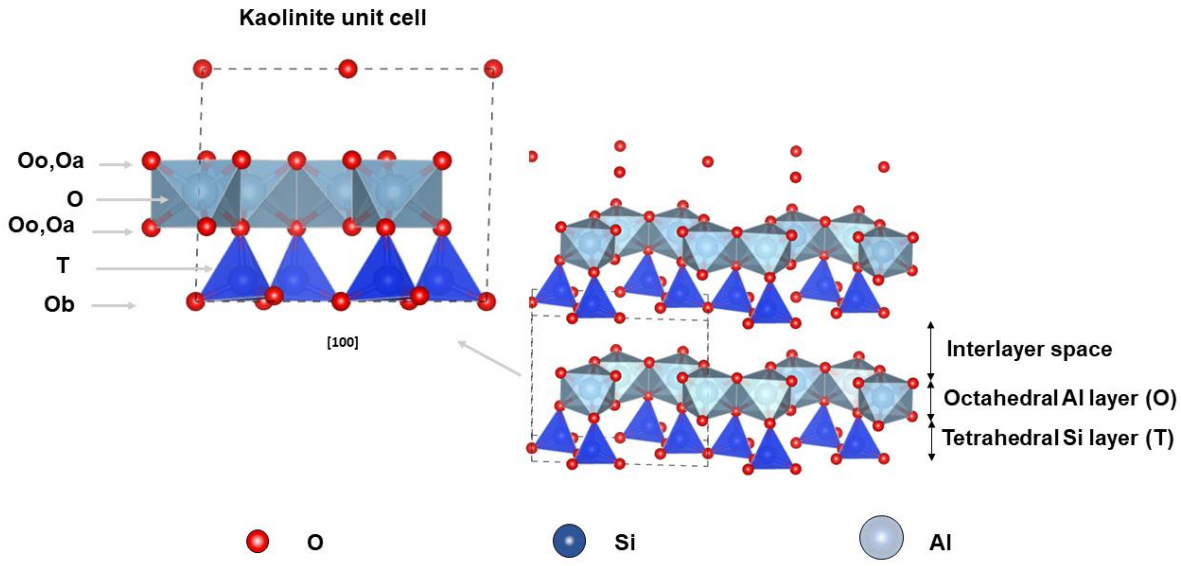

Source: Author using VESTA (MOMMA; IZUMI, 2011)

The first representation of the crystal structure of kaolinite was presented by Gruner (1932), since then scholars have been dedicated to the characterization of its crystal structure (BRIGATTI; GALÁN; THENG, 2013). One of the most divergent features of kaolinite is its structural order and disorder. One possible way to observe such differences is by X-ray diffraction. Ordered kaolinite shows intense and narrow peaks, while its disordered shows less defined, broad and asymmetric peaks (BRIGATTI; GALÁN; THENG, 2013).

The montmorillonite's interlayers are bonded by weak oxygen bridges and contain a lot of active sites and exchangeable cations, which allows the entrance of water molecules or cations such as Na, Mg or Ca (MA *et al.*, 2020) (Figure). Therefore, montmorillonite has strong adsorption and cation exchange, shrinkage, intercalation and swelling capacity (MA *et al.*, 2020; MANDALIA; BERGAYA, 2006). As a 2:1 clay mineral, it also exhibits isomorphic substitution, resulting in a net negative charge balanced by interlayer cations (Ca, Na, or K) coordinated to H_2O molecules in the interlayer region (GARG, 2015). Such characteristics, the structure, chemical composition, high surface area, high viscosity in solution, exchange cations, swelling and adsorptive capacities are the most significant differences compared with

kaolinite clay mineral (MURRAY, 2006a). Illite is also an abundant and typical 2:1 clay mineral but it is not discussed here.

Figure 3 - Crystal structure of Ca.montmorillonite, 2:1 structure showing double layer of tetrahedral Si (T) with octahedral Al layer (O), Oa apical oxygen atoms, Oo octahedral anions and interlayer space with cations (ICSD, 161171)

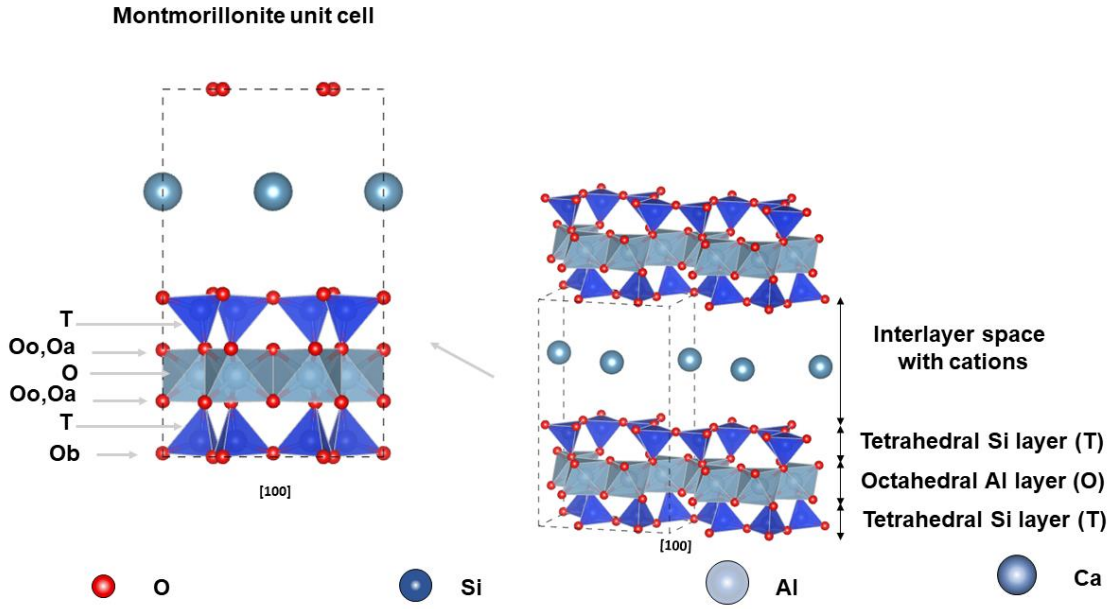

Source: Author using VESTA (MOMMA; IZUMI, 2011)

2.1.3 Kaolin and bentonite clays and their availability

Clay minerals can be found in different ways in nature such as rock, soils or clays. Kaolinite and montmorillonite, for instance, can occur as main clay minerals in kaolin and bentonite clays, respectively. Kaolin is usually a white rock formed by hydrated aluminosilicate minerals such as kaolinite and halloysite. In some regions of Brazil, kaolin is more yellowish/reddish due to the presence of iron in its composition. Even considered a high purity clay, it can contain some impurities in its composition, such as quartz, mica, feldspars, iron and titanium oxide, hydroxides, among others (ANM, 2009). Kaolin has a strong use in the paper and ceramic industry and, to a lesser extent, in the manufacture of refractory materials, plastics, paints, cements as mineral admixture, chemical products, adhesives, etc. (ANM, 2009).

Bentonite is a high montmorillonite content clay, which can be classified differently according to the commercial or academic field. In a revised 2015 standard, the Brazilian Foundry Association specifies bentonite as natural sodium bentonite, sodium-activated bentonite (Types I, II or III) or calcium bentonite (ABIFA, 1991). Natural sodium bentonite, or Na-

Montmorillonite, has swelling of a minimum of 30 mL/2g (ABIFA, 1991) due to high water adsorption ability, which is about 13 times higher than cement at the same workability (CHEN *et al.*, 2018). Despite this, it may perform better when used in mortars than Ca-montmorillonite. This is because its high absorption helps to reduce porosity due to its expansion that reduces pore size and its more dispersed particle size that favors greater formation of hydrated cement products (LIU *et al.*, 2020). Sodium-activated bentonite is a product resulting from a chemical process called sodium activation with sodium carbonate solution (Na_2CO_3), where occurs interlayer cation replacement by Na^+ by means of cations exchange (CARMO; ANGÉLICA; PAZ, 2021). Such sodium-activated bentonite is classified by means of mechanical performance, swelling, and adsorption capacity. The highest results are attributed to Type I, Type II, and Type III, respectively (ABIFA, 1991). On the other hand, calcium bentonite, or Ca-montmorillonite, has no swelling capacity or wet tensile strength (ABIFA, 1991).

The great variety of exchangeable cations in the interlayer of montmorillonite structure leads to a broader classification in the academic scope. Thus, bentonite can also be categorized as sodium, calcium, potassium, magnesium, and mixed-cationic or polycationic (CARMO; ANGÉLICA; PAZ, 2021). Such exchangeable cations properties lead the bentonite clays for variable applications. For instance, sodium bentonites can be used in freshwater drilling muds, to pelletize iron ore, in aerosols, etc. Calcium bentonites are used in some catalytic cracking of petroleum processes, absorbents, etc. In addition, when acids activate calcium bentonite to form sodium-activated bentonite, it can be used as a refining and clarifying agent in producing edible oils, industrial oils and waxes. Calcium and sodium bentonites can be used as bonds for the foundry sand, cat litter, and bid animal fed into pellets, among several applications (MURRAY, 2006b).

Kaolin and bentonite clays have both widely available around the world. Their arable reserves are estimated at 44,000 Mt of kaolin and 16,000 Mt of bentonite worldwide (USGS, 2021). In Brazil, kaolin's reserves and other common clays are estimated at 7,170.0 Mt and 5,949.0 Mt (ANM, 2010), whereas the bentonite clays are around 54.1 Mt (ANM, 2018). The principal kaolin reserves are in Amazonas and Pará, which comprise 98.4% of national resources. Also, kaolin's reserves are more distributed around the country than bentonite. The bentonite's reserves have lower availability in Brazil; 49.8% of them are located in Paraíba, 33.6% in São Paulo, and Bahia 15.3% (ANM, 2018), as shown in Figure .

Figure 4 – Distribution and geographical availability of kaolin and bentonite clay arable reserves in Brazil. Gray pentagons represent the location of the cement industries

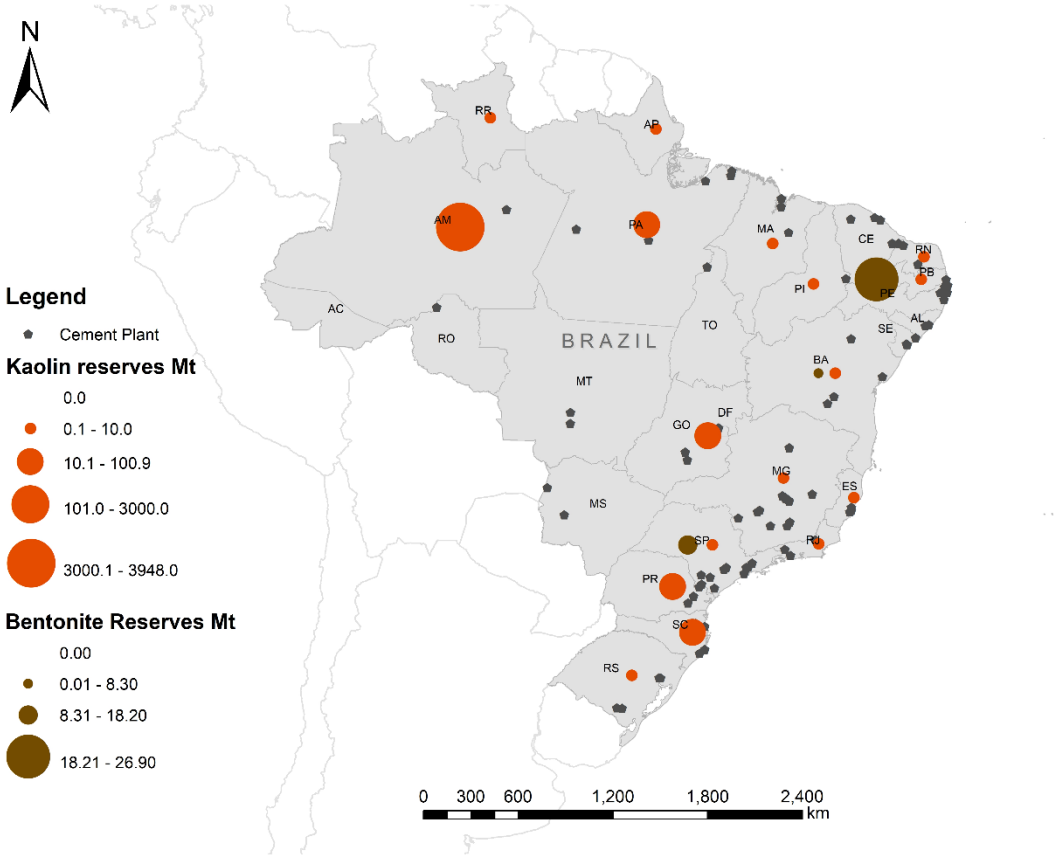

Source: Author based on (ANM, 2010, 2018) and (SNIC, 2019) database

Figure also shows that such arable reverses are distributed near cement plants across the country. Although using of SCMs as clinker replacement is a well-established practice in Brazil, each national region uses SCMs depending on their availability, local economic activity, and logistical convenience of obtaining them locally (SNIC, 2019). For instance, due to the localization of coal-fired power plants, Southern Brazil predominantly uses fly ashes as a clinker substitute by up to 50% (32-37%) followed by limestone (5%-7%). In Southeast Brazil, granulated blast furnace slag is more consolidated, with around 75% of clinker substitution followed by limestone (6.5%-8.5%). The use of calcined clays is more common in Northern (14%-16%), Midwest (8-10%) and Northeastern (4.5%-6.5%) (SNIC, 2019). Therefore, incorporating kaolin and bentonite clay as SCM is more interesting for such regions due to large natural clay reserves.

2.2 CALCINED CLAYS AS SCMs

2.2.1 Reactivity of calcined clays

In Natura clays usually have low or almost no chemical reactivity to be used as SCM in the composition of cements. Mechanical, chemical, or thermal processes can be used to increase their reactivity ease their reactivity, mechanical, chemical, or thermal processes can be used. Mechanical (or mechanochemical) activation of clays consists of intensive grinding able to promote a certain degree of amorphism to the clays; but can be costly and inefficient, respectively, due to longer grinding times and agglomeration of the particles during the process (TOLE; HABERMEHL-CWIRZEN; CWIRZEN, 2019). The chemical processes are associated with the use of chemicals that "attack" the hydroxyl groups (OH) and promote the removal of structural water from the clays through the dissolution of Si and Al (FLEGAR *et al.*, 2019); however, they are costly due to the use of reagents in large quantities. Calcination is the most interesting alternative available to increase clays' reactivity used from the industrial point of view, especially related to the cement production industry. This is based on a consolidated practice in Portland cement production, which consists of using high-temperature kilns for raw material transformation. Together with grinding, the reactivity of these materials can be further increased.

2.2.1.1 The role of calcination

Calcination is crucial in the thermal activation of clays since it can promote amorphism of such materials at high temperatures that remove free water, organic matter, and promote the dehydroxylation. In kaolinite clays, the structural water formed from hydroxyl groups evaporates to transform the crystalline clay mineral kaolinite ($Si_2Al_2O_5(OH)_4$) into a reactive phase called metakaolin ($Si_2Al_2O_7$), as well as in montmorillonite or illite/mica clay minerals, where calcined materials have an improved reactivity (FLEGAR *et al.*, 2019).

Metakaolin has been a well-known and widely used material due to its high reactivity and worldwide availability of kaolinite clay mineral (FERNANDEZ; MARTIRENA; SCRIVENER, 2011a). On the other hand, it is an expensive material, which can increase the desire for alternative clays to use as SCM, such as the 2:1 group. Hollanders et al., (2016) showed that among the 2:1 minerals, montmorillonite has higher pozzolanic reactivity than illite. Calcium montmorillonite have more pozzolanic reactivity than sodium montmorillonite due to its grater content of amorphous phases after calcination. The authors also emphasize

the importance of an adequate calcination temperature in increasing the reactivity of the clay minerals.

The phenomena behind this reactivity are based on modifications of crystalline structure, which can be observed by TGA/DTG, XRD, solid-state NMR (GARG, 2015), or FTIR (LIU *et al.*, 2017) methods. Such modifications are linked to characteristic mass losses that can be distinguished in 3 different stages: dehydration (I), dehydroxylation (II) and recrystallization (III) (Figure). Each one is described as bellow (CAO *et al.*, 2021; FERNANDEZ; MARTIRENA; SCRIVENER, 2011a):

Figure 5 - Representative thermal analysis of kaolinite and montmorillonite clay minerals

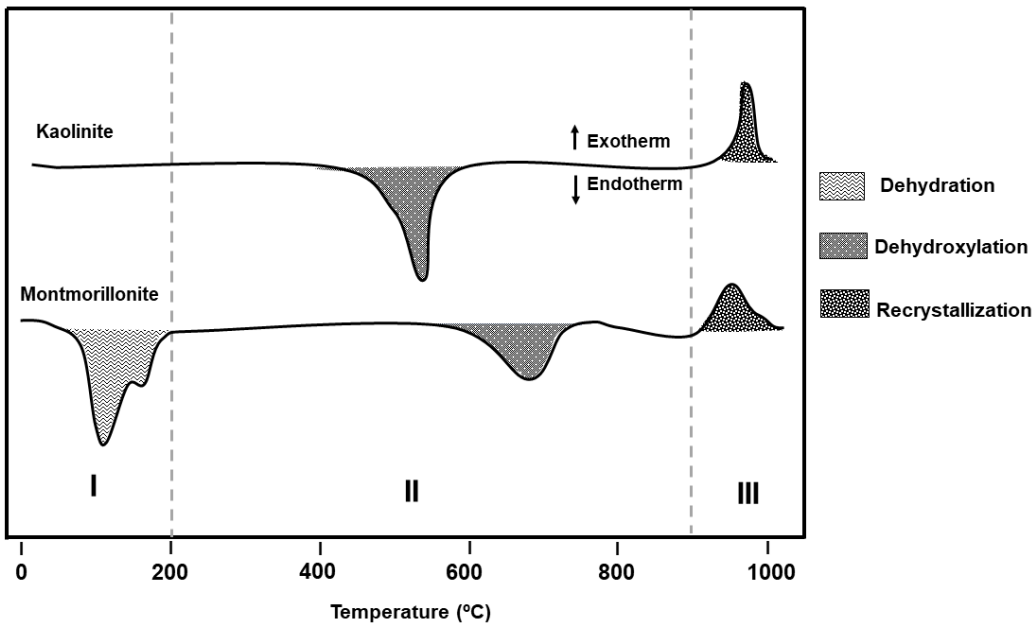

Source: adapted from (SNELLINGS; MERTENS; ELSEN, 2012)

I: Dehydration process: mass loss from room temperature to 200 ºC is related to the evaporation of adsorbed/free water (Eq. 1) or decomposition of organic matter. Montmorillonite shows a more significant loss of water, which may be due to its higher interlayer water.

$$H_2O(l) \xrightarrow{\sim 200\ ^\circ C} H_2O(g) \quad \text{Eq. 1}$$

II: Dehydroxylation process: mass loss between 400ºC~900 ºC is related to the dehydroxylation of structural water to form amorphous phases (Eq. 2). Usually, dehydroxylation of kaolinite occurs at 600ºC, whereas montmorillonite around 550-850 ºC

(FERNANDEZ; MARTIRENA; SCRIVENER, 2011a). The presence of impurities/secondary minerals in kaolinitic clays contribute to a mass loss between 200~400 ºC which can be related to gibbsite decomposition (CAO *et al.*, 2021)

$$Al_2O_3.2SiO_{2.}H_2O \xrightarrow{400\sim900\,^{\circ}C} Al_2O_3.2SiO_{2.}(s) + 2H_2O(g) \quad \text{Eq. 2}$$

III: Recrystallization process: exothermic transition without mass loss above 900 ºC. In the amorphous phase (MK), for example, may occur a molecular reorganization to form spinel (Eq. 3) or mullite phases (Eq. 4). Hence, the morphology of kaolinite clays can present a circular contour and inner voids. In contrast, montmorillonite is possible the formation of glassy phase (FERREIRO *et al.*, 2019).

$$Silicon-spinel: 2[Al_2O_3.2SiO_2](s) \xrightarrow{\sim925\,^{\circ}C} Al_2O_3.2SiO_{2.}(s) + SiO_2(s) \quad \text{Eq. 3}$$

$$1{:}1\ mullite-type\ phase: 2Al_2O_3.3SiO_2(s) \xrightarrow{\sim1100\,^{\circ}C} Al_2O_3.2SiO_{2.}(s) + SiO_2(s) \quad \text{Eq. 4}$$

Note that both clay minerals present stages of mass loss with the same behavior (I, II, II). However, 2:1 clay mineral, such as montmorillonite, has a less efficient decomposition upon thermal treatment than kaolinite. This is because their hydroxyl groups (OH) may be present at the broken edges of the particles, at the core of a layer, or between two tetrahedral sheets (MA *et al.*, 2020), which tends to preserve their TOT sheets from decomposition. Thus, the pozzolanic activity tends to be compromised. In addition, montmorillonite is more susceptible to agglomeration during calcination (FERNANDEZ; MARTIRENA; SCRIVENER, 2011a), leading to further grinding efforts.

There are many parameters related to the calcination efficiency of clays such as the calcination time, temperature, particle size and shape (JASKULSKI; JÓŹWIAK-NIEDŹWIEDZKA; YAKYMECHKO, 2020), the technology of the equipment (SCRIVENER *et al.*, 2019), fineness of the raw clay (FERREIRO *et al.*, 2019), etc. However, several studies have paid most attention to the calcination temperature (JASKULSKI; JÓŹWIAK-NIEDŹWIEDZKA; YAKYMECHKO, 2020).

Kaolinite can reach its complete dehydroxylation at a lower temperature than montmorillonite. However, the calcination range of the clay minerals is around 400-900 ºC. Some decades ago, it was believed that at least 450 ºC was possible to convert kaolinite into metakaolin (HE et al., 1995). Nowadays, it has been sown that to reach the highest pozzolanic reactivity, the calcination temperature of kaolinite clays should be around 700-850 ºC (RASHAD, 2013). Ca-montmorillonite and Na-montmorillonite complete their dehydroxylation at 730 ºC and 740 ºC, respectively (HE; OSBAECK; MAKOVICKY, 1995). In this sense, 800 ºC has been considered the upper limit of the optimal calcination temperature (GARG; SKIBSTED, 2015; HOLLANDERS *et al.*, 2016).

The solid-state NMR method is a good approach to explain the impact of the temperature on the structural derangement of clays. Kaolinite and montmorillonite have their higher pozzolanic reactivity when a total dehydroxylation is complete in calcination. By ^{27}Al NMR is possible to observe a well-ordered structure by $Al^{(VI)}$ peak from raw kaolinite (Figure). The increasing temperature rises an $Al^{(V)}$ at a maximum point at 800 ºC, indicating a disorder of crystalline structure by calcination, which removes OH groups. Montmorillonite only shows $Al^{(IV)}$ and $Al^{(VI)}$, located at 28ppm and 56ppm, respectively. Such results confirm that the modification of structural crystallinity of kaolinite and montmorillonite is entirely different (FERNANDEZ; MARTIRENA; SCRIVENER, 2011a).

Figure 6 - ^{27}Al NMR spectra of raw and calcined clay minerals

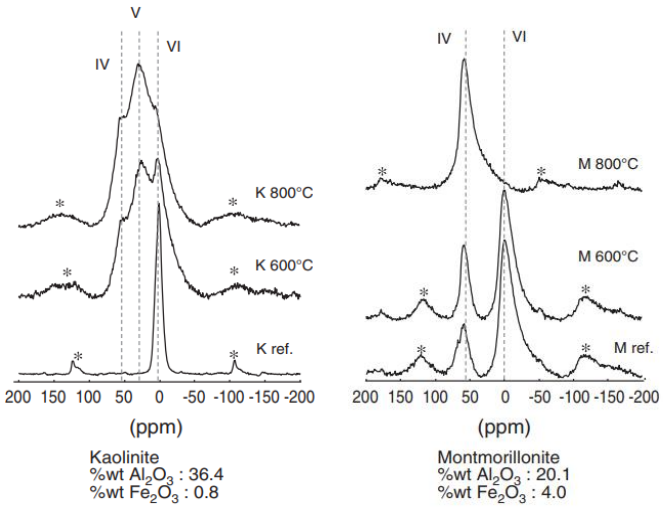

Source: (FERNANDEZ; MARTIRENA; SCRIVENER, 2011a)

2.2.1.2 Dissolution

Cement hydration reactions are known as dissolution precipitation processes. After cement comes into contact with water, the dissolution of anhydrous phases occurs, leading to the

formation of hydrated products. The use of calcined clays as SCM in cementitious materials or geopolymers (CHEN *et al.*, 2016) leads studies of the kinetics of clay dissolution to a level of great importance, since, among other factors, the greater the dissolution of Si and Al ions, the greater the reactivity of these materials (KHALIFA *et al.*, 2020). Thus, the solubility of clay (minerals) can justify their pozzolanic activity.

The outer layers' dissolution controls the clay minerals' dissolution rate (BAUER; BERGER, 1998; HUERTAS; CHOU; WOLLAST, 1999; YOKOYAMA; KURODA; SATO, 2005). This means that the hydrolysis of tetrahedral and octahedral layers at surfaces occur while the dissolution of kaolinite and montmorillonite minerals takes place, especially under alkaline conditions (BAUER; BERGER, 1998). Yokoyama et al., (2005) also indicated that the dissolution rate of montmorillonite depends on the edge surface rather than the total surface area in alkaline conditions, based on atomic force microscopy (AFM) analysis.

Despite the same mechanism involved, kaolinite and montmorillonite have different dissolution rates due to their structural characteristics and the calcination temperature that impacts their degree of amorphism, according to Garg and Skibsted (2015). They showed that optimally calcined kaolinite (at 700 ºC) has a Si an Al dissolution 12 times higher than montmorillonite at optimally calcined temperature (at 800 ºC) (figure x). This was explained by ^{27}Al NMR results that show more reactive $Al^{(v)}$ sites than montmorillonite. Montmorillonite at 800ºC presented higher amorphism than at 900ºC, dissolving Si faster than Al. When comparing the same mineral clay, there was a greater relationship between the dissolution of the clay at its optimum calcination temperature than the specific surface area (SSA).

The relation between the reactivity of common calcined clays and Si and Al dissolution was recently studied by Maier et al., (2021). They demonstrated an optimal correlation (R^2=0.98) between these factors from analysis by R^3, a method of measuring the heat release in clinker-free simplified systems (AVET *et al.*, 2016). Thus, the higher the solubility of calcined clays, in terms of Si and Al, the higher the pozzolanic activity of this material. However, such dissolution was performed by the ICP-OES technique, an expensive technique, which may hinder this approach in the analysis of clays reactivity.

Figure 7 – Impact of calcination temperature on Si and Al dissolution of kaolinite (K) and montmorillonite (MT) clay minerals

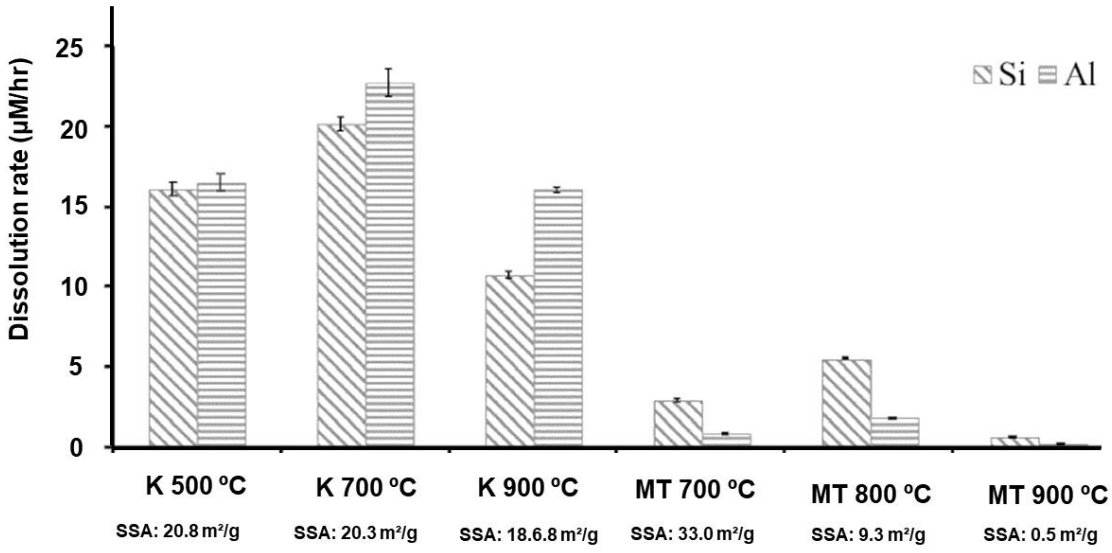

Source: adapted from Garg and Skibsted (2015)

The dissolution of SCM, such as calcined clays, affects the hydration products formed and the microstructure of cement-based materials. Dhandapani and Santhanam (2019) discussed that the high dissolution rate of calcined clay produces some hydration products and shifts their chemical composition, e.g., lower Ca/Si ratio, which can change C-(A)-S-H composition. Beuntner et al. (2016) also reported that the dissolution of sulfate ions from mixed-layer calcined clays can lead to a smaller ettringite formation. Thus, it was possible to conclude that the dissolution of calcined clays plays a role in microstructural development, affecting the macroscopy properties.

2.2.2 Evaluation of pozzolanic reactivity

Pozzolans can be siliceous or aluminosilicate materials, which in their natural state have little or no binding properties, but when finely ground in an alkaline environment, they react with the hydroxide at room temperature, forming compounds with binding properties (ABNT, 2015; ASTM C125-20, 2010). Besides the chemical and physical requirements (ABNT, 2015; ASTM C125-20, 2010), there are tests to evaluate the pozzolanic reactivity of materials that can be classified as direct or indirect methods. The first ones are conducted in simplified systems that simulate alkaline conditions to quantify Portlandite (CH) consumption by the pozzolanic activity. The most common is the Chapelle test (ABNT, 2010b), Frattini test (EN 196-5, 2011), followed by the R^3 test (AVET *et al.*, 2016); and less usual the saturated lime

test (SL) (DONATELLO; TYRER; CHEESEMAN, 2010) or lime consumption test (LC) (TIRONI *et al.*, 2013). Indirect methods evaluate the pozzolanic contribution on some change in characteristics such as mechanical performance of mortars by Strength Activity Index (SAI)(ASTM C311, 2018), also called Performance Index (PI), or electrical conductivity of saturated solution of CH (TIRONI *et al.*, 2013). Table 3 shows a comparison between the most common pozzolanic reactivity methods.

Table 3 – Comparison between usual reactivity pozzolanic methods

Technique/method	**Curing time**	**Temperature**	**Source of CH**	**CH: Pozzolan**	**Involved activity**
Chapelle test	16h ± 1h	90 ºC	Calcium hydroxide	1:1	CA
Frattini Test	8, 28, and 90days	40 ºC	Cement hydration	1:1	CA
R³	1 day 7 days	40 ºC 20 ºC	Calcium hydroxide	1:3	CA
SL	Not specified	40 C	Saturated lime solution	0.15: 1	CA
SAI	7 and 28 days	20 ± 2 ºC	Cement hydration	1:1	C-PA

CA: chemical activity; C-PA: chemical and physical activity.

Source: Adapted from (DONATELLO; TYRER; CHEESEMAN, 2010)

Table 4 shows recent studies where the main objectives are assessing the pozzolanic reactivity of calcined clays. The assessments are based on one or multiple techniques. The Chapelle test is one of the most usual for this purpose. In general, the capacity to consume CH tends to be higher for calcined kaolinite (or kaolinitic) clays than other clay minerals, which agrees with what has been discussed about their different minerals properties. The capacity of binding CH is impacted by several factors, such as calcination temperature and type of clay minerals. The better performance seems to be attributed to 700~900ºC to kaolinite clays, 800 ºC and 900 ºC to montmorillonite and illite, respectively. Frattini and SAI have a good correlation because they reflect the effects of pozzolanic materials in hydrated products formed; hence, porosity refinement is increased (TIRONI *et al.*, 2013).

Recently, R³ (reliable, rapid, relevant) test was proposed to evaluate the pozzolanic reactivity of kaolinitic clays (AVET *et al.*, 2016). The study proves the method's effectiveness, showing good a correlation with released heat flow by isothermal calorimetry, hydrated products, and compressive strength of mortar samples. Although indicated for kaolinitic clays, the method is also suggested for other SCM such as fly ash, blast furnace slag (AVET *et al.*, 2016), etc.

Each SCM will likely have a different reactivity measured by heat flow achieved, even calcined clays. Besides physical factors (fineness, specific surface area), sample condition (raw *vs.* calcined), etc; the type, quantity of minerals, and the degree of order/disorder of the kaolinite were pointed out as additional factors affecting the reactivity of clays, as discussed by Maier; Beuntner and Thienel (2021). According to the authors, 2:1 clay minerals (illite, smectite or mixed-layer minerals) significantly contributed to the pozzolanic activity of 13 different clay-rich materials. The kaolinite disorder also impacts the heat flow development but not cumulative heat. Such aspects highlight the importance of pozzolanic reactivity studies of lower purity but clay-rich materials such as SCM.

Table 4 – Comparison between usual reactivity pozzolanic methods

Calcined clays assessed / calcination temperature	**Test/technique**	**Objective**	**Result**	**Reference**
Bentonite (900 ºC)	Chapelle Test	Binding capacity of $Ca(OH)_2$ by calcined clay	545 mg/$Ca(OH)_2$ / g of calcined clay	(TRÜMER *et al.*, 2019)
Calcined coal-series kaolin (800ºC, 500 ºC, 600 ºC, 700 ºC, 800 ºC, 900 ºC)	Chapelle test, Frattini, SAI	Test coal-series kaolin as a potential pozzolanic material	Example: Chapelle: (689, 1296, 1360, 1440, 1351); SAI_{3days} (2%,4%,6,8%, 10%, 7%)	(LIU *et al.*, 2017)
Kaolinite clays: KGA-1 (500ºC, 700ºC, 800ºC and 900 ºC), KGA-2 (500ºC, 700ºC, 800ºC and 900 ºC) Na-montmorillonite (700ºC, 800 ºC, 900 ºC); Ca-montmorillonite (700 ºC, 800 ºC, 900ºC); Calcined hectorite (700 ºC, 800 ºC, 900 ºC) Calcined illite (700ºC, 800 ºC, 900ºC).	Chapelle Test	Determine the pozzolanic reactivity of eight clay samples at different calcination temperature	mg/$Ca(OH)_2$: KGA-1 (~1400, ~1550, ~1470, ~1600) KGA-2 (~1500, ~1500, ~1450, ~1500) Na-montmorillonite (-450, ~1400, ~700) Ca-montmorillonite (~650, ~1410, ~190) Calcined hectorite (~250, ~200, ~50) Calcined hectorite (~180, ~250, ~930)	(HOLLANDERS *et al.*, 2016)
Kaolinite clay (600 ºC, 700 ºC, 750 ºC, 800 ºC, 850 ºC)	R^3	Determine the pozzolanic reactivity of eight clay samples	R^3 (J/g): (600 ºC: ~101, 700 ºC:~115, 750 ºC: ~116, 800 ºC: ~118, 850 ºC: ~100)	(SCRIVENER *et al.*, 2019)
Common clays (AC, OC, SCW, CCW, KT, HUP, FUP, RKUP, SW, SLS, MOSM, KBZ, KK)	R^3	Characterization and reactivity test of 13 common clays suitable as SCMs	Example: R^3 (J/g) (AC: 279, OC: 233, SCW: 399, CCW: 208, KT: 174, KUP: 246, FUP: 611, RKUP: 457, SW:	(MAIER; BEUNTNER; THIENEL, 2021)

			67, SLS:113 , MOSM: 141, KBZ: 780, KK: 749)	
Kaolinite clays AE23 (700 ºC, 800 ºC), AE24 (700 ºC, 800 ºC), AE27(700 ºC, 800 ºC), AE28 (700 ºC, 800 ºC), AE29 (700 ºC, 800 ºC)	Chapelle, PI, R³	Valorization of non-beneficiated clays as SCM in cement-based mortars	Example: Chapelle mg/Ca(OH): AE23 (700 ºC: 947.9, 800 ºC: 1027.9), AE24 (700 ºC: 680.3, 800 ºC:717.5), AE27(700 ºC: 591.1, 800 ºC: 583.6), AE28 (700 ºC: 933.1, 800 ºC: 888.5), AE29 (700 ºC: 823.4, 800 ºC: 724.9)	(DE OLIVEIRA *et al.*, 2021)

Source: Author (2021)

Another way to check the pozzolanic reactivity of the materials is through the consumption of CH over time, which can be followed up with common techniques such as XRD, TGA, and NMR, among others.

2.3 LIMESTONE CALCINED CLAY CEMENTS

2.3.1 Early-age hydration

Previous knowledge about the hydration of cementitious materials was mainly based on studies in their hardened states. Nowadays, developing new analytical techniques in micro/nanoscale and with higher sensitivity allows monitoring the development of hydration reactions in real-time and at an early age. Therefore, hydration studies at earlier ages have been the target to explain the hydration mechanisms of Portland cement and its main constituent phases: the silicates (C_3S and C_2S) and aluminates (C_3A and C_4AF). This approach has motivated several studies to refute weakly grounded theories and to create hypotheses about the main phenomena related to cement dissolution: precipitation of hydrated products such as induction period, acceleration and deceleration (BULLARD *et al.*, 2011; SCRIVENER, K. *et al.*, 2019; SCRIVENER; JUILLAND; MONTEIRO, 2015), that can be observed by techniques such as isothermal calorimetry.

The increasing substitution of clinker by SCMs makes understanding the hydration mechanisms even more complex. SCMs properties affect the reactivity of blended cements by physical and chemical effects. The increased number of nucleation sites, filler effect, and space for the further precipitation of hydrated products are some of the major physical impacts of SCMs at an early age (SKIBSTED; SNELLINGS, 2019). At the same time, the chemical effects are based on Si and Al amorphous minerals present in SCM, which influence the

amount, type, or composition of hydrated formed products (LOTHENBACH; SCRIVENER; HOOTON, 2011).

The LC^3 is the main example of ternary (or blended) cements based on limestone and calcined clays as SCM. Different mix proportions of LC^3 systems were studied by Zunino (2020), but the most promising and more usual has been the LC^3-50, which consists of 55% of cement (clinker+calcium sulfate), 30% calcined clay, and 15% limestone (% weight). The relation 2:1 (metakaolin (MK): limestone (LS)) is based on the stoichiometric formation of the monocarboaluminate phase (Mc), where 1 mol of metakaolin reacts with 1 mol of calcium carbonate to form 1 mol of Mc in aqueous calcium solution (ANTONI *et al.*, 2012b). However, such dosage considered MK and LS as a pure mineral sources. Costa (2021) proposed ternary cement dosage based on amorphous content in the calcined clay and calcium carbonate of waste raw materials rather than simple mass proportion. The amounts of clinker: gypsum in LC^3-50 is around 45~55%, depending on whether sulfate adjustment is made.

A common way to observe the early hydration kinetics of cement is through the heat flow released in the hydration reactions, which can be monitored by isothermal calorimetry. Such heat flow curves can be broken up into 4 periods or 3 periods according to the author's discussion (BULLARD et al., 2011; SCRIVENER et al., 2019; SCRIVENER; SNELLINGS; LOTHENBACH, 2016), as shown in Figure . Period I defines the initial reactions; Period II is the induction period; III is the acceleration period or IV decelerating period (BULLARD *et al.*, 2011; SCRIVENER; SNELLINGS; LOTHENBACH, 2016). The approach in 3 distinct periods differs from the previous one by grouping periods I and II together as published by (SCRIVENER et al., 2019).

Figure 8 – Different phases of cement hydration as seen in an isothermal calorimetric measurement with IV phases. I (initial reactions), II (induction period), III(acceleration period) IV (deacceleration period).

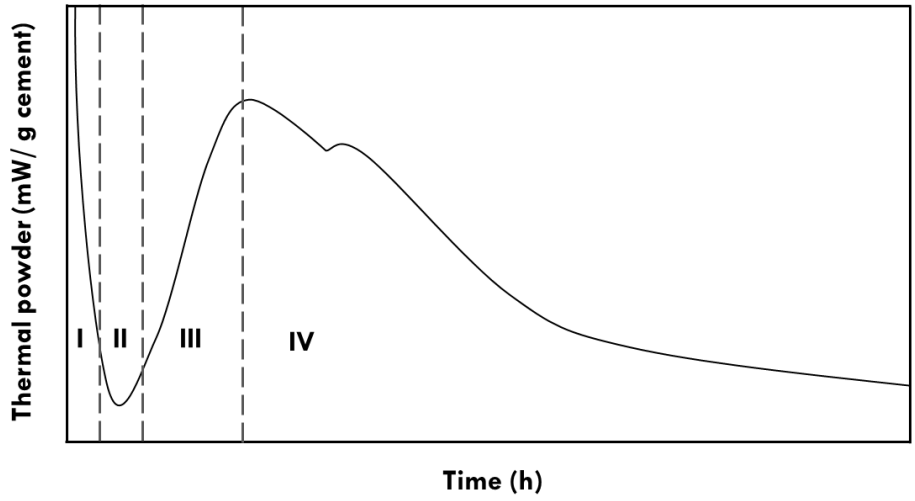

Source: Adapted from Scrivener; Snellings and Lothenbach (2016)

The early hydration kinetics between OPC and LC³ cements are pretty different. A typical heat flow curve by isothermal calorimetry of OPC and LC³ is illustrated in Figure 9 of this section. Both cements are in a properly sulfated condition. Otherwise, the reactions would be unbalancing that can change the heat flow curves (further discussion on the sulfate balance is presented in the 2.2.3 section). The initial reactions (I) are characterized by the dissolution processes, which involve reactions of C_3S and water (BULLARD *et al.*, 2011) and C_3A and gypsum to form ettringite ($C_6A\$_3H_{32}$, AFt) in the first minutes (SCRIVENER et al., 2019) (Eq. 5). Due to the speed and high heat flow released after contact of the cement with the water, some studies have excluded initial heat measurement in LC³ pastes (ZUNINO; SCRIVENER, 2019, 2020, 2021a, 2021b) which does not affect the understanding of the main hydration phenomena.

$$C_3A + 3CaSO_4.2H_2O + 26H \rightarrow C_6A\$_3H_{32} \quad \text{Eq. 5}$$

The induction period (II) is common in both OPC and LC³ but can be prolonged by the addition of chemical admixtures (e. g., PCE), as observed by (AVET; SCRIVENER, 2018b). The resumption of reactions characterizes the silicate peak (Period III). At this time, there is a rapid dissolution of C_3S with heterogeneous nucleation and growth of C-S-H, mainly outer, on the alite surface (BULLARD *et al.*, 2011; SCRIVENER; JUILLAND; MONTEIRO, 2015). Portlandite can also grow rapidly (BULLARD *et al.*, 2011; SCRIVENER; JUILLAND; MONTEIRO, 2015). Such silicate peak is common for OPC and LC³ but tends to start faster for LC³ than OPC due to the filler effect promoted by calcined clays and limestone.

Consequently, the slope and intensity of the silicate's peak increase (AVET; SCRIVENER, 2018b).

Figure 9 – Typical heat flow curves of OPC and LC³ with IV phases (proper sulfated systems): I (initial reactions), II (induction period), III(acceleration period) and IV (deaccelerating period). SD: sulfate depletion. AFm: Formation of AFm phases (Hc+Mc).

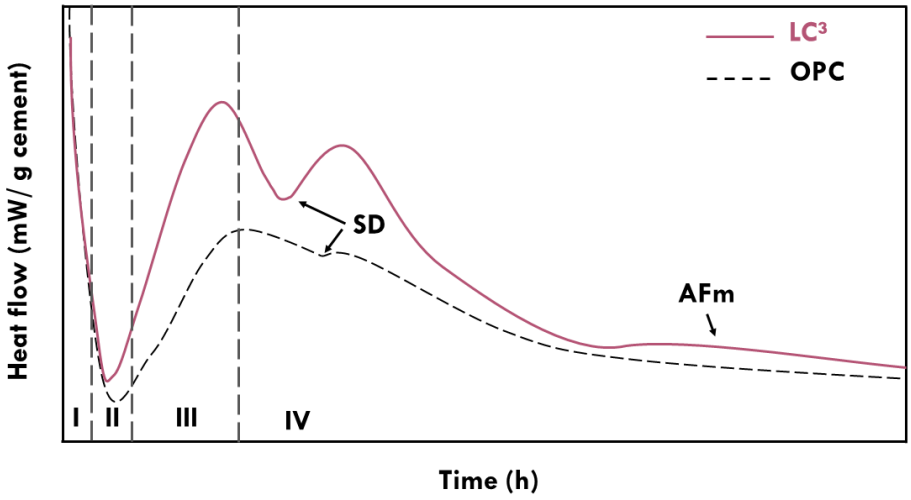

Source: Author (2021)

The most pronounced distinctions between the early-age hydration of OPC and LC³ are observed in the deceleration period (IV). After the silicate peak, a deceleration occurs until all the sulfate is consumed, leading to what is also called "sulfate depletion"(SD) (ANDRADE NETO; DE LA TORRE; KIRCHHEIM, 2021)Figure . As previously mentioned, the sulfate ions initially available are partially combined with C_3A to form the first ettringite crystals. The remaining amount is gradually adsorbed to C-S-H, reducing its availability in solution (NONAT *et al.*, 2011) with gradually changing C-S-H morphology (BÉRODIER; MULLER; SCRIVENER, 2020). The chemical and physical mechanisms associated with the SCMs present in LC³ may indicate this faster sulfate depletion. However, there is a lot of discussion on the most impacting factor. Such SCMs increase C-S-H formation from the acceleration period (III) by filler effect, where sulfate ions can be adsorbed. In addition, as an Al-rich SCM, metakaolin increases the alumina ions concentration in the pore solution, and consequently higher is the ettringite formed (ZUNINO; SCRIVENER, 2020). Such interactions among C-S-H, C_3A (from clinker), and extra alumina (from MK) increase the sulfate demand to ensure a proper sulfated system.

The SD also marks the onset of a second (aluminate) peak. At this point, a new and rapid dissolution of the C_3A occurs while sulfate ions are desorbed from the C-S-H to an 2nd and

intensified ettringite precipitation (ANDRADE NETO; DE LA TORRE; KIRCHHEIM, 2021; ZUNINO; SCRIVENER, 2019). The amount of ettringite and AFm phases at 24h tends to intensify from the onset of the aluminate peak, as Zunino and Scrivener (2019) discussed. Such authors demonstrate a high correlation between the formation of such phases and the aluminate peak's intensity (R^2=0.97) from its deconvolution by supersulfated comparison systems. The position of this peak is dependent on the time for sulfate depletion, while the intensity of this peak may be associated with physical factors, such as the greater specific surface area (SSA) provided by the calcined clays (ZUNINO; SCRIVENER, 2019), or chemical factors such as the calcined kaolinite content (AVET; SCRIVENER, 2018b; da SILVA et al., 2021).

The synergistic reaction between metakaolin and limestone leads to a third peak associated with the formation of CO_3-AFm phases, so-called carboalumination phases. The calcium carbonate (Cc, from limestone) reacts with aluminates phases such C_3A and alumina from MK to form hemicarboaluminate ($C_4A.0.5H_{12}$, Hc) (Eq.6) and monocarboaluminate ($C_4AH_{11,}$ Mc) (Eq. 7), instead of calcium monosulfoaluminate ($C_4A\$H_{12,}$ SO_4- AFm) (DAMIDOT *et al.*, 2011; PUERTA-FALLA *et al.*, 2015), respectively. Hc and Mc appear after the 2nd ettringite formation is concluded, which this may occur around ~24h in LC^3 hydrated properly sulfated (ANTONI et al., 2012b; MALACARNE et al., 2021; ZUNINO; SCRIVENER, 2019), although this is more common at late ages.

$$C_3A + 0.5Cc + 12H \rightarrow C_4A.0.5H_{12} \quad \text{Eq. 6}$$

$$C_3A + Cc + 11H \rightarrow C_4AcH_{11} \quad \text{Eq. 7}$$

Zunino and Scrivener (2021) have recently investigated the influence of metakaolin and sulfate contents and water to binder ratio on the position and intensity of this third peak in LC^3. As results, they affirmed that MK and sulfate affects the amount of Hc+Mc precipitation. As higher is the calcined kaolinite content, earlier is such precipitation, whereas the higher is sulfate addition, the latter is Hc+Mc precipitation. Water to binder ratio affects the delay in the third peak. Therefore, balancing these parameters is necessary and will be further discussed in the following section.

There are few studies involving the hydration of cements blended with calcined montmorillonite. Most research is limited to binary systems cements, where the effects of calcined montmorillonite on the fresh and hardened properties of mortar and/or concrete are investigated at different levels of Portland cement replacement (AL-HAMMOD; FRAYYEH; ABBAS, 2021; MADHUKAR MASKE; KRISHNARAO PATIL; DEEPAK KATDARE, 2021; MESBOUA *et al.*, 2021; REHMAN *et al.*, 2020; YANG *et al.*, 2019). As a pozzolan, the hydration of cementitious materials with calcined montmorillonite is usually evaluated at later ages. In this context, Scanning Electron Microscopy (SEM) - EDS has been a usual technique to observe the morphology and chemical composition of hydrated products. Some authors have found needle-like products with higher Al and Si content (such as C-(A)-S-H) on the surface or edge of montmorillonite particles. Such parts of montmorillonite are based on Si-O or Al-O chemicals bonds that contribute as nucleation sites for further cement reaction (LIU *et al.*, 2020; YANG *et al.*, 2019). In addition, there are common hydration products such as CH and AFt (LUO *et al.*, 2019), or monosulfoaluminate in subsulfated systems, (MESBOUA *et al.*, 2021).

A deeper study on the hydration of binary cements with calcined montmorillonite (70% white PC - 30% calcined montmorillonite) was conducted from 1 day to 365 days by Garg and Skibsted (2015). Based on ^{29}Si MAS NMR spectra, after 1 day of hydration, aluminosilicate chains and Al/Si ratios were higher than the white Portland cement (WPC), despite the lower degree of reaction of the calcined clay (4.4%) compared to kaolinite. The highest reaction gain of the montmorillonite was reached at 7 days (~60%), with little difference up to 1 year. The ^{27}Al MAS NMR spectra showed the formation of C-S-H phases with the presence of Al in their composition. Furthermore, in addition to ettringite (AFt) phase formation (at 1 day), a higher monosulfoaluminate (SO_4-AFm) formation than WPC was observed at 7 days. This may indicate a reduction of the SO_3/Al ratio (due to the dissolution of alumina from the clay) with the consequent conversion of ettringite to monosulfoaluminate. Thus, it is possible to assume that in ternary cements such as LC^3, a synergistic reaction will occur between limestone and calcined montmorillonite, marked by the formation of CO_3-AFm phases instead of SO_4-AFm; but to a less accelerated degree than mixtures with calcined kaolinite clays. Moreover, despite being less reactive, montmorillonite normally has a high specific surface area, which instigates the investigation of its filer effect in this hydration process.

Thus, the use of calcined montmorillonite (CM) in ternary cements is rarely reported. However, some efforts have been made on its potential use combined with metakaolin

(calcined kaolinite clay) in partial cement replacements (TAYLOR-LANGE *et al.*, 2015; WEI *et al.*, 2019) and with limestone (SHI *et al.*, 2019). The synergy between both calcined clays increased the CH consumption and compressive strength (TAYLOR-LANGE *et al.*, 2015). In addition, increasing this amount of MK+MT, more C-(A)-S-H gel pores, hydrogarnet, and strätlingite are formed at late ages (WEI *et al.*, 2019). Limestone and calcined montmorillonite clay in blended cements were studied by Shi et al., (2019). However, only aspects related to sulfate resistance, pozzolanic reactivity, and porosity at different calcined clays were assessed. No further attention was paid to the hydration of such blended systems, especially at early ages.

2.3.2 Sulfate balance

2.3.2.1 The importance of sulfate balance

Portland cement is one of the world's most critical human-made products. Its production involves calcination of limestone and clay at high temperatures to produce clinker, which result in a huge environment impact due to CO_2 emissions related to the processes. After the 'clinkerization', the material is cooled, finely ground, and mixed with calcium sulfate to control the flash-set of the clinker in contact with water (JACKSON, 2003). Mineral admixtures (e.g., limestone, blast furnace, fly ash) are usually inserted in the final stage of the production of Portland cement (ABNT, 2018) or the concrete mixtures.

Calcium sulfate is an inorganic compound that can be found in several forms in nature. Its dihydrated structure is called gypsum ($CaSO_4.2H_2O$), which gives its name to the gypsum rock. Such minerals can lose crystallization water through calcination or due to the temperature increase during grinding of the clinker and transform itself into hemihydrate ($CaSO_4.{}_{1/2}H_2O$) or anhydrite ($CaSO_4$) (SCRIVENER; SNELLINGS; LOTHENBACH, 2016). Calcium sulfate is added to the cement and initially interact with the aluminate phases, especially tricalcium aluminate (C_3A), which has a strong dissolution after contact with water (YE *et al.*, 2020) and considerable influence on the setting and early hardening of the cement (KIRCHHEIM *et al.*, 2011).

The adequate calcium sulfate balance is especially related to the C_3S and C_3A phases reactions. Undersulfated systems (with low levels of calcium sulfate) may not ensure the control of setting times and a high initial compressive strength due to the rapid and early ettringite formation without adequate hydration of the C_3S to form C-S-H (SCRIVENER, K.

et al., 2019). While super-sulfated systems (with high sulfate contents) have a prolonged sulfate depletion and late return of C_3A reactions (QUENNOZ; SCRIVENER, 2013), reflecting in low strength at early age. Besides that, such systems are more susceptible to the delayed ettringite formation (DEF) capable of damaging concrete structures due to expansive effects (MOHAMMED; SAFIULLAH, 2018). Properly sulfated systems are those where calcium sulfate content ensures that the C_3S reaction occurs before the C_3A reactions (SCRIVENER et al., 2019) providing the highest compressive strength, lowest chemical shrinkage, lowest expansibility, and avoid cracking at late ages (MOHAMMED; SAFIULLAH, 2018). Therefore, the adequate addition of calcium sulfate into cement is of great importance. Besides controlling the setting times and the initial strength of the cement, it can impact the durability of structures at long ages.

Currently, the desgin of calcium sulfate to Portland cement is done in terms of total SO_3 content. The Brazilian standard for Portland cement requirements (ABNT, 2018) and European standard (EN 197-1, 2018) limits the SO_3 content to 4.5% and 3.5%-4% as a precaution against possible expansive effects. On the other hand, American standard does not limit the SO_3 content as long as it is proven that the levels used in the cement formulation do not present a short expansibility (~0.03mm) at 14 days (ASTM, 2020). The usual techniques/procedures to determine the optimum SO_3 content are mechanical strength, calorimetry, setting time, (chemical) shrinkage, probability of DEF (ANDRADE NETO; DE-LA-TORRE and KIRCHHEIM, 2021). The first three mentioned promoting operational speed since it can quickly provide the optimum SO_3 content (e.g., 1-3 days). Even though not considerate the durability of the cements, such approach has been usual by cement producers following their performance criteria.

The determination of the optimum sulfate content, here call as $SO_{3optimum}$, is a difficult task because it is affected by several factors; such as physicochemical and mineralogical properties of clinker, sulfate source, chemical admixtures, SCMs, among others as discussed by Andrade Neto et al. (2021). The replacement of Portland cement by SCMs has been one of the most successful strategies to reduce CO_2 emissions related to the cement production chain (IEA, 2018). However, these practices with SCMs such as slag, fly ash, and calcined clay cause an accelerated sulfate depletion compared to OPC (DE LA VARGA *et al.*, 2018; NIEMUTH; BARCELO; WEISS, 2012; SUN *et al.*, 2020; ZUNINO; SCRIVENER, 2019). The blended cements with limestone and calcined clays, e. g. LC^3, has presented the acceleration of sulfate depletion even higher due to the large amounts of SCMs in its composition, approximately

~45% in LC³-50. Thus, an extra addiction of gypsum is required to achieve high compressive strength at 24h (ANTONI *et al.*, 2012b; SCRIVENER *et al.*, 2019).

2.3.2.2 How has sulfate adjustment been performed in LC³ cements?

The sulfate balance adjustment in blended cements such as LC³ is usually based on the heat released by isothermal calorimetry results. Several authors define the optimum gypsum content basically when the aluminate peak occurs after and silicate peak curves (AVET et al., 2016; AVET; BOEHM-COURJAULT; SCRIVENER, 2019; AVET; SCRIVENER, 2018b, AVET; SCRIVENER, 2020). Such determination is made by adding extra gypsum beside that already used during the clinker grinding. Avet and Scrivener (2020) adjusted the sulfate balance with 2% extra gypsum at 10 ºC and 20 ºC, and 3.5% at 40 ºC and 60 ºC of analysis. The total SO_3 content were 2.6% and 3.3%, respectively. The extra gypsum of 2% was defined as the optimum sulfate content by several authors (AVET *et al.*, 2016; AVET; BOEHM-COURJAULT; SCRIVENER, 2019; AVET; SCRIVENER, 2018b).

However, such approach of determining proper sulfate content only with heat flow results have some disadvantages. First, the replacement of OPC (clinker + gypsum) by SCMs decreases only the total amount of gypsum but does not affect its proportion regarding clinker, as discussed by (ANDRADE NETO; DE LA TORRE; KIRCHHEIM, 2021). Second, by physical and chemical effects, SCMs will increase the sulfate demand. Andrade Neto et al. (2021) mention that such demand will be higher relative to clinker and not as higher relative to total cement mass. Thus, the increase in sulfate demand related to the impact of SCMs on clinker should be a more appropriate approach than their impact related to total cement mass. Another disadvantage is that the distinction between silicate and aluminate peaks can occur over long-time intervals impacting the compressive strength at early age.

There are several methods to better determine the proper cement sulfate content. For instance, the standard C563-18 (ASTM 2019) describes the determination of approximate $SO_{3optimum}$ as maximum performance at different levels of cement substitution by means of heat flow released isothermal calorimetry or compressive strength test. The first one is based on cumulative heat flow at a specific age in different levels of SO_{3total}. Usually, the heat released is a good indication of the reactivity of SCM in cement pastes (SCRIVENER; SNELLINGS; LOTHENBACH, 2016). However, this systematic relationship is not always found in subsulfated LC³ systems (PY, 2021), as the overlap between heat peaks can impact on the heat flow released at 72h and on the compressive strength. The sulfate optimization based on

thermal analysis can be a good strategy for optimum sulfate determination. Such technique can provide the bound/combined water, which has good relationship with compressive strength results (JOHN *et al.*, 2019), and Portlandite content (CH) of cement. Different levels of SO_{3total} could be tested in pastes samples at different ages. The optimum sulfate content may be defined as the high-bound water mixture to a lower CH content. The chemical shrinkage can also contribute to the optimum SO_3 determination. Such test can be performed in pastes of different SO_3 levels to determine which one has the highest chemical shrinkage at the specific age.

2.3.2.3 The impact of the calcined clays on the sulfate balance

As discussed before, comparing to Ordinary Portland cement (OPC), the blended cements have shown an accelerated setting time, low compressive strength at an early age and a rheology characterized by an increase of viscosity, yield stress and water demand (MALACARNE et al., 2021) as well as higher chemical admixture dosage required to achieve a specific workability (SCRIVENER *et al.*, 2019). In addition, it is known that physical characteristics such as high fineness, high Specific Surface Area (BET method) (SSA_{BET}) and lamellar morphological structure of the clays, especially in kaolinitic clays, have a major impact on the rheological behavior mentioned. However, the physical and chemical impact of calcined clays on the sulfate balance is still under discussion. Three hypotheses based on the clay minerals properties can be highlighted: the filler effect, ionic dissolution under alkaline environment and adsorption of calcium sulfate on the clays' surface.

The physical and chemical effects of the calcined clays on the sulfate balance are still under discussion. Zunino and Scrivener (2019) concluded that the increase of sulfate demand in blended cements is related to the additional surface area that impacts the total C-S-H and ettringite formation due to their competition for sulfate ions rather than the clays' chemical composition. Besides that, the authors concluded that the additional alumina content of the calcined clays would not influence the need for sulfate for adequate sulfation. Such conclusions were made in non-systematic comparisons. On the other hand, Avet and Scrivener (2018) and da Silva et al. (2021) suggest that an accelerated sulfate depletion dependent more on the kaolinite content of the clays than on the SSA_{BET} provided by kaolinitic clays, which leads to extra aluminum driving hydration to an undersulfated system and accelerated ettringite formation.

The dissolution of calcined clay minerals can also impact on sulfate depletion. For instance, Maier et al. (2021) concluded that, using ICP-OES of illite and kaolinite clay minerals in alkaline solutions, an acceleration of sulfate depletion in blended cements is caused by an alumina interactions (from C_3A and calcined clays minerals) for calcium sulfate-based. In calcined clays, such dissolution is dependent on clay minerals and related to their SSA, reactivity and dehydroxylation degree, according to Garg and Skibsted 2019. For example, in kaolinite, Si and Al dissolution are 4 and 12 times larger than in montmorillonite as explained by ^{27}Al NMR results, which showed a highly and preferential dissolution of pentahedral aluminum sites (Al^{V}).

The acceleration of sulfate depletion can also be influenced by ions adsorption during the cement hydration. Such arguments were pointed out by Maier et al. (2021) in blended cement concerning to kaolinite and illite clays minerals. The authors have proposed that the adsorption processes of SO_4 ions and/or Ca-SO_4-complexes on the surface of calcined clays impact the rapid sulfate depletion during the hydration process according to their zeta potential analysis at a specific age. The affinity of the clay minerals with ions Ca^{+2} was previously presented by Lei and Plank (2014), where the kaolinite, montmorillonite and muscovite showed increased adsorption as a function of Ca^{+2} into solution. However, the calcium sulfate adsorption on the montmorillonite clay surface, such as calcium bentonite, has not yet been evaluated. Therefore, the present study will also evaluate this property between clays and a fixed calcium sulfate content over time.

2.3.3 Artificial pore solution

The better understanding of pore solution of hydrated cements has a crucial importance on their durability and hydration kinetics of cementitious systems, but studies on the topic are generally overlooked. The pore solution can be extracted either in the liquid phase by vacuum filtration or centrifugation or hardening pastes by pore press device, then the chemical composition of the pore water can be assessed by different analytical methods such as ICP-OES, AAS, IC, among others (BARBARA; RUBEN; HAUFE, 2016). The results provide insights about hydration kinetics that involve dissolution-precipitation processes and determine the stability or dissolution of phases (BARBARA; RUBEN; HAUFE, 2016) from a variety of ion concentrations present in the pore water extracted.

SCMs in blended systems change the hydration reactions and products formed when compared to OPC. They reduce the amount of portlandite, change the C-S-H composition, can

increase the amount of ettringite or even the type of AFm phases in a cement hydrated (LOTHENBACH; SCRIVENER; HOOTON, 2011). SCM additions can also affect the pore solution composition due to dilution of alkalis and alkalis binding to C-A-S-H[1] (HONG; GLASSER, 1999). Most studies focus on the impacts caused by traditional SCMs such as limestone, blast furnace slag, fly ash and silica fume on the pore solution composition (BARBARA; RUBEN; HAUFE, 2016; CHERIF *et al.*, 2017; FU *et al.*, 2020; KOLANI *et al.*, 2012; SCHÖLER *et al.*, 2017). Recently, the combined clinker replacement by limestone with calcined clays in blended cements such as LC³ has increasingly gained attention in this sense.

Usually, pore solution has been extracted at different ages of hydration for many purposes in LC³ systems, such as simple characterization, to verify the impact of grinding aids into hydration kinetics, the influence of calcined kaolinite content into ions concentration and pH, etc (ZUNINO; SCRIVENER, 2020; NGUYEN et al., 2018; AVET; SCRIVENER, 2018b; DHANDAPANI; SANTHANAM, 2019). Given the low water to binder (w/b) ratios (<1.0), the pore extraction has been done by high-pressure equipment. pH measurements are made right after the extraction showing values ~13 and acid solution (NHO_3) are used to correct the pH value and limit further precipitation of hydrated products. The ion concentration is measured by ICP-OES analytical method.

The impact of the calcined clays on the pore solution composition of LC³ blends is of most interest due to their large amount utilized (e.g., 30% in LC³-50). Metakaolin, for instance, increase the concentrations of Si and Al ions on the pore solution, as these are its predominant elements. Therefore, Al ions has been the focus of the studies. The amount of Al released into solution as a function of kaolinite content was first investigated by (AVET; SCRIVENER, 2018b). As higher is the calcined kaolinite content, greater is the availability of Al ions in the solution, but the dissolution of Si is barely altered at 28 days. To a lesser extent, there is a change in solution pH and reduction Ca ions concentration, indicating pozzolanic reactions that consume portlandite and modifications of the C-(A)-S-H composition, respectively (AVET; SCRIVENER, 2018b). In addition, the increase of Al concentration on the pore solution and C-(A)-S-H composition was also observed by Avet; Boehm-Courjault and Scrivener (2018) using either SEM-EDS or STEM-EDS techniques. The Al/Ca ratios of C-A-S-H show a significant increase of aluminum with the level of calcined kaolinite content of

[1] C-A-S-H [1]: "Consists of a calcium oxide polyhedral layers flanked with tetrahedral (alumina) silicate chains – on both sides - and water as well as counter-ions (e. g., $Ca^{2+}$and OH) in an interlayer between two such layers" (BARZGAR *et al.*, 2021). It is a hydration product resulting from the incorporation of Al into the C-S-H structure. Although it is common in cements with Al-rich SCMs, such as calcined clays, its major formation occurs at long ages and therefore will not be deeply detailed in this study.

calcined clay (SEM-EDS and STEM-EDS) whereas Si/Ca also show higher than OPC and also increasing with calcined kaolinite content (STEM-EDS). Dhandapani and Santhanam (2019) observed in Al/Ca and Si/Ca atomic ratios obtained by SEM-EDS that there is an increase in Al in C-(A)-S-H compared to OPC pozzolanic cement with fly ash. Therefore, the pore solution chemistry can also indicate alteration of hydrated products (e.g., C-(A)-S-H) which are assessed by other techniques.

A new perspective aiming to analyze the impact of calcined clays in alkaline conditions near Portland cement has been the artificial pore solution. Although not the real pore condition of pastes, mortars or concretes, the approach promotes a faster and more practical solution, as it does not require the use of specific equipment and apparatus to extract the pore solution. In addition, it removes the impact of alkalis and ions from the hydrated phases, focusing on the real contribution of the clays on the chemical solution. It consists in preparing mixtures of different solutes capable of simulating some of the main ions present in the cement chemical solution and the pH during hydration.

The behavior of calcined clays under alkaline conditions have been studied for decades, specially to better understand their dissolution rates. Bauer and Berger (1998), for instance, conducted experiments measuring kaolinite and smectite dissolution in high KOH solution, with batch reactors at 35° and 80°C . As results, the main differences in dissolution rates were explain by structural differences, such as the organization of tetrahederal and octahedral layers. Garg and Skibsted (2019), in experiments between calcined kaolinied and montmorillonite, used NaOH (pH=13.0) solution to assess the dissolution of calcined clays. Beuntner and Thienel (2016) verified the solubity of calcined clay with four different alkaline solution (CH, 2 solutions of NaOH+KOH and KOH). They concluded that the kinetics of pozzolanic reaction and the products formed are affected by the type of alkaline solution and the presence of sulfate or carbonates in the pore solution.

Recently, the first MOK solution based 50 mmol/l NaOH and 300 mmol/l KOH (pH 13.57), suggest by Beuntner and Thienel (2016), has been used due to close conditions to real Portland cement pH (13) to create a model pore solution environment. The solution has bee used to correlate dissolution of Si and Al with R^3 tests, XRD quantifications, reaction kinetics in free-clinker systems, etc. (MAIER; BEUNTNER; THIENEL, 2021; SCHERB *et al.*, 2020, 2021). Thus, it seems a suitable approach to help the assessment of the dissolution and zeta potential of calcined clays in this study.

REFERENCES

ABNT. **NBR 16697: Cimento Portland-Requisitos**. [*S. l.: s. n.*], 2018. Disponível em: www.abnt.org.br. .

ANDRADE NETO, José S. *et al.* Hydration of C3S and Al-doped C3S in the presence of gypsum. **Cement and Concrete Research**, [*s. l.*], v. 152, p. 106686, 2022.

ANDRADE NETO, José S. *et al.* The role of sodium and sulfate sources on the rheology and hydration of C3A polymorphs. **Cement and Concrete Research**, [*s. l.*], v. 151, 2022.

ANDRADE NETO, José da Silva; DE LA TORRE, Angeles G.; KIRCHHEIM, Ana Paula. Effects of sulfates on the hydration of Portland cement – A review. **Construction and Building Materials**, [*s. l.*], v. 279, 2021.

ANTONI, M. *et al.* Cement substitution by a combination of metakaolin and limestone. **Cement and Concrete Research**, [*s. l.*], v. 42, n. 12, p. 1579–1589, 2012.

ASTM. **C1608-12, Standard Test Method for Chemical Shrinkage of Hydraulic Cement Paste, ASTM International, West Conshohocken, PA, 2012, www.astm.org**. [*S. l.: s. n.*], 2012.

ASTM. C563:18 - Standard Guide for Approximation of Optimum SO3 in Hydraulic Cement 1. [*s. l.*], 2018. Disponível em: www.astm.org,.

AVET, François *et al.* Development of a new rapid, relevant and reliable (R3) test method to evaluate the pozzolanic reactivity of calcined kaolinitic clays. **Cement and Concrete Research**, [*s. l.*], v. 85, p. 1–11, 2016.

AVET, François; BOEHM-COURJAULT, Emmanuelle; SCRIVENER, Karen. Investigation of C-A-S-H composition, morphology and density in Limestone Calcined Clay Cement (LC 3). **Cement and Concrete Research**, [*s. l.*], v. 115, p. 70–79, 2019. Disponível em: https://doi.org/10.1016/j.cemconres.2018.10.011. Acesso em: 9 ago. 2021.

AVET, François; SCRIVENER, Karen. Effect of temperature on the water content of C-A-S-H in plain Portland and blended cements. **Cement and Concrete Research**, [*s. l.*], v. 136, 2020. Disponível em: www.elsevier.com/locate/cemconres. Acesso em: 2 jul. 2021.

AVET, François; SCRIVENER, Karen. Investigation of the calcined kaolinite content on the hydration of Limestone Calcined Clay Cement (LC3). **Cement and Concrete Research**, [*s. l.*], v. 107, p. 124–135, 2018.

BAKI, Vahiddin Alperen *et al.* The impact of mechanochemical activation on the physicochemical properties and pozzolanic reactivity of kaolinite, muscovite and montmorillonite. **Cement and Concrete Research**, [*s. l.*], v. 162, 2022.

BERGAYA, F.; LAGALY, G. General Introduction: Clays, Clay Minerals, and Clay Science. **Developments in Clay Science**, [*s. l.*], v. 5, p. 1–19, 2013.

BERODIER, E.; SCRIVENER, K. Understanding the filler effect on the nucleation and growth of C-S-H. **Journal of the American Ceramic Society**, [*s. l.*], v. 97, n. 12, p. 3764–3773, 2014.

BEUNTNER, Nancy *et al.* **Solubility and kinetics of calcined clay: study of interaction by pore solution**. [*S. l.: s. n.*], 2016. Disponível em:

https://www.researchgate.net/publication/309426709. .

BULLARD, Jeffrey W. *et al.* Mechanisms of cement hydration. **Cement and Concrete Research**, [*s. l.*], v. 41, n. 12, p. 1208–1223, 2011.

CANBEK, Oğulcan *et al.* A quantitative approach to determining sulfate balance for LC3. **CEMENT**, [*s. l.*], v. 12, p. 100063, 2023. Disponível em: https://linkinghub.elsevier.com/retrieve/pii/S2666549223000099. Acesso em: 6 mar. 2023.

CEMENTIR HOLDING. **The Cement of the Future Is now Here: Cementir Launches FUTURECEM™ With up to 30 Percent Lower Carbon Emissions | Cementir Holding N.V.** [*S. l.*], 2020. Disponível em: https://www.cementirholding.com/en/media/whats-new/cement-future-now-here-cementir-launches-futurecemtm-30-percent-lower-carbon. Acesso em: 10 jun. 2021.

DA SILVA, Micael Rubens Cardoso *et al.* Valorization of kaolin mining waste from the Amazon region (Brazil) for the low-carbon cement production. **Case Studies in Construction Materials**, [*s. l.*], v. 15, p. e00756, 2021.

DE LA VARGA, Igor *et al.* Evaluating the hydration of high volume fly ash mixtures using chemically inert fillers. **Construction and Building Materials**, [*s. l.*], v. 161, p. 221–228, 2018.

DE MATOS, P.R. *et al.* Effect of superplasticizer addition time and metakaolin source on the early-age hydration of limestone calcined clay cement (LC3). **Materials and Structures - Under Revision (2022)**, [*s. l.*], 2022.

ECTORS, D. **Advances in the analysis of cementitious reactions and hydrate phases-Fortschritte in der Analyse von zementären Reaktionen und Hydratphasen**. 2016. [*s. l.*], 2016. Disponível em: https://opus4.kobv.de/opus4-fau/frontdoor/index/index/docId/7174.

EN 197-1. **EN 197-1 Cement-Part 1: Composition, specifications and conformity criteria for common cements**. [*S. l.: s. n.*], 2018. Disponível em: www.mbsmw.org. Acesso em: 5 jul. 2021.

FERNANDEZ, Rodrigo; MARTIRENA, Fernando; SCRIVENER, Karen L. The origin of the pozzolanic activity of calcined clay minerals: A comparison between kaolinite, illite and montmorillonite. **Cement and concrete research**, [*s. l.*], v. 41, p. 113–122, 2011. Disponível em: http://ees.elsevier.com/CEMCON/default.asp. Acesso em: 31 jul. 2021.

FLEGAR, Matea *et al.* Overview of clay as supplementarycementitious material. **SIMPOZIJ DOKTORSKOG STUDIJA GRAĐEVINARSTVA**, [*s. l.*], 2019. Disponível em: https://doi.org/10.5592/CO/PhDSym.2019.14. Acesso em: 10 jun. 2021.

GARG, Nishant. **STRUCTURE, REACTIVITY, AND DISSOLUTION OF CALCINED CLAYS BY SOLID-STATE NMR**. 2015. - Aarhus University, Denmark , 2015.

GARG, Nishant; SKIBSTED, Jørgen. Dissolution kinetics of calcined kaolinite and montmorillonite in alkaline conditions: Evidence for reactive Al(V) sites. **Journal of the American Ceramic Society**, [*s. l.*], v. 102, n. 12, p. 7720–7734, 2019. Disponível em: https://ceramics.onlinelibrary.wiley.com/doi/full/10.1111/jace.16663. Acesso em: 11 jul. 2021.

GEIKER, METTE. Characterisation of development of cement hydration using chemical

shrinkage. *In*: SCRIVENER, Karen; SNELLINS, Ruben; LOTHENBACH, Barbara (org.). **A Practical Guide to Microstructural Analysis of Cementitious Materials** . 1. ed. [*S. l.*]: CCR Press, 2016. v. 1, p. 75–106.

HE, Changling; OSBAECK, Bjarne; MAKOVICKY, Emil. Pozzolanic reactions of six principal clay minerals: Activation, reactivity assessments and technological effects. **Cement and Concrete Research**, [*s. l.*], v. 25, n. 8, p. 1691–1702, 1995.

IEA. **International Energy Agency, Iea. Technology Roadmap - Low-Carbon Transition in the Cement Industry**. [*S. l.: s. n.*], 2018. Disponível em: www.wbcsdcement.org. Acesso em: 10 jun. 2021.

ITO, Akihiko; WAGAI, Rota. Global distribution of clay-size minerals on land surface for biogeochemical and climatological studies. **Scientific Data**, [*s. l.*], v. 4, n. 1, p. 1–11, 2017. Disponível em: www.nature.com/sdata/. Acesso em: 10 jun. 2021.

JANSEN, D. *et al.* The early hydration of OPC investigated by in-situ XRD, heat flow calorimetry, pore water analysis and 1H NMR: Learning about adsorbed ions from a complete mass balance approach. **Cement and Concrete Research**, [*s. l.*], v. 109, p. 230–242, 2018.

JOHN, Vanderley M. *et al.* **Rethinking cement standards: Opportunities for a better future**. [*S. l.*]: Elsevier Ltd, 2019.

JUENGER, Maria C.G.; SNELLINGS, Ruben; BERNAL, Susan A. **Supplementary cementitious materials: New sources, characterization, and performance insights**. [*S. l.*]: Elsevier Ltd, 2019.

KURDOWSKI, Wieslaw. **Cement and Concrete Chemistry**. 1. ed. Dordrecht: Springer Netherlands, 2014. v. 1

LEI, L; PLANK, J. A study on the impact of different clay minerals on the dispersing force of conventional and modified vinyl ether based polycarboxylate superplasticizers. [*s. l.*], 2014. Disponível em: http://dx.doi.org/10.1016/j.cemconres.2014.02.009. Acesso em: 12 ago. 2022.

LOTHENBACH, B.; DURDZI´NSKI, P. T.; DE WEERDT, K. Thermogravimetric analysis. *In*: SCRIVENER, K.; SNELLINGS, R.; LOTHENBACH, B. (org.). **A Practical Guide to Microstructural Analysis of Cementitious Materials**. [*S. l.*]: CCR Press, 2016. v. 1st ed., p. 177–212.

LU, Z. C. *et al.* Characterization data of reference cement CEM III/A 42.5N used for priority program DFG SPP 2005 “Opus Fluidum Futurum – Rheology of reactive, multiscale, multiphase construction materials”. **Data in Brief**, [*s. l.*], v. 30, p. 105524, 2020.

MA, Yihan *et al.* **Research progress on polycarboxylate based superplasticizers with tolerance to clays - A review**. [*S. l.*]: Elsevier Ltd, 2020.

MAIER, Matthias *et al.* Hydration of cubic tricalcium aluminate in the presence of calcined clays. **Journal of the American Ceramic Society**, [*s. l.*], v. 104, n. 7, p. 3619–3631, 2021.

MAIER, Matthias *et al.* Particle characteristics of calcined clays and limestone and their impact on early hydration and sulfate demand of blended cement. **Cement and Concrete Research**, [*s. l.*], v. 154, p. 106736, 2022. Disponível em: https://linkinghub.elsevier.com/retrieve/pii/S0008884622000278.

MALACARNE, C. *et al.* Influence of low-grade materials as clinker substitute on the

rheological behavior, hydration and mechanical performance of ternary cements. **Case Studies in Construction Materials**, [*s. l.*], v. 15, p. e00776, 2021.

MANDALIA, Tushar; BERGAYA, Faïza. Organo clay mineral–melted polyolefin nanocomposites Effect of surfactant/CEC ratio. **Journal of Physics and Chemistry of Solids**, [*s. l.*], v. 67, n. 4, p. 836–845, 2006.

MOHAMMED, Siline; SAFIULLAH, Omary. Optimization of the SO3 content of an Algerian Portland cement: Study on the effect of various amounts of gypsum on cement properties. **Construction and Building Materials**, [*s. l.*], v. 165, p. 362–370, 2018. Disponível em: https://doi.org/10.1016/j.conbuildmat.2017.12.218. Acesso em: 30 jul. 2021.

MURRAY, Haydn H. Chapter 6 Bentonite Applications. *In*: DEVELOPMENTS IN CLAY SCIENCE. [*S. l.: s. n.*], 2006. v. 2, p. 111–130.

MYERS, Rupert J *et al.* Role of Adsorption Phenomena in Cubic Tricalcium Aluminate Dissolution. [*s. l.*], 2016. Disponível em: https://pubs.acs.org/sharingguidelines. Acesso em: 15 out. 2021.

NIEMUTH, Mark D.; BARCELO, Laurent; WEISS, Jason. Effect of Fly Ash on Optimum Sulfate Levels Measured Using Heat and Strength at Early Ages. **Advances in Civil Engineering Materials**, [*s. l.*], v. 1, n. 1, p. 1–18, 2012. Disponível em: http://www.astm.org/DIGITAL_LIBRARY/JOURNALS/ACEM/PAGES/ACEM20120012.htm. Acesso em: 12 ago. 2021.

PY, Lucas Goldenberg. **Balanceamento de sulfatos e hidratação de cimentos ternários à base de calcários e argilas calcinadas**. 2021. - Universidade Federal do Rio Grande do Sul, Porto Alegre, 2021.

QUENNOZ, Alexandra; SCRIVENER, Karen L. Interactions between alite and C3A-gypsum hydrations in model cements. **Cement and Concrete Research**, [*s. l.*], v. 44, p. 46–54, 2013.

SCHERB, Sebastian *et al.* Reaction kinetics during early hydration of calcined phyllosilicates in clinker-free model systems. **Cement and Concrete Research**, [*s. l.*], v. 143, p. 106382, 2021.

SCHERB, Sebastian *et al.* Reactivity of metakaolin in alkaline environment: Correlation of results from dissolution experiments with XRD quantifications. **Materials**, [*s. l.*], v. 13, n. 10, 2020.

SCHMID, Marlene; PLANK, Johann. Interaction of individual meta clays with polycarboxylate (PCE) superplasticizers in cement investigated via dispersion, zeta potential and sorption measurements. **Applied Clay Science**, [*s. l.*], v. 207, p. 106092, 2021.

SCHÖLER, Axel *et al.* Hydration of quaternary Portland cement blends containing blast-furnace slag, siliceous fly ash and limestone powder. **Cement and Concrete Composites**, [*s. l.*], v. 55, p. 374–382, 2015.

SCRIVENER *et al.* Impacting factors and properties of limestone calcined clay cements (LC 3) . **Green Materials**, [*s. l.*], v. 7, n. 1, p. 3–14, 2019.

SCRIVENER, K. *et al.* Advances in understanding cement hydration mechanisms. **Cement and Concrete Research**, [*s. l.*], v. 124, p. 105823, 2019.

SHI, Zhenguo *et al.* Sulfate resistance of calcined clay-Limestone-Portland cements.

Cement and Concrete Research, [*s. l.*], v. 116, p. 238–251, 2019. Disponível em: https://doi.org/10.1016/j.cemconres.2018.11.003.

SKIBSTED, Jørgen; SNELLINGS, Ruben. **Reactivity of supplementary cementitious materials (SCMs) in cement blends**. [*S. l.*]: Elsevier Ltd, 2019.

SUN, Huaqiang *et al.* Optimization of gypsum and slag contents in blended cement containing slag. **Cement and Concrete Composites**, [*s. l.*], v. 112, 2020.

TANG, Fulvio J.; GARTNER, Ellis M. Influence of sulphate source on Portland cement hydration. **Advances in Cement Research**, [*s. l.*], v. 1, n. 2, p. 67–74, 1988.

TAYLOR-LANGE, Sarah C. *et al.* Calcined kaolinite-bentonite clay blends as supplementary cementitious materials. **Applied Clay Science**, [*s. l.*], v. 108, p. 84–93, 2015.

WADSÖ, L. *et al.* Calorimetry. *In*: SCRIEVENER, Karen; SNELLINGS, Ruben; LOTHENBACH, Barbara (org.). **A Practical Guide to Microstructural Analysis of Cementitious Materials**. 1. ed. [*S. l.*]: CCR Press, 2016. v. 1, p. 37–74.

WEI, Jianqiang; GENCTURK, Bora. Hydration of ternary Portland cement blends containing metakaolin and sodium bentonite. **Cement and Concrete Research**, [*s. l.*], v. 123, 2019.

YOKOYAMA, Shingo; KURODA, Masato; SATO, Tsutomu. Atomic force microscopy study of montmorillonite dissolution under highly alkaline conditions. **Clays and Clay Minerals 2005 53:2**, [*s. l.*], v. 53, n. 2, p. 147–154, 2005. Disponível em: https://link.springer.com/article/10.1346/CCMN.2005.0530204. Acesso em: 3 ago. 2021.

ZUNINO, Franco; SCRIVENER, Karen. Insights on the role of alumina content and the filler effect on the sulfate requirement of PC and blended cements. **Cement and Concrete Research**, [*s. l.*], v. 160, p. 106929, 2022. Disponível em: https://linkinghub.elsevier.com/retrieve/pii/S0008884622002216.

ZUNINO, Franco; SCRIVENER, Karen. Microstructural developments of limestone calcined clay cement (LC3) pastes after long-term (3 years) hydration. **Cement and Concrete Research**, [*s. l.*], v. 153, p. 106693, 2022.

ZUNINO, Franco; SCRIVENER, Karen. The influence of sulfate addition on hydration kinetics and C-S-H morphology of C3S and C3S/C3A systems. **Cement and Concrete Research**, [*s. l.*], v. 160, p. 106930, 2022. Disponível em: https://linkinghub.elsevier.com/retrieve/pii/S0008884622002228.

ZUNINO, Franco; SCRIVENER, Karen. The influence of the filler effect on the sulfate requirement of blended cements. **Cement and Concrete Research**, [*s. l.*], v. 126, 2019. Disponível em: www.elsevier.com/locate/cemconres. Acesso em: 2 jul. 2021.

ZUNINO, Franco; SCRIVENER, Karen. The reaction between metakaolin and limestone and its effect in porosity refinement and mechanical properties. **Cement and Concrete Research**, [*s. l.*], v. 140, p. 106307, 2021a.

ZUNINO, Franco; SCRIVENER, Karen. The reaction between metakaolin and limestone and its effect in porosity refinement and mechanical properties. **Cement and Concrete Research**, [*s. l.*], v. 140, 2021b.

3 PART 2: Exploring sulfate optimization techniques in Limestone Calcined Clay Cements (LC^3): limitations and insights

3.1 Introduction

Sulfates play an important role during the hydration of Portland cement (PC) (ANDRADE NETO; DE LA TORRE; KIRCHHEIM, 2021). The adequate addition of calcium sulfate into cement ensures proper sulfated systems. The so-called optimum sulfate content is the sulfate content that ensures that the C_3S reaction occurs before sulfate depletion and the renewed C_3A reactions during the cement hydration (ZUNINO; SCRIVENER, 2019), providing the highest compressive strength, highest chemical shrinkage, lowest expansibility, and avoiding cracking at late ages (MOHAMMED; SAFIULLAH, 2018). On the other hand, inappropriate calcium sulfate additions can lead to under-sulfated or super-sulfated systems. Under-sulfated systems (with low levels of calcium sulfate) may not ensure the control of setting times and high initial compressive strengths due to the rapid and early ettringite formation without adequate C_3S hydration to form C-S-H [2]. While super-sulfated systems (with high sulfate contents) have a prolonged sulfate depletion and late return of C_3A reactions (QUENNOZ; SCRIVENER, 2013). Also, there is a higher susceptibility to delayed ettringite formation (DEF), which can damage concrete structures due to expansive effects [3]. Therefore, sulfate optimization is essential to balance the early and later reactions occurring during hydration of PC.

Currently, the design of calcium sulfate to PC is done regarding total SO_3 content. The Brazilian standard for PC requirements (ABNT, 2018) and European standard (EN 197-1, 2018) limit the SO_3 content to 4.5% and 3.5% - 4.0%, respectively, as a precaution against possible expansive effects. Meanwhile, the American standard does not limit the SO_3 content if it is proven that the levels used in the cement formulation present a short expansibility (~0.03mm) at 14 days (ASTM, 2018). Most of these standards suggest determining the optimum SO_3 content using common procedures/techniques such as mechanical strength, calorimetry, setting time, (chemical) shrinkage, and probability of DEF measurements (ANDRADE NETO; DE LA TORRE; KIRCHHEIM, 2021). Mechanical strength, calorimetry, and setting time measurements offer rapid assessment of the optimum SO_3 content (e.g., 1-3 days, and has been typical in the performance criteria of common cement producers.

Determination of the optimum sulfate content, here call as $SO_{3optimum}$, is a difficult task because it is affected by several factors, such as physicochemical and mineralogical properties of clinker, sulfate source, chemical admixtures, supplementary cementitious materials (SCMs), among others (ANDRADE NETO; DE LA TORRE; KIRCHHEIM, 2021). The reduction of clinker ratio using SCMs has been one of the most successful strategies to reduce CO_2 emissions associated with cement production chain (IEA, 2018). However, when blended with Portland cement, the SCMs in most common use - such as slag, fly ash, and calcined clay - cause an accelerated sulfate depletion compared to PC without addition of SCMs (DE LA VARGA *et al.*, 2018; NIEMUTH; BARCELO; WEISS, 2012; SUN *et al.*, 2020; ZUNINO; SCRIVENER, 2019). Blended Portland cements with limestone and calcined clays, e.g., LC^3, have presented the acceleration of sulfate depletion even higher due to the large amounts of SCMs in its composition, approximately ~45 wt.% in LC^3-50. Thus, an extra addition of gypsum ($CaSO_4.2H_2O$) is required to balance the initial reactions.

In Portland cement systems, the heat flow peaks observed by isothermal calorimetry can be divided into 4 or 3 periods according to the author's discussion (Figure 1). Period I defines the start of reactions; Period II is the induction period; III is the acceleration period (heat flow peak of silicates) and IV decelerating period (heat flow peaks of aluminates and/or AFm are observed) (BULLARD *et al.*, 2011; WADSÖ *et al.*, 2016). The approach in 3 distinct periods differs from the previous one by grouping periods I and II together as published by (SCRIVENER, K. *et al.*, 2019). During the decelerating period, a heat flow aluminate peak is observed. The most pronounced distinctions between the early-age hydration of OPC and LC^3 are observed in the deceleration period (IV). After the silicate peak, a deceleration occurs until all the sulfate is consumed, leading to what is also called "sulfate depletion"(SD) (ANDRADE NETO; DE LA TORRE; KIRCHHEIM, 2021).

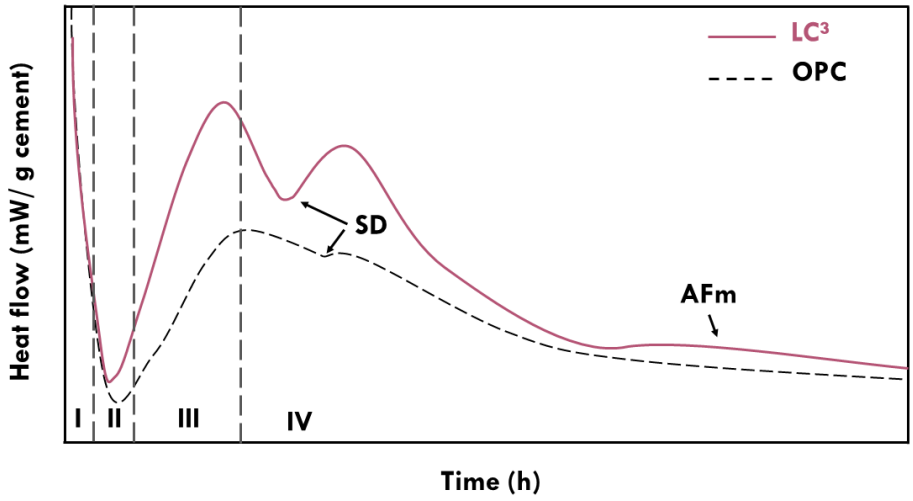

Fig.1 Typical heat flow curves of OPC and LC³ with IV phases (proper sulfated systems): I (initial reactions), II (induction period), III(acceleration period) and IV (deaccelerating period). SD: sulfate depletion. AFm: Formation of AFm phases (Hc+Mc).

The sulfate balance adjustment in blended cements such as LC³ is usually based on the optimum gypsum content when the aluminate peak occurs after silicate peak (AVET; BOEHM-COURJAULT; SCRIVENER, 2019; AVET; SCRIVENER, 2018, 2020). Such determination is made by adding extra gypsum besides that already used during the clinker grinding. Avet and Scrivener (2020) adjusted the sulfate balance with 2% extra gypsum at 10 ºC and 20 ºC, and 3.5% at 40 ºC and 60 ºC of analysis. The total SO_3 contents were 2.6% and 3.3%, respectively. Some authors defined the extra gypsum of 2% as the optimum sulfate content (AVET; SCRIVENER, 2018).

However, the approach of determining proper sulfate content by using isothermal calorimetry has some disadvantages. First, the replacement of Portland cement (clinker + gypsum) by SCMs decreases the total amount of gypsum but does not affect its proportion regarding clinker, as discussed by (ANDRADE NETO; DE LA TORRE; KIRCHHEIM, 2021). Second, by physical and chemical effects, SCMs will increase the sulfate demand. Andrade Neto et al. (ANDRADE NETO; DE LA TORRE; KIRCHHEIM, 2021) noted that such demand will be higher when normalized by gram of clinker over total cement mass, thus, the first normalization to observed the effects of the SCMs on the sulfate demand is more appropriate. Third, high additions of gypsum lead to longer-time intervals between silicate and aluminate heat flow peaks, delaying the early reactions. Also, sulfate balance solely based on heat flow released is an empirical approach.

Other methods also attempt to determine the optimum sulfate content in cement. For instance, the C563-18 standard (NIEMUTH; BARCELO; WEISS, 2012) describes the determination of approximate $SO_{3optimum}$ as maximum performance at different levels of cement substitution by means of isothermal calorimetry or compressive strength tests. The first is based on total heat released at different days (such as 3, 7, 28 days) in cements containing different levels of SO_{3total}. Usually, the heat released is a good indication of the reactivity of SCM in cement pastes (WADSÖ *et al.*, 2016). However, this systematic correlation is not always found in subsulfated LC³ systems (PY, 2021), as the overlap between heat peaks can impact the heat flow released at 72h and the compressive strength. In addition to isothermal calorimetry and compressive strength tests, sulfate optimization based on thermal analysis can be a useful strategy for optimum sulfate determination. According to John et al. (JOHN *et al.*, 2019) the bound/combined water fraction (*cwf*) has a high correlation (R^2=0.98) with compressive strength results. This allows pastes produced from cements comprising different levels of SO_{3total} to be tested in samples cured for different ages. Finally, chemical shrinkage can also contribute to the optimum SO_3 determination, as the cement reactivity is indicated by the volume reduction of the paste. Such tests can be performed in pastes produced from cements comprising different SO_3 levels to determine which one has the highest chemical shrinkage at a specific age, indicating its reactivity.

Most of the research seeking to understand the sulfate balance of LC^3s is based on calcined kaolinite clay (typically called metakaolin), while no attention has been given to clays with different mineralogy, such as montmorillonite clays. As far as we know, a Danish company is the first to develop cements mixed with clay and calcined bentonite (clay-rich in montmorillonite) for large scale applications (CEMENTIR HOLDING, 2020). This shows that concerns over transport distance and shortages of kaolin reserves, as in Denmark, can stimulate the increasing production of these novel cements. Therefore, it is vital to investigate the use of different calcined clays and their effect on the sulfate optimization of blended cements, to further enhance the performance of these cements, and expedite their widespread implementation in industry.

This research aimed to determine the optimum sulfate content, in terms of total SO_3, in LC³ with kaolinite and montmorillonite calcined clays using the main existing techniques. This work provides new insight into approaches for sulfate optimization in LC^3, information critical to achieving widespread implementation of these low-carbon cements.

3.2 Experimental program

3.2.1 Raw materials characterization

Two clays were evaluated in this study: a natural clay (high purity kaolinite clay) and commercial sodium bentonite (Na-montmorillonite main clay mineral), obtained from Pantano Grande, southern Brazil, and Buschle & Lepper S.A., respectively. Sodium bentonite's technical specifications provided by the sale company are shown in Supplementary Material (SM), Table S1. Mineral gypsum ($CaSO_4.2H_2O$) (GYP) as calcium sulfate, Portland clinker (PC) and limestone (LS) were provided by the cement industry. In addition, a commercial quartz powder (QP) was used as inert material.

Both clays were kept in an oven at 100 ºC to eliminate free water. The dried materials were sieved through a 2.4-mm opening sieve to ensure a consistent particle size distribution (PSD) and homogenous calcination. The calcination was carried out in a static oven at 800 °C for 1 hour (heating rate 10 °C/min), followed by a thermal shock which consisted of the abrupt opening of the furnace to bring the sample to room temperature. This calcination temperature was based on the TGA results to achieve the highest dehydroxylation of main clay minerals (kaolinite and montmorillonite). 100g of calcined montmorillonite clay (CM) was ground in a disc grinding mill for 50min (see grinding tests in SM, Table S.2) to reach a PSD smaller than 40 µm and closer to that of clinker, while for the calcined kaolinite clay (CK) no grinding was needed to reach this PSD. R³ test was used to predict the pozzolanic activity of the calcined clays. Such test simulates the hydration environment of blended cements from the heat flow released by simplified systems (AVET *et al.*, 2016). The R³ reactivity test results are shown in Fig.2.

The materials' PSD was measured by laser granulometry in triplicate with 60 seconds of ultrasound/each repetition and dispersion in isopropanol or water. All the specific surface area were measure using BET method (SSA_{BET}), heating rate 20 °C/min with gas nitrogen atmosphere. The chemical composition was assessed by X-Ray fluorescence (XRF) in Sequential X-ray fluorescence spectrometer between 400 and 4000 cm-1 wavelengths. All characterization is presented in Table 1.

Thermogravimetry analysis was done by 20 ºC/min heating rate configuration from 40 ºC to 1000 ºC and constant nitrogen flow of 20 mL/min. X ray diffraction was done by Bragg-

Brentano geometry, with CuKα source operated at 30 kV and 30 mA. Samples were scanned from 5 to 70° 2θ, with a step of 0.0167° 2θ, 2s per step. TGA/DTG and XRD of the materials are presented in Fig. S1 and Fig. S2, respectively (see SM).

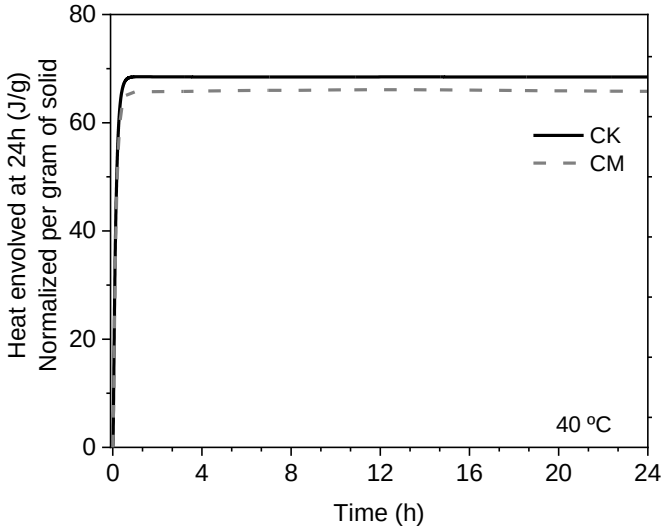

Fig. 2 Reactivity of calcined clays by R³ test

Table 1 Materials characterization

Characterization	**Portland clinker (PC)**	**Quartz powder (QP)**	**Calcined kaolinite clay (CK)**	**Calcined montmo-rillonite clay (CM)**	**Limestone (LS)**	**Gypsum (GYP)**
D_{v90} (μm)	27.79	13.01	37.85	39.83	37.18	34.83
D_{v50} (μm)	9.01	4.66	14.87	15.80	10.24	8.97
D_{v10} (μm)	1.61	0.89	2.86	2.63	1.44	1.85
Dvmean	12.67	6.19	18.73	19.58	15.91	14.73
Span ($\frac{D_{v90}-D_{v10}}{D_{v50}}$)	2.90	2.60	2.36	2.35	3.49	3.67
SSA_{BET} (m^2/g)	2.51	2.71	12.00	15.35	1.02	5.11
Oxide compositions (wt.%) as determined by X-ray fluorescence analysis						
SiO_2	19.97	96.98	45.70	61.93	0.23	0.72
Al_2O_3	3.96	2.22	38.20	19.73	0.08	0.21
Fe_2O_3	3.11	-	0.65	5.02	0.05	0.11
CaO	60.43	-	0.31	1.30	55.06	33.27
MgO	7.64	-	-	3.01	0.44	0.59
SO_3	1.21	0.34	-	1.28	0.07	43.48

K_2O	1.39	0.10	0.39	0.45	0.01	0.05
P_2O_5	0.08	-	-	0.09	0.09	-
MnO	0.15	-	-	0.02	0.01	0.03
ZnO	-	0.09	-	-	-	-
SrO	0.04	-	-	0.02	0.23	0.18
Na_2O	0.20	-	-	2.92	0.05	-
TiO_2	0.20	0.06	0.13	0.51	-	0.01
ZrO_2	-	-	-	-	-	-
LOI	1.37	14.62	10.54	3.53	43.61	21.62
Others	0.2	-	4.08	0.02	0.01	-
%Total	99.8	100	95.92	99.8	99.9	100

3.2.2 Mix proportions

The blended cements were prepared based on the mix proportions that Antoni et al. (2012) suggested for Limestone-Calcined Clay Cements (LC³): 50 wt.% clinker, 30 wt.% calcined clay, 15 wt.% limestone and 5 wt.% gypsum. The contents of calcined clay (or quartz powder in the reference system) and limestone were kept constants for all cements. Clinker and gypsum proportions were adjusted based on 5 levels of SO_{3total} (2.0 wt.%, 2.5 wt.%, 3.0 wt.%, 3.5 wt.%, 4 wt.%) under 4.5 wt.% SO_{3total} according to the chemical requirements of portland cement (ABNT, 2018). The SO_{3total} was calculated by Equation 1 (ASTM, 2018). Where $M_{calcium\ sulfate}$ = the mass of calcium sulfate (gypsum); M_{cement} = the mass of cement; $SO_{3\text{-}calcium\ sulfate}$ = the mass percentage of SO_3 in the calcium sulfate; and $SO_{3\text{-}cement}$ = the mass percentage of SO_3 in the cement. SO_3 values of each material were obtained from the XRF results.

$$SO_{3total} = \frac{M_{calcium\ sulfate}}{M_{calcium\ sulfate} + M_{cement}} x\ SO_{3-calcium\ sulfate} + \frac{M_{cement}}{M_{calcium\ sulfate} + M_{cement}} x\ SO_{3-cement} \quad (1)$$

The mixes were evaluated with 5 levels of $SO_{3,total}$ for the cements LC³-QP, LC³-CK and LC³-CM (totaling fifteen mixes) at water:cement (w:c) ratio of 0.5. The proportion of calcined clay (or quartz powder):limestone was the same for the 3 cements (2:1) investigated. The amount of clinker and gypsum was calculated based on $SO_{3,total}$ (Equation 1). The nomenclature used for identifying the cement samples throughout this study is as follow:

cement type-clay/quartz powder_SO_{3total} (e.g., LC³-CK_2.5%$\bar{S}$). Table 2 presents the mix proportions used to prepare the cement samples in this study.

Table 2 Mix proportions used to prepare the cement samples in this study

Cement	PC	GYP	LS	QP	CK	CM	$SO_{3\ total}$
LC³-QP_2.0%$\bar{S}$	52.11	2.89	15.00	30.00	-	-	2
LC³-QP_2.5%$\bar{S}$	50.93	4.07	15.00	30.00	-	-	2.5
LC³-QP_3.0%$\bar{S}$	49.74	5.26	15.00	30.00	-	-	3
LC³-QP_3.5%$\bar{S}$	48.56	6.44	15.00	30.00	-	-	3.5
LC³-QP_4.5%$\bar{S}$	47.38	7.62	15.00	30.00	-	-	4
LC³-CK_2.0%$\bar{S}$	51.87	3.13	15.00	-	30.00	-	2
LC³-CK_2.5%$\bar{S}$	50.68	4.32	15.00	-	30.00	-	2.5
LC³-CK_3.0%$\bar{S}$	49.50	5.50	15.00	-	30.00	-	3
LC³-CK_3.5%$\bar{S}$	48.32	6.68	15.00	-	30.00	-	3.5
LC³-CK_4.0%$\bar{S}$	47.14	7.86	15.00	-	30.00	-	4
LC³-CM_2.0%$\bar{S}$	52.78	2.22	15.00	-	-	30.00	2
LC³-CM_2.5%$\bar{S}$	51.59	3.41	15.00	-	-	30.00	2.5
LC³-CM_3.0 %$\bar{S}$	50.41	4.59	15.00	-	-	30.00	3
LC³-CM_3.5%$\bar{S}$	49.23	5.77	15.00	-	-	30.00	3.5
LC³-CM_4.0%$\bar{S}$	48,04	6.96	15.00	-	-	30.00	4

PC: Portland clinker; GYP: Gypsum; LS: Limestone; QP: quartz powder; CK: calcined kaolinite clay; CM: calcined montmorillonite clay; w/c: water:cement ratio.

3.3 Test conducted

3.3.1 Isothermal calorimetry

The test was performed on a TA instruments TAM Air calorimeter. 100 grams of dry material was placed in a stainless-steel container and mixed with deionized water at 0.5 w/c (wt.%). The pastes were manually mixed with a threaded rod for 30 seconds, after 20 seconds of resting, the paste was mechanically mixed for 70 seconds in a 10,000-rpm mixer. About 5 grams of paste was added to the equipment for monitoring hydration for 72 hours. Deionized water was used as a reference sample. Key points such as alite heat flow peak, onset of aluminate peak/sulfate depletion point (SD), maximum aluminate peak were determined by heat flow derivate as shown in Fig.3. The heat flow area of the aluminate peak was determined by the integral of the aluminate peak analyzed. Thus, a supersulfated system (ex.: >6% $\overline{S}$) or interpolation between the SD and peak initiation of the carbo-aluminate phases in LC^3 systems is suggested.

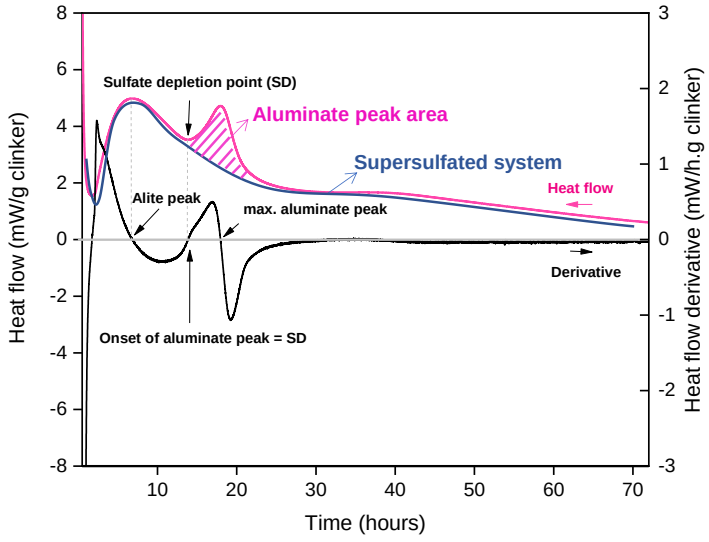

Fig.3 Representation of calorimetry curves and its derivative.

3.3.2 Thermogravimetry analysis: Bound water and portlandite content

TGA was performed in METTLER TOLEDO (TGA-2) equipment. The samples (~10 mg) were placed in alumina crucibles, pre-heated at 40 ºC for 10 minutes, then heated up to 1000 ºC at a heating rate of 20 ºC/min. The bound water ($BW_{measured}$) was determined by the weight loss (in percentage) from 40 to 550 ºC. The portlandite content ($Ca(OH)_{2,measured}$) was obtained according to Equation 2. These results were rescaled to 100 g of anhydrous cement, according to Equations 3-4 (LOTHENBACH; DURDZI´NSKI; DE WEERDT, 2016).

$$Ca(OH)_{2,measured} = WL_{Ca(OH)_2} \cdot \frac{m_{Ca(OH)_2}}{m_{H_2O}} \quad (2)$$

$$BW_{rescaled} = \frac{BW_{measured}}{m_{600\,°C}} \quad (3)$$

$$Ca(OH)_{2,rescaled} = \frac{Ca(OH)_{2,measured}}{m_{600\,°C}} \quad (4)$$

Where $WL_{Ca(OH)_2}$ is the weight loss due to the decomposition of portlandite determined by integrating the DTG peak located in the temperature range from ~400 and ~500 °C, using the tangential method [24] the $m_{Ca(OH)_2}$ is the molecular mass of portlandite (74 g/mol), m_{H_2O} is the molecular mass of water (18 g/mol), $m_{600\,°C}$ is the weight of the sample at 600 °C (in percentage).

Finally, the combined water fraction (*cwf*) was calculated using Equation 5 (JOHN *et al.*, 2019) . Where $Bw_{rescaled}$ is the bound water content rescaled to 100g of anhydrous cement and Tw is the total water content used in the mix.

$$cwf = \frac{BW_{rescaled}}{TW} \quad (5)$$

3.3.3 Compressive strength

After the mixing procedure described at 2.3.1 (isothermal calorimetry), all the SO_3 mix pastes were cast in cubic forms (1cm³) and cured at room temperature. Then, compressive strength test was conducted at 3, 7 and 28 days with a press model EMIC under constant load (0.2 N/s). The compressive strength results were the mean of 5 samples for each age (in MPa) plotted versus SO_3 levels. The approximate $SO_{3optimum}$ content was defined as the mix with the highest compressive strength at the age evaluated. Fig. 4 presents an example of the determination by the Visual fit method in mortar samples, illustrated by standard C563 (ASTM, 2018).

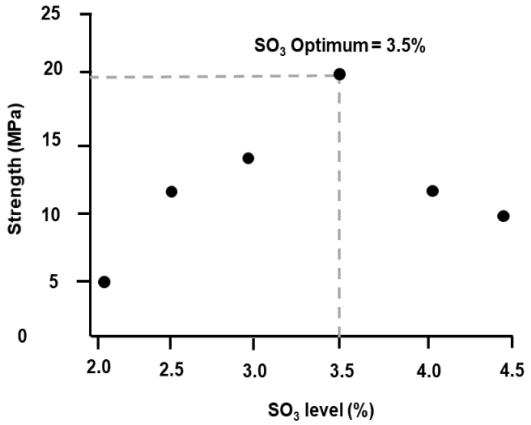

Fig. 4 Representation of the Visual fit method. Adapted from ASTM (ASTM, 2018)

The data were analyzed for normality using the Shapiro-Wilke test and homoscedasticity using the Levene test. Confirming data normality and homogeneity of variance, data were compared using one-way analysis of variance (ANOVA ONE-WAY) since there were more than two experimental conditions, complemented by Tukey's test when necessary for multiple data analysis. Differences were considered significant when P.value < 0.05 (P<0.05).

All figures are represented as mean and error bars represent ± standard deviation and F (F.D) are the freedom degrees. Furthermore, although the Shapiro-Wilk and Levene tests revealed that all data present normal distribution and homogeneity in variances, the data were represented as points (raw data) in the graphical representations because the number of repetitions is considered low for only the standard deviation to represent the behavior of the data distribution around the mean.

Distinguished lowercase letters indicate statistical difference when comparing the pastes for the same variable (one-way ANOVA; complemented by Tukey's test); for example, if in the column graph, there are the letters “a” in the first column, "b" in the second column and "a" the third column, it means that the variable in the first and third columns behave similarly, which in turn behave differently from the variable in the second column.

3.3.4 Chemical Srinkage using Dilametry

The chemical shrinkage was monitored by dilatometry following C1608 – 12 (ASTM, 2012). After mixing, the pastes were inserted into test containers at room temperature (23 ± 2 ºC).

Measurements started after the temperature equilibrium of the samples (~1h). The results were registered as the volume change in millimeters due to the cement pastes hydration. The chemical shrinkage per unit mass of cement at time t is expressed by equation 6, according to the C1608 standard (ASTM, 2012):

$$CS_{(t)} = \frac{h(t)-h(t_{ref})}{M_{cement}} \quad (6)$$

Where $CS_{(t)}$ is the chemical shrinkage at time t (millimeters/gram of cement), $h(t)$ is the water level in the graduated pipette at time t (millimeters) and $h(t_{ref})$ is the water level in the pipette at the reference time (t_{ref}). The M_{cement} is the cement mass of the sample which can be calculated by the equation 7:

$$M_{cement} = (M_{vial+paste} - M_{vial})/(1+w/c), \quad (7)$$

Where M_{cement} is the mass of cement in the vial (in grams), $M_{vial+paste}$ is the mass of the vial with paste (in grams), M_{vial} is the mass of the empty vial (in grams) and w/c is the water:cement ratio. The approximate $SO_{3optimum}$ was defined as the samples that presented the highest chemical shrinkage.

3.4 Results

3.4.1 Effects of the calcined clays on the heat flow of LC³ with different SO_3 levels

Figure 5 shows the calorimetry results of the cements with calcined clays and the reference material (quartz powder) for different levels of total SO_3, normalized per gram of clinker. The induction period for all cements, regardless of the SO_3 level, was approximately the same (~2h). Next, an accelerated and increasing reaction occurs, indicated by the large heat flow peak at approximately 10 hours after hydration, due to the dissolution of C_3S and precipitation of the first C-S-H, where part of the calcium sulfate ions will be adsorbed [1]. The intensity of this silicate heat flow peak exhibited no difference between all the cements examined, with average values of 4.80 mW/g of clinker to LC³-QP (4.75-4.83 mW/g of clinker), 4.79 mW/g of clinker to LC³-CK (4.65-4.88 mW/g of clinker) and 4.89 mW/g of clinker to LC³-CM (4.86-4.98 mW/g of clinker). Considering the variability of the isothermal calorimetry results can show, as observed by Lu et al. (LU *et al.*, 2020), these minor differences in the values obtained

here are negligible, and it can be concluded that there are no significant differences between the main heat flow peak in the cements assessed.

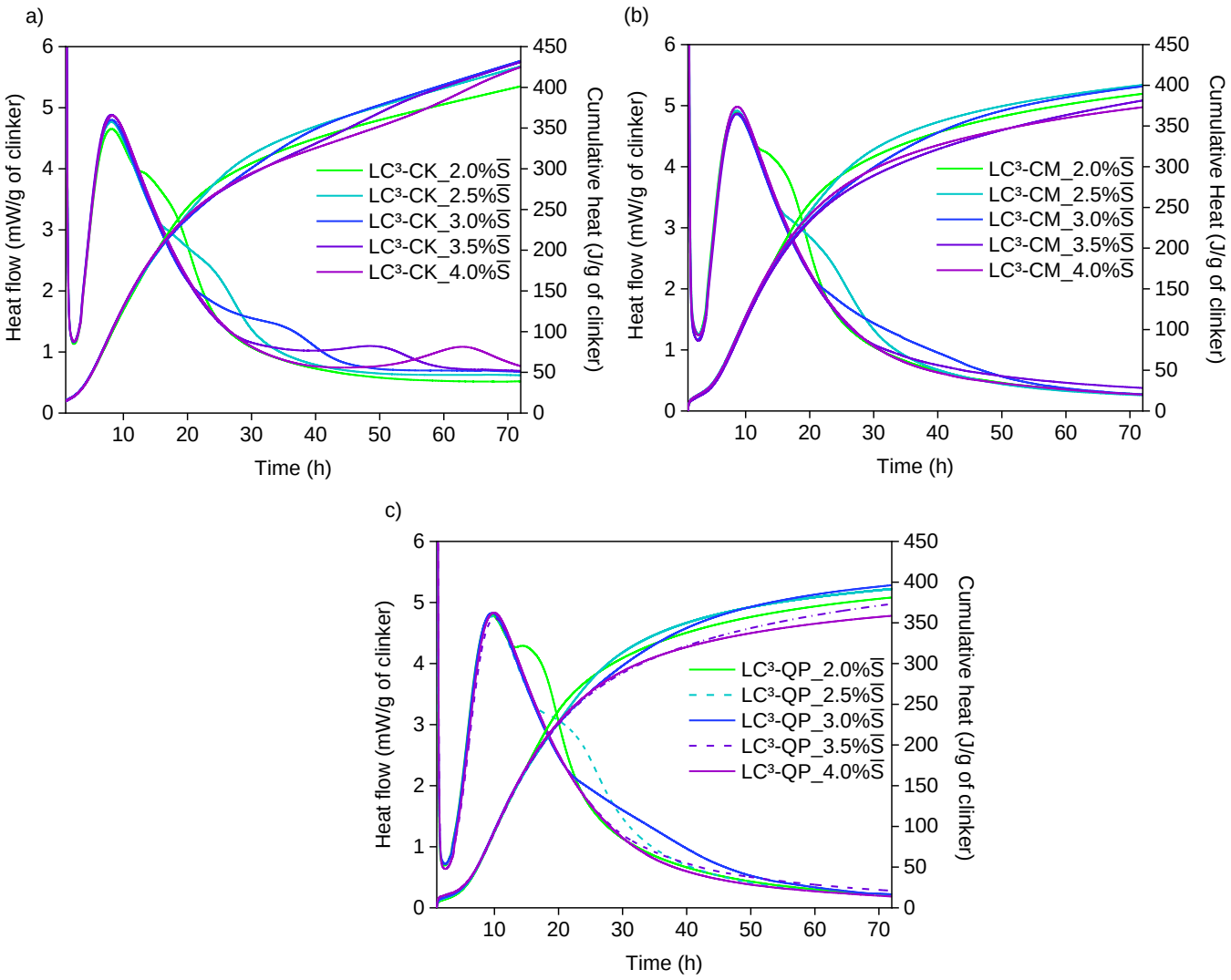

Fig. 5 Effects of the calcined clays on the heat flow of LC^3 mixes with different SO_3 levels

The main difference between all cements occurs in the second peak of the reactions (the aluminate heat flow peak). As expected, the interval between the silicate heat flow peak and the lower point representing sulfate depletion (SD, Fig.3) tended to be longer in cements containing greater gypsum content (i.e. SO_3). After sulfate depletion, the resumption of aluminate reactions occurred faster in LC³-CK mixes for all of the $SO_{3,total}$ levels investigated, likely due to both physical and chemical effects. The C_3S reaction in LC^3 blends is enhanced by the filler effect of the SCMs (calcined clays and limestone) (AVET; SCRIVENER, 2018). This leads to faster formation of C-S-H where calcium sulfate ions can be adsorbed. The chemical effect can be related to the higher availability of Al ions in kaolinite over

montmorillonite clays minerals, which enables more Al ions to participate in the second ettringite formation, which is marked by the second intensified heat peak.

The aluminate peak flows were more intense and visible in the LC³-CK cement. The area of the aluminate peak flow (see SM, table S.3) were 12.2-25.7 J/g of clinker, 15.1-28.4 J/g and 11.1 to 22.4 J/g of clinker to -CK, -CM, -QP cements, respectively. According to Zunino and Scrivener (ZUNINO; SCRIVENER, 2019), these calculated areas have a good linear fitting (R^2=0.97) with the formation of ettringite and AFm phases in hydrated pastes, which suggests the higher reactivity (in terms of products formed) of the (LC^3)-CK compared to -CM or -QP in this study. Note that the 2.0-2.5% SO_3 contents had a very similar behavior among all the cements, which suggests that, at lower SO_3 contents, the C_3A of the clinker is sufficient to lead to sulfate depletion, whereas at higher levels, sulfate depletion is not exclusively due to it.

3.4.2 Effects of calcined clays on TGA results of LC³ with different levels of SO_{3total} at 3, 7 and 28 days

Figure 6 shows the DTG curves of the LC^3 pastes with different SO_3 contents at 3, 7 and 28 days. One can note peaks related to the decomposition of ettringite (at ~ 110 °C), AFm phases (at ~ 150 °C), C-S-H (50 to 600 °C), portlandite (between 400 and 500 °C) and calcium carbonates (between 650 and 800 °C) (LOTHENBACH; DURDZI´NSKI; DE WEERDT, 2016).

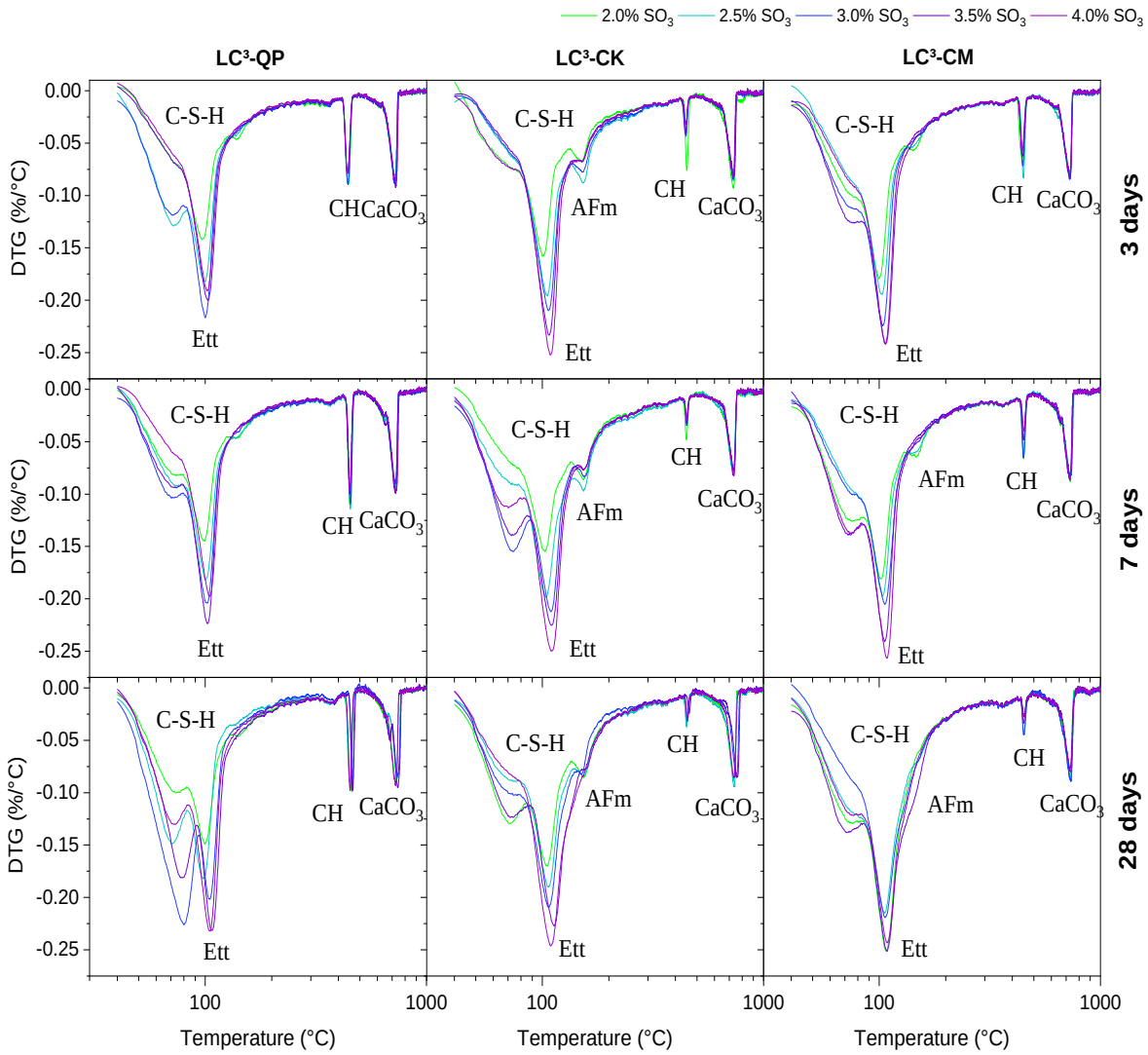

Fig. 6 DTG curves of the LC^3 pastes at 3, 7 and 28 days

By comparing the DTG data for each cement, differences can be observed in the ettringite and AFm peaks' intensity. The AFm peak is present in all LC^3-CK mixes at 3, 7 and 28 days, while it only appears from 7 days on for the LC^3-CM mixes at lower SO_3 content (2.0 and 2.5 %SO_3). Finally, the AFm peak is not clearly distinguished in the DTG curves of the LC^3-QP mixes. Regarding the sulfate content, a higher SO_3 content results in a higher peak intensity due to ettringite, and a lower intensity of the peak due to AFm. These results are directly related to the Al_2O_3/SO_3 ratio of the system. An increase in the Al_2O_3/SO_3 ratio should increase the AFm phases over the ettringite content. The alumina content was different despite the mixes having the same SO_3 content (2.0 – 4.0%). The LC^3-CK mixes are expected to have

higher alumina content in the solution in the first days due to the high reactivity of the metakaolinite clay to interact with limestone (and dolomite in gypsum), which explains the well-defined AFm DTG peaks at 3 days. In turn, as the montmorillonite clay has lower reactivity, the AFm peaks on the DTG curves of the LC^3-CM mixes only appeared from 7 days on and only for the lower sulfate content mixes. Finally, as the quartz powder does not have amorphous aluminum in its composition, its mixes presented lower amounts of AFm.

Figure 7(a-b) shows the mixes' bound water and portlandite contents, determined by TGA. Regarding the bound water, one can note that at 3 days, the LC^3-CK and LC^3-CM pastes presented slightly higher values than the LC^3-QP (considering the highest value in each group – 22.0% and 22.6% for the systems with CK and CM, respectively, and 19.8 for the systems with QP). At 7 days, the LC^3-CK pastes had higher bound water contents than the other cements (up to 26.9% *vs.* 19.1% and 23.7% for the systems with QP and CM). This result evidenced the higher reactivity of the CK clay. Finally, at 28 days, the LC^3-CK and LC^3-CM pastes presented similar values and were higher than the bound water content of the LC^3-QP pastes. This higher bound water content compared to the LC^3-QP can be explained by the pozzolanic reaction of the calcined clays.

For all ages tested, the LC^3-CK exhibited lower portlandite content in comparison with the reference cement, LC^3-QP, indicating that the CK clay already presented pozzolanic activity at early age (3 days). These results agree with previous studies showing early pozzolanic activity for metakaolin clays (MAIER *et al.*, 2022; The reaction between metakaolin and limestone and its effect in porosity refinement and mechanical propertiesZUNINO; SCRIVENER, 2021a). In turn, the LC^3-CM showed similar portlandite content to the LC^3-QP at 3 days, an intermediate content at 7 days, and a similar content to the LC^3-CK at 28days. This result showed that CM clay had pozzolanic activity, consuming the portlandite, but that was much slower when compared with CK clay, which agrees with the R^3 test (Figure 1).

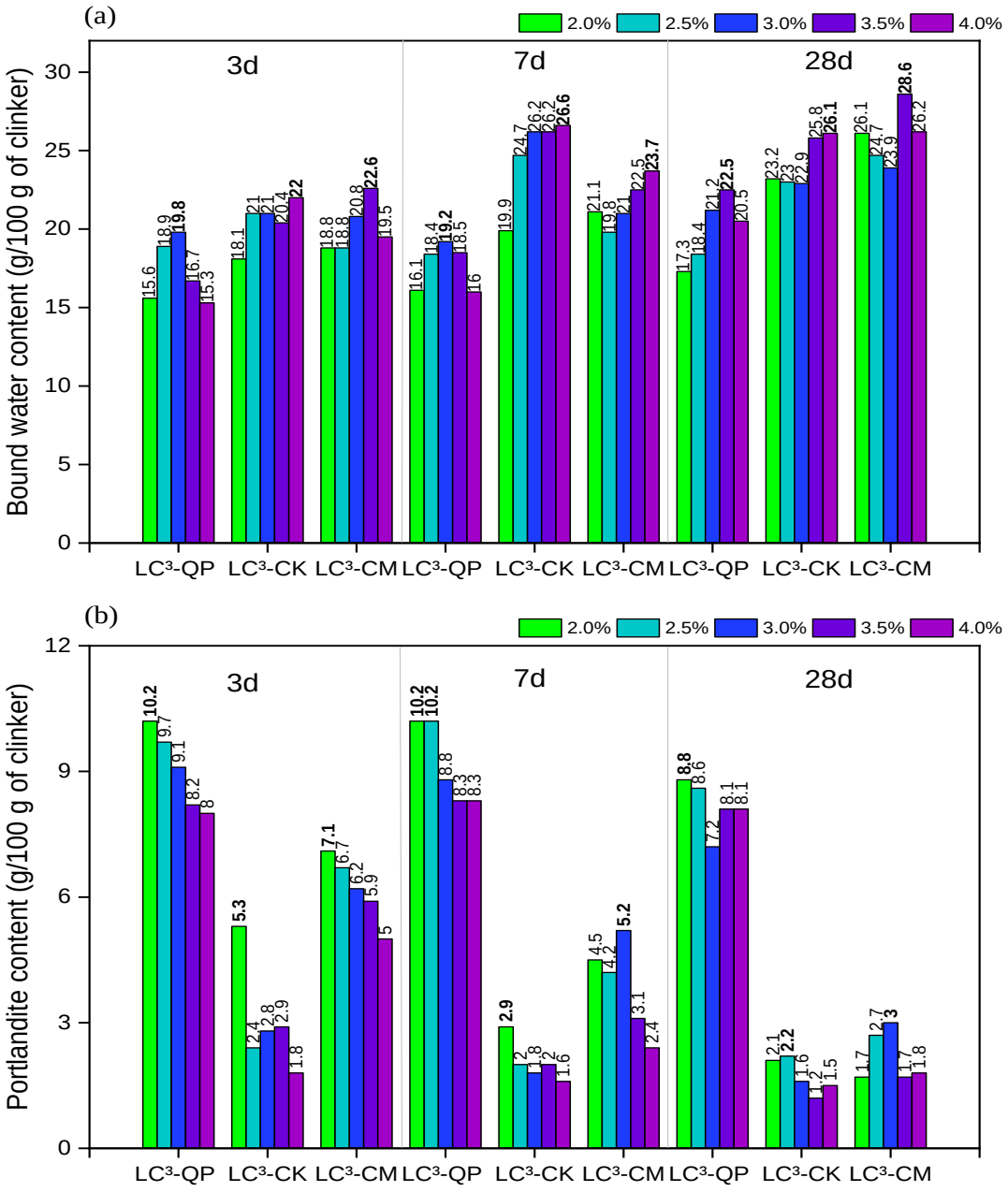

Fig. 7 Bound water content (a) and portlandite content (b) versus SO_3 level

In addition, by increasing the sulfate content in the mixes, the portlandite content was reduced. The same behavior was observed in several previous studies(Hydration of C3S and Al-doped C3S in the presence of gypsumANDRADE NETO *et al.*, 2022; HE; OSBAECK; MAKOVICKY, 1995). This occurs as the increase of sulfate increases ettringite precipitation (as observed in the DTG curves, Figure 6), which also consumes calcium ions.

3.4.3 Effects of calcined clays on compressive strength of LC³ with different levels of $SO_{3,total}$ at 3, 7 and 28 days

Figure 8 shows the compressive strength of cements pastes with different $SO_{3,\ total}$ levels at 3, 7 and 28 days. At 3 days, in most cases, there is no significant difference in the compressive strength between the SO_3 total levels for the same cement ($P<0.05$). For instance, 2.0-2.5% or 3.0%-4.0% levels for (LC^3)-QP behave similarly. The statistical comparison between cements for the same SO_3 content shows that most are similar at 3 days ($P<0.05$, See SM). This is likely due to the filler effect of SCMs equally driving the cement hydration at early ages (SKIBSTED; SNELLINGS, 2019) where the chemical influence of the SCMs was not observed.

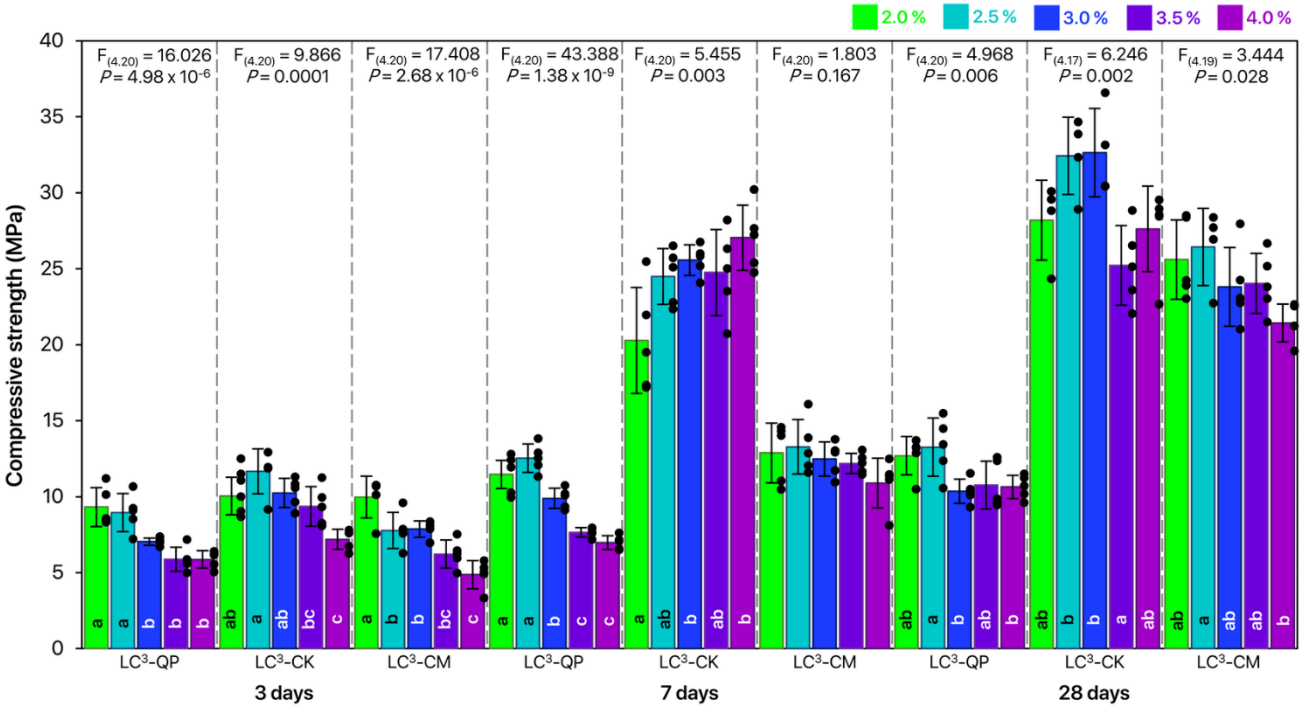

Fig. 7 Compressive strength versus SO_3 level

Only at 7 days was obtained a significant difference in the results when comparing (LC^3)-CK with -CM and -QP. LC_3-CK had the highest average results in all $SO_{3,\ total}$ levels (2.0-4.0% $SO_{3,\ total}$) due to the synergic effect of calcined kaolinite clays with limestone forming CO^3-AFm phases. This is one of the main characteristics of LC³ blends, as reported in previous studies (ANTONI *et al.*, 2012; MALACARNE *et al.*, 2021). Moreover, the greater availability and dissolution of Al ions into pore solution of (LC^3)-CK than in -CM may have intensified the formation of AFm phases, also justifying the greater strength gain. Also, it was not possible to observe the effect of the variation of the $SO_{3,\ total}$ on the compressive strength of

the LC^3-CM at 7 days (2.0-4.0% $SO_{3,\ total}$) since the results did not present significant differences between them (P>0.05).

Interestingly, the LC^3-CM compressive strength increased from 7 to 28 days achieving average results similar to LC^3-CK mixes. The results showed that this cement is still promising in terms of strength gains at later ages despite the lower reactivity of CM than a metakaolin (here called CK). Despite a limited amount of alumina to participate in the hydration reactions of the blended cements (such as ettringite, carboaluminate phases, C-(A)-S-H formation, etc.) cements with calcined montmorillonite clays may present an advantage over high purity kaolinite clays (in terms of high kaolinite content). According to Avet and Scrivener (AVET; SCRIVENER, 2018), clays with high kaolinite content (>80%), despite an intensified strength gain at early ages, have limited reaction progress. They concluded that it occurs due to the refinement of porosity to a critical point where hydration products have no more space to grow up. On the other hand, such porosity refinement does not seem to affect the compressive strength results of the CM cement negatively. The results also suggest that such clay reacts as the most common pozzolanic additions, such as fly ash, with greater strength gain at late ages (MALACARNE *et al.*, 2021). These factors justify the more expressive strength gain of LC^3-CM from 7 to 28 days. Further studies on the mechanical performance and porosity in larger LC^3 with calcined montmorillonite should be done.

3.4.4 Effects of calcined clays on chemical shrinkage results of LC^3 with different levels of SO_{3total} at 3, 7 and 28 days

The impact of the calcined clays on the cement chemical shrinkage with different levels of SO_{3total} was monitored for 28 days. The results are shown in Figure 8.

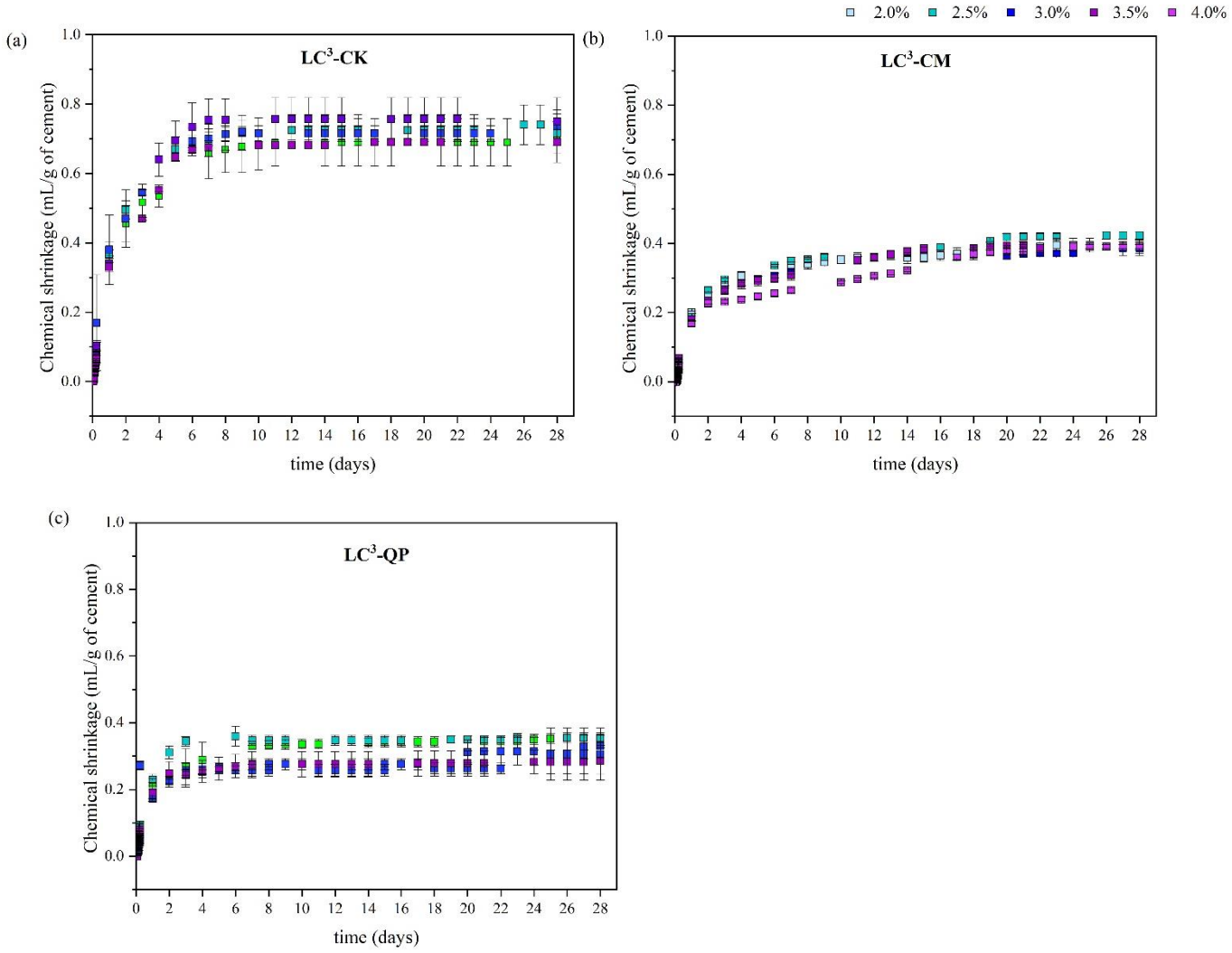

Fig. 8 Chemical shrinkage of the LC^3 mixes with different SO_3 levels

In general, LC³-CK showed the highest chemical shrinkage during the dilatometry test, followed by LC³-CM and LC³-QP. At 3 days, the mean values to gram of cement were from 0.47 mL to 0.52 mL to LC³-CK, from 0.23 mL to 0.29 mL to LC³-CM, and from 0.24 mL to 0.27 mL to LC³-QP. By 7-8 days, there was an accelerated reduction in the volume of the pastes, caused by the rapid hydration reactions that occur at early ages. After that, LC^3-CK trend towards stabilization of the volume change until 28 days. For instance, at 7 days, LC³-CK reached mean values per gram of cement from 0.66 mL to 0.75 mL, while at 28 days, from 0.68 mL to 0.75 mL, a quite similar chemical shrinkage. LC³-CM mixtures slightly increased from 0.26 mL-0.35 mL /g of cement at 7 days, to 0.38 mL-0.42 mL/g of cement at 28 days. At the same interval, LC³-QP increased from 0.25mL to 0.34 mL at 7 days and from 0.28mL to 0.35 mL/g of cement at 28 days.

As observed, both calcined clays increased chemical shrinkage despite their different mineralogy and reactivity compared to the inert addition, QP. According to Schöler et al. (SCHÖLER *et al.*, 2015) whom studied blended cement with fly ash, blast furnace slag, and limestone, all reactive and inert additions had an impact on the pastes' chemical shrinkage by physical and chemical effects. Although pozzolanic reactions did not exist in LC³-QP cement, Schöler et al. (SCHÖLER *et al.*, 2015) explained that the replacement of Portland cement by quartz powder results in dilution effects, which means higher effective water: cement ratio that increases the clinker degree reaction and compensates for the lower chemical shrinkage of cements with no reactive additions.

3.5 Discussion

Table 3 summarizes the $SO_{3optimum}$ determination results of each technique used on the cements.

Table 3 - Summary of $SO_{3optimum}$ by each technique

Technique	**Objective of the optimization**	**Mixes**	**$SO_{3optimum}$**
Isothermal calorimetry	i) The optimum sulfate content is that mix where the aluminate peak occurs after the silicate peak (no longer than 30h)	LC³-QP_ (2.0%, 2.5%, 3.0%, 3.5%,4.0)$\bar{S}$	2.0%-2.5%
		LC³-CK_ (2.0%, 2.5%, 3.0%, 3.5%,4.0)$\bar{S}$	2.0%-2.5%
		LC³-CM_ (2.0%, 2.5%, 3.0%, 3.5%,4.0)$\bar{S}$	2.0%-2.5%
	ii) The mix with the highest total heat between the SO_3 levels	LC³-QP_ (2.0%, 2.5%, 3.0%, 3.5%,4.0)$\bar{S}$	3.0%
		LC³-CK_ (2.0%, 2.5%, 3.0%, 3.5%,4.0)$\bar{S}$	3.0%
		LC³-CM_ (2.0%, 2.5%, 3.0%, 3.5%,4.0)$\bar{S}$	3.0%
Thermogravimetric Analysis	i)The mix with highest bound water at each age (normalized per gram of solids)	LC³-QP_ (2.0%, 2.5%, 3.0%, 3.5%,4.0)$\bar{S}$	3.0% (3 and 7 d), 3.5% (28 d)

		LC³-CK_ (2.0%, 2.5%, 3.0%, 3.5%,4.0%)$\bar{S}$	4% (3, 7 and 28 d)
		LC³-CM_ (2.0%, 2.5%, 3.0%, 3.5%,4.0%)$\bar{S}$	3.5% (3 d), 4.0% (7 d) and 3.5% (28 d)
Compressive strength	i) The mix with the highest compressive strength at each age (3, 7 and 28 days)	LC³-QP_ (2.0%, 2.5%, 3.0%, 3.5%,4.0%)$\bar{S}$	Inconclusive
		LC³-CK_ (2.0%, 2.5%, 3.0%, 3.5%,4.0%)$\bar{S}$	
		LC³-CM_ (2.0%, 2.5%, 3.0%, 3.5%,4.0%)$\bar{S}$	
Chemical Shrinkage by Dilatometry	i)The mix with highest chemical shrinkage over time between different SO_3 levels (3,7 and 28 days)	LC³-QP_ (2.0%, 2.5%, 3.0%, 3.5%,4.0%)$\bar{S}$	Inconclusive
		LC³-CK_ (2.0%, 2.5%, 3.0%, 3.5%,4.0%)$\bar{S}$	
		LC³-CM_ (2.0%, 2.5%, 3.0%, 3.5%,4.0%)$\bar{S}$	

3.6 $SO_{3\ optimum}$ by isothermal calorimetry

The $SO_{3optimum}$ was determined by isothermal calorimetry based on two of the most used approaches observed in the literature. The first approach defines the optimum sulfate content as the sulfate content for which the aluminate peak occurs after the silicate peak curves in the isothermal calorimetry data for that cement, which is an approach used by a group of authors (AVET *et al.*, 2016; AVET; BOEHM-COURJAULT; SCRIVENER, 2019; AVET; SCRIVENER, 2018, 2020). This was observed with an increase in the amount of gypsum, which leads to a smaller, broader, and delayed second heat flow peak in LC³ (ZUNINO; SCRIVENER, 2019). This approach would include all SO_3 levels observed within 72h in the LC³-CK and only the 2-3% SO_3 levels in LC³-QP and LC³-CM cements. Nevertheless, a critical point of view is needed when making the optimum sulfate content decision.

Several reasons suggest that this is not the most suitable approach for determining the optimum sulfate content in blended cements. First, the simple criterion based on an extra addition of gypsum to cement (further added during clinker grinding) can result in higher SO_3 contents in cement. According to Mohammed and Safiullah (MOHAMMED; SAFIULLAH, 2018), high levels of calcium sulfate can impair the durability of concrete structures for many reasons, such as greater susceptibility to to delayed ettringite formation (DEF). Therefore, some cement standards follow some criteria for SO_3 design. For instance, the Brazilian standard (ABNT, 2018) limits this total value to 4.5% SO_3 and the European standard (EN 197-1, 2018) limits to 3.5-4 % SO_3, while the American standard (ASTM, 2018) does not, requesting only that the mixtures present a limited expansion. The second reason is a slight reduction of the compressive strength due to the clinker substitution by gypsum to change the cement SO_3 levels (MOHAMMED; SAFIULLAH, 2018). The third reason is that high additions of gypsum into cement lead to longer intervals of SD, i.e., the time between the start of the reactions and the onset of the aluminates peak, which can affect the kinetics of reactions, due to the time for the proper reactions of C_3A with gypsum. It is important to think carefully how to define an upper bound for optimum sulfate content – the lower bound is easy to define using isothermal calorimetry, but the upper bound is more challenging. Based on this discussion, ~30 hours seem a reasonable upper bound, resulting in $aSO_{3optimum}$ of 2%-2.5% to all the cements, as shown in Table 3.

The second approach to determinate $SO_{3optimum}$ by means of isothermal calorimetry defines the mix of the highest total 72h cumulative heat (or just total heat) released between all the SO_3 levels assessed. This approach identifies the mixture that exhibits the highest reactivity. As shown in Fig. 9, the SO_3 level which presented the highest total heat was 3% for all the cements, indicating the $SO_{3\ optimum}$. Note that this determination based only on total heat released leads to a determination of the mixes with SD intervals very varied among cements. Therefore, using solely qualitative isothermal calorimetry is insufficient to determine the $SO_{3optimum.}$ Such an approach is very empirical and more tests should be performed to help define this parameter. Qualitative methods in isothermal calorimetry results can help assess the sulfate balance. For instance, using a stepwise regression model, Canbek et al. (CANBEK *et al.*, 2023) confirmed the predominant impact of metakaolin fraction and the effects of finer

limestone particle and w:c ratio on the sulfate balance. Further studies along these lines are promising and can help in the decision making of optimal sulfate content.

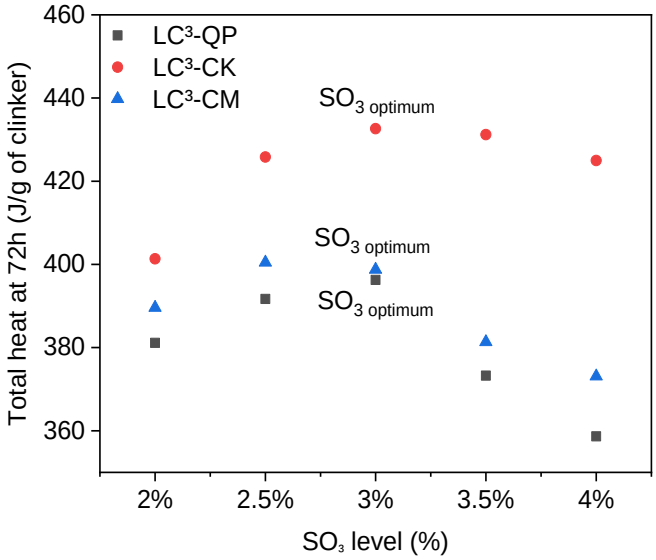

Fig. 9 Total heat at 72h versus SO_3 levels shows 3% as $SO_{3\ optimum}$ level

3.7 $SO_{3\ optimum}$ by TGA at 3, 7 and 28 days

TGA can also be used to determine the $SO_{3optimum}$. Here, the optimum sulfate content is defined as the one that results in the highest bound water content. Figure 10 presents the bound water content as a function of the SO_3 level. The $SO_{3optimum}$ of LC^3-QP was 3.0, 3.0 and 3.5 $\%SO_3$ at 3, 7, and 28 days, respectively. In turn, the $SO_{3optimum}$ of LC^3-CK is 4.0 $\%SO_3$ for all ages tested. Finally, the $SO_{3optimum}$ of LC^3-CM is 3.5, 4.0 and 3.5 $\%SO_3$ at 3, 7 and 28 days. One can note that these values were higher than the optimum sulfates contents determined by

calorimetry. However, the same trend was observed: the LC³-CK had the highest sulfate demand, and the LC³-QP the lowest.

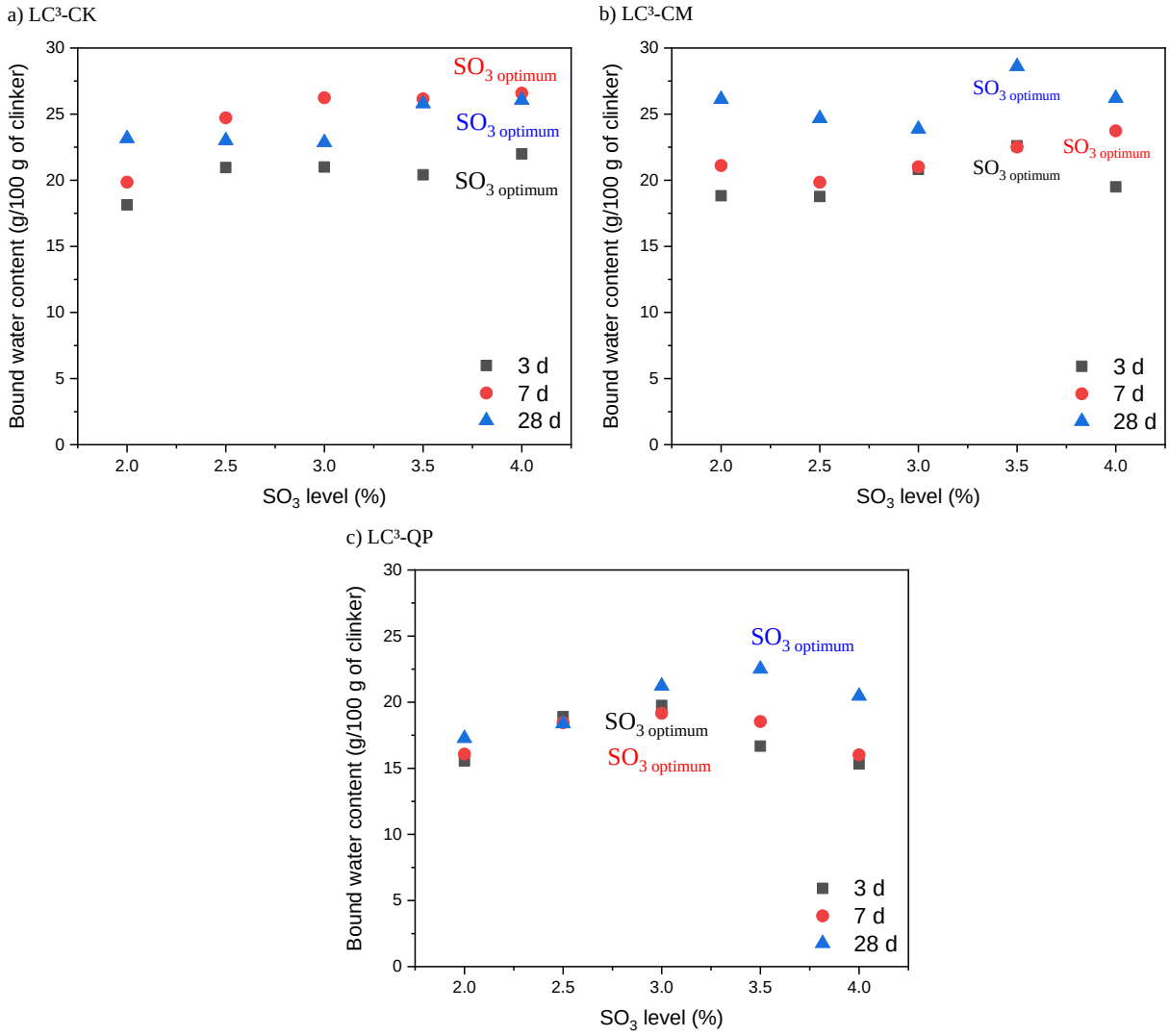

Fig. 10 Bound water content as a function of the SO_3 level with the indication of the $SO_{3\ optimim}$ for the (a) LC³-QP, (b) LC³-CK and (c) LC³-CM cements.

The bound water content is related to the cement's degree of hydration (DoH). For the same cement, the higher the bound water, the higher the DoH. Therefore, the SO_3 content that results in the higher bound water content (*i.e.*, the highest DoH) should be optimum. However, as the SO_3 content will greatly influence the phase assemblage (especially the amount of ettringite), an increase in the bound water does not necessarily mean an increase in the DoH of cement (especially the DoH of alite, that ultimately will control the mechanical performance of the cement).

3.8 $SO_{3\ optimum}$ by compressive strength at 3, 7 and 28 days

The approach of determining the optimum sulfate content in terms of the highest compressive strength was insufficient to provide a specific $SO_{3optimum}$ result. At 3 days, the values between ~2.0-3.0% $SO_{3,total}$ levels would be sufficient to provide properly sulfated systems without significantly decreasing the pastes compressive strength. Greater additions of gypsum into cement to reach higher $SO_{3,total}$ levels (3.5%-4.0%), may decrease the compressive strength, as it results in a slight reduction of the clinker content (See Table 2). Furthermore, comparing compressive strength with the heat flow curves from calorimetry (Fig 4) seems reasonable within 72h. The 2.0-3.0% SO_3 contents showed higher compressive strength and followed the criterion of the aluminate peak occurring after the silicate peak in the calorimetry data. By calculating some $SO_{3,\ total}$ of properly sulfated LC_3 systems in previous studies (DA SILVA *et al.*, 2021; MALACARNE *et al.*, 2021), it was also possible to find $SO_{3,total}$ around 2.82-3.03% for LC^3 mixes at 3 days, further corroborating the values obtained here.

At 7 days is still impossible to define a single $SO_{3optimum}$ level; across each of the cements investigated this would be between 2.0%-2.5% for LC^3-(QP), 2.5%-4.0% for -CK and all $SO_{3,\ total}$ levels for -CM. The increase of the $SO_{3optimum}$ in LC^3 mixes with metakaolin was previously observed by some authors (KURDOWSKI, 2014; PY, 2021). According to Kurdowski (KURDOWSKI, 2014), that is caused by the maximum volume of aluminates hydration phases at each age. On the other hand, Andrade Neto et al. (ANDRADE NETO; DE LA TORRE; KIRCHHEIM, 2021) declare that is not fully understood, and further studies are needed on this topic. According to these authors, the optimum sulfate content should decrease with age because although calcium sulfate accelerates the hydration of C_3S at early ages, which increases strength, over time, there would occur a reduction in density and formation of C-S-H.

Such phenomena that may explain the increased sulfate content required to promote properly sulfated LC^3 systems are mainly related to the formation of hydration products such as ettringite. In blended cements, such as LC^3, an intense and prolonged ettringite formation occurs, which can be related to two main factors. At early ages, there is an extra ettringite formation as result of the reaction of the alumina from metakaolin with the calcium from portlandite [29]. At later ages, it occurs during the transformation of the hemicarbonate (Hc) phase into monocarbonate (Mc). Zunino and Scrivener (Microstructural developments of

limestone calcined clay cement (LC3) pastes after long-term (3 years) hydrationZUNINO; SCRIVENER, 2022) observed in a study of LC³ pastes after long hydration periods (3 years) that sulfate ions were incorporated into the Hc structure. Over time, this phase transforms into Mc, promoting an additional sulfate availability. This sulfate can interact with the alumina dissolved by the calcined clays to form more ettringite, increasing the $SO_{3optimum}$.

The 28 days results suggest again a $SO_{3optimum}$ between 2.0%-2.5% for LC³-(QP), 2.0%-3% for -Ck and 2.0-3.5% for -CM. Although there was an increase of the paste's compressive strength over time, the $SO_{3optimum}$ remained the same as at 7 days. It would be expected an increase of the optimum sulfate content over time. Py (PY, 2021), for instance, observed that from 7 days to 28 days, the $SO_{3optimum}$ was about 4-4.5% in some ternary cements. However, this does not mean that $SO_{3optimum}$ for all cements assessed in this study will increase. Py (PY, 2021) using cements with higher fineness materials than those used in this study observed that fineness had an essential impact on the sulfate balance, as Zunino and Scrivener (ZUNINO; SCRIVENER, 2019) mentioned.

3.8.1 Compressive strength vs. Total heat

The approach of correlating the calorimetry results with compressive strength is a rapid and practical alternative for predicting cement compressive strength since the heat released is a good indication of the reactivity of SCM in cement pastes. However, this systematic relation was not found in LC³ systems of this study. When the total heat at 72h (excluding the heat of the wetting peak) was plotted versus the LC³ compressive strength results, there was no

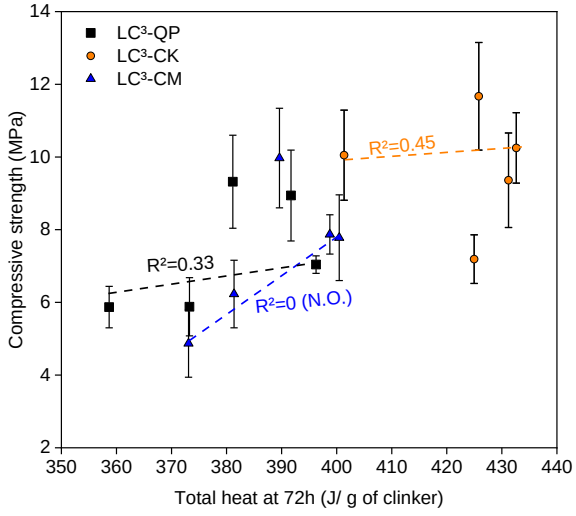

satisfactory linear fit, as depicted in Figure 11. R^2 values were 0.33, 0.45 and N/O (not observed) for LC³-QP, -CK and -CM cements, respectively.

Fig. 11 Total heat at 72h vs paste's compressive strength

In the case of LC³ cements, it is common to observe an intense and well-defined second peak, the so-called aluminate peak, of reaction. Such peak provides an "extra heat" to the total heat of LC³ mixtures, not observed in other types of cement, which is related to the formation of ettringite. That reliable comparison between calorimetry and compressive strength results might be possible in types of cement with high clinker content since the higher clinker content, the higher the total heat released from the silicate reactions. To validate such a hypothesis, Ordinary Portland cement (OPC) was made with different SO_3 levels and was tested by isothermal calorimetry and compressive strength test for 72 hours, as shown in Figure 12.

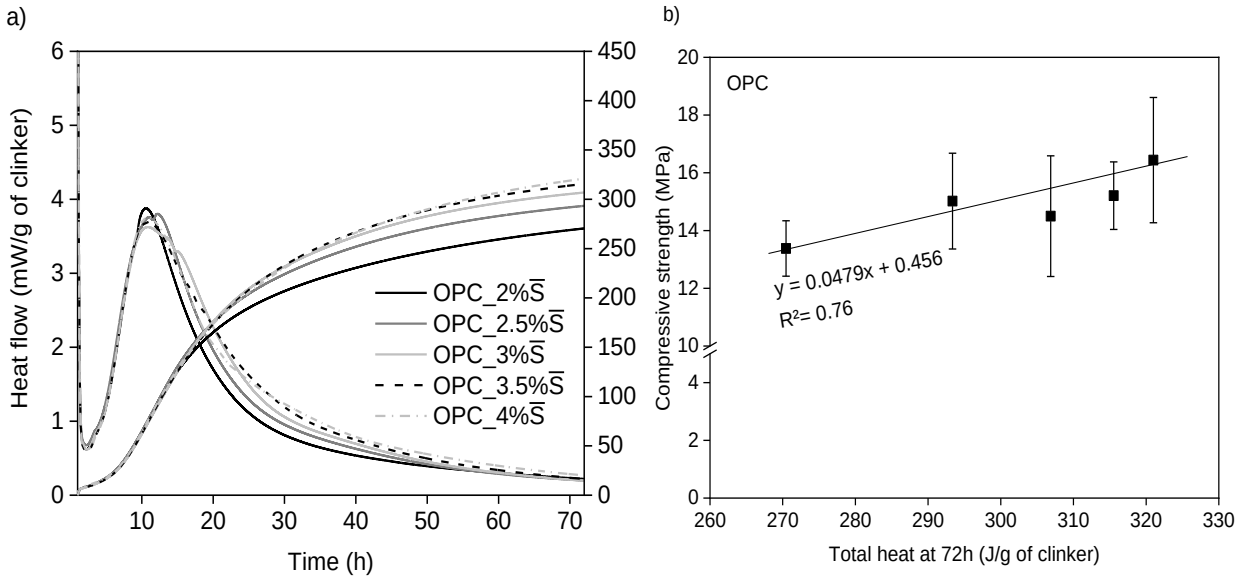

Fig. 12 Compressive strength versus SO_3 level of the OPC

All mixtures generally showed the same induction period and acceleration of the silicate peaks. The increase of SO_3 levels led to a slightly higher silicate peak intensity, but it was impossible to provide an intense and well-defined aluminate peak as much as LC³ cements do. Moreover, the total heat was higher as the SO_3 levels increased due to the contribution of gypsum to the C_3S hydration, as previously mentioned. This indicates that such correlation was more reliable to OPC than LC³. Thus, comparing total heat and compressive strength was not appropriate for LC³.

3.8.2 Compressive strength vs. *Cwf*

Figure 13(a-c) present the relation between combined water fraction, *cwf*, and compressive strength of (LC³)-QP, -CK, -CM pastes.

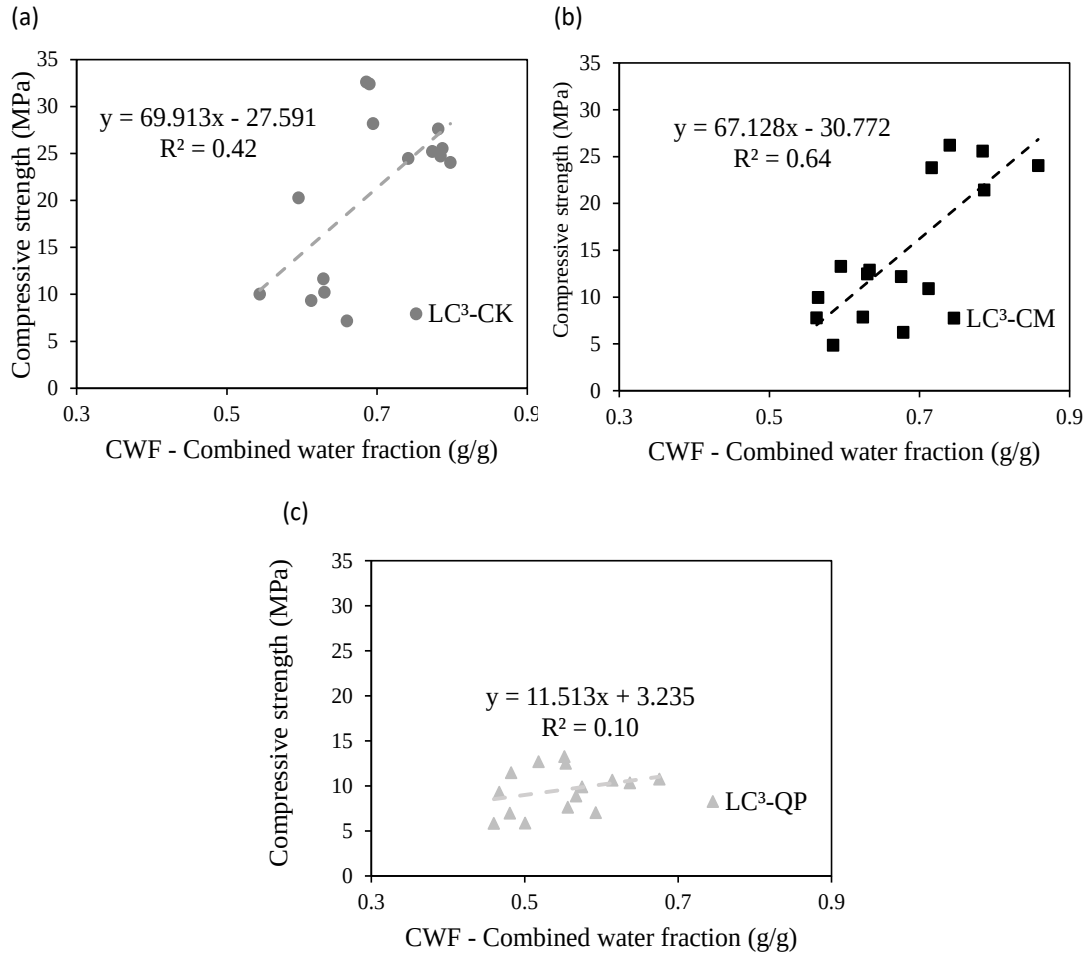

Fig. 13 Correlation between compressive strength and combined water fraction of the LC³ systems

The linear correlation between these properties was low for the mixes tested here, which is evidenced by the low R^2 values (0.09 – 0.63). This result did not agree with John et al. (JOHN *et al.*, 2019) observations, which noted a high (R^2 = 0.91) linear correlation between *cwf* and compressive strength for several types of cement, including LC³. This might be related to the variation of the sulfate level in the present study, which greatly influences the amount of ettringite. Ettringite has a high amount of combined water, which contributes to a significant increase in the paste's *cwf* but does not necessarily result in a great increase of strength (when compared to C-S-H, which has a low amount of water). This result indicated that, at least for the cements tested here, the *cwf* does not seem to agree well with the compressive strength.

3.8.3 $SO_{3optimum}$ by chemical shrinkage using dilatometry for 28 days

The objective of the sulfate optimization using dilatometry was to determine the SO_3 level at which it should be possible to observe the highest chemical shrinkage for each cement. For the same group of cement, all the SO_3 levels had quite similar chemical shrinkage over time. If the standard deviation is disregarded, the highest chemical shrinkage should be approximately 3.5%SO_3 mix to LC³-CK (at 7 and 28 days), whereas for LC³-CM and QP something between 2-2.5% of SO_3 level, consistent with compressive strength result. However, this was an inconclusive approach and must be performed with additional tests.

Chemical shrinkage using dilatometry is a simple and reproducible technique. According to Geiker (GEIKER, 2016), the main advantages of chemical shrinkage measurements are the long testing periods, inexpensive equipment and low training required. Despite this, such a technique was not sensitive enough to detect subtle differences caused by changing the total SO_3 content (additions of 0.5%) in blended cement, such as LC³. When the comparison was made between the shrinkage values of the cements, differences were observed, especially CK cement, compared to CM and QP cement. Therefore, this technique is restricted to comparative purposes of the reactivity of SCMs or different cements rather than determining an optimum sulfate content.

4 Conclusions

This study explored the effects of calcined clays with different mineralogy on the reaction mechanisms and kinetics, phase assemblage, compressive strength, and shrinkage of LC³ mixes containing different SO_3 content; also, the most appropriate techniques to determine the optimum sulfate content in these cements. The main conclusions found were:

- The mineralogy of the analyzed clay affected its reactivity in LC^3 cements but not the nature of the reactions involved. The more reactive the clay (in this case CK) the higher, the faster or the more intensified the mechanism/characteristics involved.
- It is known that metakaolin (MK) is a commercial calcined clay of high reactivity in Portland cement systems. Nevertheless, calcined montmorillonite clay, when

combined with limestone in LC^3 blends showed satisfactory results without the problem of accelerated sulfate depletion.

- The optimum sulfate content in LC^3 systems will depend on the criteria established by the decision-maker (academia or industry), either kinetics reactions, phase assemblage, compressive strength at a specific curing time or shrinkage of LC^3 mixtures containing different SO^3 content. Also, sulfate optimization in terms of $SO_{3,\ total}$ level over the addition of gypsum (wt.%) is encouraged.
- There is no single best technique to predict sulfate optimization in LC^3 but carefully combining multiple techniques can assist in more coherent decision-making. For instance, the visual observation of the isothermal calorimetry results within 30 hours and compressive strength after 3 days (72 hours) were consistent. On the other hand, compressive strength with *cwf* did not show a higher correlation expected from some authors to commercial types of cement.

The paper opens a discussion on the importance that should be given to addressing sulfate optimization in LC^3 systems. The information provided on the behavior of these cements with kaolinite alternative clays (bentonite) demonstrates the potential for further application. Researchers, engineers, and cement manufacturers will be able to discuss further and propose more efficient approaches to the clinker: gypsum ratio instead of the conventional formulation (45:5%) suggested for LC^3-50, based on optimum sulfate content.

References

ABNT. **NBR 16697: Cimento Portland-Requisitos**. [*S. l.: s. n.*], 2018. Disponível em: www.abnt.org.br. .

ANDRADE NETO, José S. *et al.* Hydration of C3S and Al-doped C3S in the presence of gypsum. **Cement and Concrete Research**, [*s. l.*], v. 152, p. 106686, 2022.

ANDRADE NETO, José S. *et al.* The role of sodium and sulfate sources on the rheology and hydration of C3A polymorphs. **Cement and Concrete Research**, [*s. l.*], v. 151, 2022.

ANDRADE NETO, José da Silva; DE LA TORRE, Angeles G.; KIRCHHEIM, Ana Paula. Effects of sulfates on the hydration of Portland cement – A review. **Construction and Building Materials**, [*s. l.*], v. 279, 2021.

ANTONI, M. *et al.* Cement substitution by a combination of metakaolin and limestone. **Cement and Concrete Research**, [*s. l.*], v. 42, n. 12, p. 1579–1589, 2012.

ASTM. **C1608-12, Standard Test Method for Chemical Shrinkage of Hydraulic**

Cement Paste, ASTM International, West Conshohocken, PA, 2012, www.astm.org. [*S. l.: s. n.*], 2012.

ASTM. C563:18 - Standard Guide for Approximation of Optimum SO3 in Hydraulic Cement 1. [*s. l.*], 2018. Disponível em: www.astm.org,.

AVET, François *et al.* Development of a new rapid, relevant and reliable (R3) test method to evaluate the pozzolanic reactivity of calcined kaolinitic clays. **Cement and Concrete Research**, [*s. l.*], v. 85, p. 1–11, 2016.

AVET, François; BOEHM-COURJAULT, Emmanuelle; SCRIVENER, Karen. Investigation of C-A-S-H composition, morphology and density in Limestone Calcined Clay Cement (LC 3). **Cement and Concrete Research**, [*s. l.*], v. 115, p. 70–79, 2019. Disponível em: https://doi.org/10.1016/j.cemconres.2018.10.011. Acesso em: 9 ago. 2021.

AVET, François; SCRIVENER, Karen. Effect of temperature on the water content of C-A-S-H in plain Portland and blended cements. **Cement and Concrete Research**, [*s. l.*], v. 136, 2020. Disponível em: www.elsevier.com/locate/cemconres. Acesso em: 2 jul. 2021.

AVET, François; SCRIVENER, Karen. Investigation of the calcined kaolinite content on the hydration of Limestone Calcined Clay Cement (LC3). **Cement and Concrete Research**, [*s. l.*], v. 107, p. 124–135, 2018.

BAKI, Vahiddin Alperen *et al.* The impact of mechanochemical activation on the physicochemical properties and pozzolanic reactivity of kaolinite, muscovite and montmorillonite. **Cement and Concrete Research**, [*s. l.*], v. 162, 2022.

BERGAYA, F.; LAGALY, G. General Introduction: Clays, Clay Minerals, and Clay Science. **Developments in Clay Science**, [*s. l.*], v. 5, p. 1–19, 2013.

BERODIER, E.; SCRIVENER, K. Understanding the filler effect on the nucleation and growth of C-S-H. **Journal of the American Ceramic Society**, [*s. l.*], v. 97, n. 12, p. 3764–3773, 2014.

BEUNTNER, Nancy *et al.* **Solubility and kinetics of calcined clay: study of interaction by pore solution**. [*S. l.: s. n.*], 2016. Disponível em: https://www.researchgate.net/publication/309426709. .

BULLARD, Jeffrey W. *et al.* Mechanisms of cement hydration. **Cement and Concrete Research**, [*s. l.*], v. 41, n. 12, p. 1208–1223, 2011.

CANBEK, Oğulcan *et al.* A quantitative approach to determining sulfate balance for LC3. **CEMENT**, [*s. l.*], v. 12, p. 100063, 2023. Disponível em: https://linkinghub.elsevier.com/retrieve/pii/S2666549223000099. Acesso em: 6 mar. 2023.

CEMENTIR HOLDING. **The Cement of the Future Is now Here: Cementir Launches FUTURECEM™ With up to 30 Percent Lower Carbon Emissions | Cementir Holding N.V.** [*S. l.*], 2020. Disponível em: https://www.cementirholding.com/en/media/whats-new/cement-future-now-here-cementir-launches-futurecemtm-30-percent-lower-carbon. Acesso em: 10 jun. 2021.

DA SILVA, Micael Rubens Cardoso *et al.* Valorization of kaolin mining waste from the Amazon region (Brazil) for the low-carbon cement production. **Case Studies in Construction Materials**, [*s. l.*], v. 15, p. e00756, 2021.

DE LA VARGA, Igor *et al.* Evaluating the hydration of high volume fly ash mixtures using chemically inert fillers. **Construction and Building Materials**, [*s. l.*], v. 161, p. 221–228,

2018.

DE MATOS, P.R. *et al.* Effect of superplasticizer addition time and metakaolin source on the early-age hydration of limestone calcined clay cement (LC3). **Materials and Structures - Under Revision (2022)**, [*s. l.*], 2022.

ECTORS, D. **Advances in the analysis of cementitious reactions and hydrate phases-Fortschritte in der Analyse von zementären Reaktionen und Hydratphasen**. 2016. [*s. l.*], 2016. Disponível em: https://opus4.kobv.de/opus4-fau/frontdoor/index/index/docId/7174.

EN 197-1. **EN 197-1 Cement-Part 1: Composition, specifications and conformity criteria for common cements**. [*S. l.: s. n.*], 2018. Disponível em: www.mbsmw.org. Acesso em: 5 jul. 2021.

FERNANDEZ, Rodrigo; MARTIRENA, Fernando; SCRIVENER, Karen L. The origin of the pozzolanic activity of calcined clay minerals: A comparison between kaolinite, illite and montmorillonite. **Cement and concrete research**, [*s. l.*], v. 41, p. 113–122, 2011. Disponível em: http://ees.elsevier.com/CEMCON/default.asp. Acesso em: 31 jul. 2021.

FLEGAR, Matea *et al.* Overview of clay as supplementarycementitious material. **SIMPOZIJ DOKTORSKOG STUDIJA GRAĐEVINARSTVA**, [*s. l.*], 2019. Disponível em: https://doi.org/10.5592/CO/PhDSym.2019.14. Acesso em: 10 jun. 2021.

GARG, Nishant. **STRUCTURE, REACTIVITY, AND DISSOLUTION OF CALCINED CLAYS BY SOLID-STATE NMR**. 2015. - Aarhus University, Denmark , 2015.

GARG, Nishant; SKIBSTED, Jørgen. Dissolution kinetics of calcined kaolinite and montmorillonite in alkaline conditions: Evidence for reactive Al(V) sites. **Journal of the American Ceramic Society**, [*s. l.*], v. 102, n. 12, p. 7720–7734, 2019. Disponível em: https://ceramics.onlinelibrary.wiley.com/doi/full/10.1111/jace.16663. Acesso em: 11 jul. 2021.

GEIKER, METTE. Characterisation of development of cement hydration using chemical shrinkage. *In*: SCRIVENER, Karen; SNELLINS, Ruben; LOTHENBACH, Barbara (org.). **A Practical Guide to Microstructural Analysis of Cementitious Materials** . 1. ed. [*S. l.*]: CCR Press, 2016. v. 1, p. 75–106.

HE, Changling; OSBAECK, Bjarne; MAKOVICKY, Emil. Pozzolanic reactions of six principal clay minerals: Activation, reactivity assessments and technological effects. **Cement and Concrete Research**, [*s. l.*], v. 25, n. 8, p. 1691–1702, 1995.

IEA. **International Energy Agency, Iea. Technology Roadmap - Low-Carbon Transition in the Cement Industry**. [*S. l.: s. n.*], 2018. Disponível em: www.wbcsdcement.org. Acesso em: 10 jun. 2021.

ITO, Akihiko; WAGAI, Rota. Global distribution of clay-size minerals on land surface for biogeochemical and climatological studies. **Scientific Data**, [*s. l.*], v. 4, n. 1, p. 1–11, 2017. Disponível em: www.nature.com/sdata/. Acesso em: 10 jun. 2021.

JANSEN, D. *et al.* The early hydration of OPC investigated by in-situ XRD, heat flow calorimetry, pore water analysis and 1H NMR: Learning about adsorbed ions from a complete mass balance approach. **Cement and Concrete Research**, [*s. l.*], v. 109, p. 230–242, 2018.

JOHN, Vanderley M. *et al.* **Rethinking cement standards: Opportunities for a better future**. [*S. l.*]: Elsevier Ltd, 2019.

JUENGER, Maria C.G.; SNELLINGS, Ruben; BERNAL, Susan A. **Supplementary cementitious materials: New sources, characterization, and performance insights**. [*S. l.*]: Elsevier Ltd, 2019.

KURDOWSKI, Wieslaw. **Cement and Concrete Chemistry**. 1. ed. Dordrecht: Springer Netherlands, 2014. v. 1

LEI, L; PLANK, J. A study on the impact of different clay minerals on the dispersing force of conventional and modified vinyl ether based polycarboxylate superplasticizers. [*s. l.*], 2014. Disponível em: http://dx.doi.org/10.1016/j.cemconres.2014.02.009. Acesso em: 12 ago. 2022.

LOTHENBACH, B.; DURDZI´NSKI, P. T.; DE WEERDT, K. Thermogravimetric analysis. *In*: SCRIVENER, K.; SNELLINGS, R.; LOTHENBACH, B. (org.). **A Practical Guide to Microstructural Analysis of Cementitious Materials**. [*S. l.*]: CCR Press, 2016. v. 1st ed., p. 177–212.

LU, Z. C. *et al.* Characterization data of reference cement CEM III/A 42.5N used for priority program DFG SPP 2005 "Opus Fluidum Futurum – Rheology of reactive, multiscale, multiphase construction materials". **Data in Brief**, [*s. l.*], v. 30, p. 105524, 2020.

MA, Yihan *et al.* **Research progress on polycarboxylate based superplasticizers with tolerance to clays - A review**. [*S. l.*]: Elsevier Ltd, 2020.

MAIER, Matthias *et al.* Hydration of cubic tricalcium aluminate in the presence of calcined clays. **Journal of the American Ceramic Society**, [*s. l.*], v. 104, n. 7, p. 3619–3631, 2021.

MAIER, Matthias *et al.* Particle characteristics of calcined clays and limestone and their impact on early hydration and sulfate demand of blended cement. **Cement and Concrete Research**, [*s. l.*], v. 154, p. 106736, 2022. Disponível em: https://linkinghub.elsevier.com/retrieve/pii/S0008884622000278.

MALACARNE, C. *et al.* Influence of low-grade materials as clinker substitute on the rheological behavior, hydration and mechanical performance of ternary cements. **Case Studies in Construction Materials**, [*s. l.*], v. 15, p. e00776, 2021.

MANDALIA, Tushar; BERGAYA, Faïza. Organo clay mineral–melted polyolefin nanocomposites Effect of surfactant/CEC ratio. **Journal of Physics and Chemistry of Solids**, [*s. l.*], v. 67, n. 4, p. 836–845, 2006.

MOHAMMED, Siline; SAFIULLAH, Omary. Optimization of the SO3 content of an Algerian Portland cement: Study on the effect of various amounts of gypsum on cement properties. **Construction and Building Materials**, [*s. l.*], v. 165, p. 362–370, 2018. Disponível em: https://doi.org/10.1016/j.conbuildmat.2017.12.218. Acesso em: 30 jul. 2021.

MURRAY, Haydn H. Chapter 6 Bentonite Applications. *In*: DEVELOPMENTS IN CLAY SCIENCE. [*S. l.: s. n.*], 2006. v. 2, p. 111–130.

MYERS, Rupert J *et al.* Role of Adsorption Phenomena in Cubic Tricalcium Aluminate Dissolution. [*s. l.*], 2016. Disponível em: https://pubs.acs.org/sharingguidelines. Acesso em: 15 out. 2021.

NIEMUTH, Mark D.; BARCELO, Laurent; WEISS, Jason. Effect of Fly Ash on Optimum Sulfate Levels Measured Using Heat and Strength at Early Ages. **Advances in Civil**

Engineering Materials, [*s. l.*], v. 1, n. 1, p. 1–18, 2012. Disponível em: http://www.astm.org/DIGITAL_LIBRARY/JOURNALS/ACEM/PAGES/ACEM20120012.htm. Acesso em: 12 ago. 2021.

PY, Lucas Goldenberg. **Balanceamento de sulfatos e hidratação de cimentos ternários à base de calcários e argilas calcinadas**. 2021. - Universidade Federal do Rio Grande do Sul, Porto Alegre, 2021.

QUENNOZ, Alexandra; SCRIVENER, Karen L. Interactions between alite and C3A-gypsum hydrations in model cements. **Cement and Concrete Research**, [*s. l.*], v. 44, p. 46–54, 2013.

SCHERB, Sebastian *et al.* Reaction kinetics during early hydration of calcined phyllosilicates in clinker-free model systems. **Cement and Concrete Research**, [*s. l.*], v. 143, p. 106382, 2021.

SCHERB, Sebastian *et al.* Reactivity of metakaolin in alkaline environment: Correlation of results from dissolution experiments with XRD quantifications. **Materials**, [*s. l.*], v. 13, n. 10, 2020.

SCHMID, Marlene; PLANK, Johann. Interaction of individual meta clays with polycarboxylate (PCE) superplasticizers in cement investigated via dispersion, zeta potential and sorption measurements. **Applied Clay Science**, [*s. l.*], v. 207, p. 106092, 2021.

SCHÖLER, Axel *et al.* Hydration of quaternary Portland cement blends containing blast-furnace slag, siliceous fly ash and limestone powder. **Cement and Concrete Composites**, [*s. l.*], v. 55, p. 374–382, 2015.

SCRIVENER *et al.* Impacting factors and properties of limestone calcined clay cements (LC 3) . **Green Materials**, [*s. l.*], v. 7, n. 1, p. 3–14, 2019.

SCRIVENER, K. *et al.* Advances in understanding cement hydration mechanisms. **Cement and Concrete Research**, [*s. l.*], v. 124, p. 105823, 2019.

SHI, Zhenguo *et al.* Sulfate resistance of calcined clay-Limestone-Portland cements. **Cement and Concrete Research**, [*s. l.*], v. 116, p. 238–251, 2019. Disponível em: https://doi.org/10.1016/j.cemconres.2018.11.003.

SKIBSTED, Jørgen; SNELLINGS, Ruben. **Reactivity of supplementary cementitious materials (SCMs) in cement blends**. [*S. l.*]: Elsevier Ltd, 2019.

SUN, Huaqiang *et al.* Optimization of gypsum and slag contents in blended cement containing slag. **Cement and Concrete Composites**, [*s. l.*], v. 112, 2020.

TANG, Fulvio J.; GARTNER, Ellis M. Influence of sulphate source on Portland cement hydration. **Advances in Cement Research**, [*s. l.*], v. 1, n. 2, p. 67–74, 1988.

TAYLOR-LANGE, Sarah C. *et al.* Calcined kaolinite-bentonite clay blends as supplementary cementitious materials. **Applied Clay Science**, [*s. l.*], v. 108, p. 84–93, 2015.

WADSÖ, L. *et al.* Calorimetry. *In*: SCRIEVENER, Karen; SNELLINGS, Ruben; LOTHENBACH, Barbara (org.). **A Practical Guide to Microstructural Analysis of Cementitious Materials**. 1. ed. [*S. l.*]: CCR Press, 2016. v. 1, p. 37–74.

WEI, Jianqiang; GENCTURK, Bora. Hydration of ternary Portland cement blends containing metakaolin and sodium bentonite. **Cement and Concrete Research**, [*s. l.*], v.

123, 2019.

YOKOYAMA, Shingo; KURODA, Masato; SATO, Tsutomu. Atomic force microscopy study of montmorillonite dissolution under highly alkaline conditions. **Clays and Clay Minerals 2005 53:2**, [*s. l.*], v. 53, n. 2, p. 147–154, 2005. Disponível em: https://link.springer.com/article/10.1346/CCMN.2005.0530204. Acesso em: 3 ago. 2021.

ZUNINO, Franco; SCRIVENER, Karen. Insights on the role of alumina content and the filler effect on the sulfate requirement of PC and blended cements. **Cement and Concrete Research**, [*s. l.*], v. 160, p. 106929, 2022. Disponível em: https://linkinghub.elsevier.com/retrieve/pii/S0008884622002216.

ZUNINO, Franco; SCRIVENER, Karen. Microstructural developments of limestone calcined clay cement (LC3) pastes after long-term (3 years) hydration. **Cement and Concrete Research**, [*s. l.*], v. 153, p. 106693, 2022.

ZUNINO, Franco; SCRIVENER, Karen. The influence of sulfate addition on hydration kinetics and C-S-H morphology of C3S and C3S/C3A systems. **Cement and Concrete Research**, [*s. l.*], v. 160, p. 106930, 2022. Disponível em: https://linkinghub.elsevier.com/retrieve/pii/S0008884622002228.

ZUNINO, Franco; SCRIVENER, Karen. The influence of the filler effect on the sulfate requirement of blended cements. **Cement and Concrete Research**, [*s. l.*], v. 126, 2019. Disponível em: www.elsevier.com/locate/cemconres. Acesso em: 2 jul. 2021.

ZUNINO, Franco; SCRIVENER, Karen. The reaction between metakaolin and limestone and its effect in porosity refinement and mechanical properties. **Cement and Concrete Research**, [*s. l.*], v. 140, p. 106307, 2021a.

ZUNINO, Franco; SCRIVENER, Karen. The reaction between metakaolin and limestone and its effect in porosity refinement and mechanical properties. **Cement and Concrete Research**, [*s. l.*], v. 140, 2021b.

4.1 PART 3: Effects of kaolinite and montmorillonite calcined clays on the sulfate balance, early hydration and artificial pore solution of limestone calcined clay cements (LC3)

5 Introduction

Clays are mainly composed of minerals widely available in the earth's crust, including kaolinite, montmorillonite, and illite/mica as the most abundant (ITO; WAGAI, 2017). Kaolinite is a typical 1:1 clay mineral of the kaolin group with the chemical formula $Si_2Al_2O_5(OH)_4$. Its unit cell structure consists of the tetrahedral Si and octahedral Al layers joined by bonds of oxygen atoms. Montmorillonite has an extra layer of tetrahedral Si that encompasses the octahedral Al layer; hence they are known as a 2:1 group clay mineral (GARG, 2015). Also, the montmorillonite's interlayers are bonded by weak oxygen bridges and contain a lot of active sites and exchangeable cations, which allow the entrance of water molecules or cations such as Na^+, Mg^{2+} or Ca^{2+} (MA *et al.*, 2020). As a 2:1 clay mineral, it exhibits isomorphic substitution, resulting in a net negative charge balanced by interlayer cations (Ca^{2+}, Na^+, or K^+) coordinated to H_2O molecules in the interlayer region (GARG, 2015). Therefore, montmorillonite has strong adsorption and cation exchange, shrinkage, intercalation, and swelling capacity (MA *et al.*, 2020; MANDALIA; BERGAYA, 2006), contrasting significantly with kaolinite clay minerals (MURRAY, 2006).

Clay minerals can be found in different forms in nature, such as rock, soil, or clays. *In Natura*, clays usually have low or negligible chemical reactivity, limiting their application as supplementary cementitious material (SCM) by the cement industry. Thus, mechanical, chemical, or thermal processes are used to increase their reactivity. Calcination is the most common way to enhance clay reactivity, by inducing dehydroxylation and structural disorder in the clay, which provides sufficient reactivity for the calcined clay to react with products of ordinary Portland cement (OPC) hydration and reduce the environmental impact (primarily CO_2 emissions) from the cement production by high levels of clinker substitution (FLEGAR *et al.*, 2019).

It is known that the kaolinite clay mineral has the highest reactivity in the cement matrix among the clay minerals (FERNANDEZ; MARTIRENA; SCRIVENER, 2011). However,

concerns about transportation distances or shortages of raw materials may encourage other clay types to be considered for production low-carbon cements such as limestone calcined cements (LC^3) to increase CO_2 savings further. It consists of replacement of ~50% (wt.%) for limestone and calcined clays able to help reduce the CO_2 (ANTONI *et al.*, 2012). For instance, in Denmark, bentonite (a clay-rich in montmorillonite) has become a suitable alternative to develop blended cements since kaolin reserves are locally scarce (CEMENTIR HOLDING, 2020).

SCMs interact with blended cement mainly through their physical and chemical effects (JUENGER; SNELLINGS; BERNAL, 2019). Studies with fresh pastes confirm that calcined clays increase the requirement for water and chemical admixtures in LC^3 for a specific rheological behavior, mainly due to their high fineness, specific surface area (SSA_{BET}), and mineralogical structure (DA SILVA *et al.*, 2021; SCRIVENER *et al.*, 2019) The effects of such SCM features on the hydration of blended cements are still a matter of debate, especially related to their impact on the sulfate balance of blended cements.

Recent studies on LC^3 have indicated a faster sulfate depletion than OPC (ZUNINO; SCRIVENER, 2019). Clays are considered responsible for accelerating sulfate depletion in LC^3 cements. The mechanisms underpinning this behavior are still under discussion, but the calcined clay filler effect (fineness), ion dissolution, and possible sulfate ion adsorption on the clay surface have all been proposed as likely mechanisms affecting this (MAIER *et al.*, 2021; ZUNINO; SCRIVENER, 2019). The complexity of these interactions is even more remarkable considering different clay minerals other than kaolinite, such as montmorillonite, which can be incorporated into the production of these blended cements such as LC^3.

The use of calcined montmorillonite (CM) in ternary cements is rarely reported. However, some efforts have been made to assess its potential use combined with metakaolin (calcined kaolinite clay, MK) in partial cement replacements (TAYLOR-LANGE *et al.*, 2015; WEI; GENCTURK, 2019) and with limestone (SHI *et al.*, 2019). The synergy between both calcined clays increased portlandite ($Ca(OH)_2$;CH) consumption and compressive strength in ternary cements (TAYLOR-LANGE *et al.*, 2015). In addition, by increasing this amount of MK and CM, more calcium aluminosilicate hydrate (C-(A)-S-H) gel pores, hydrogarnet, and strätlingite are formed at later ages (WEI; GENCTURK, 2019). Shi et al. (2019) studied limestone and CM in blended cements. However, only aspects related to sulfate resistance, pozzolanic reactivity, and porosity of different calcined clays were assessed. No further

attention was paid to the hydration of such blended systems, especially early age aspects, such as sulfate demand.

The physical and chemical effects of the calcined clays (exclusively MK) on the sulfate balance are still under discussion. Zunino and Scrivener (ZUNINO; SCRIVENER, 2019) concluded that the increase of sulfate demand in blended cements mainly related to the additional surface area that impacts the total C-S-H and ettringite formation due to their competition for sulfate ions rather than the clays' chemical composition. Based non-systematic comparisons, the authors concluded that the additional alumina content of the calcined clays would not have a major impact on the need suitable sulfate content. On the other hand, other authors (AVET; SCRIVENER, 2018; DA SILVA *et al.*, 2021) suggest that an accelerated sulfate depletion is dependent more on the kaolinite content of the clays than on the SSA_{BET} provided by kaolinitic clays, which leads to extra aluminum driving hydration to an under-sulfated system and accelerated ettringite formation. Recently, according to Zunino and Scrivener (Insights on the role of alumina content and the filler effect on the sulfate requirement of PC and blended cementsZUNINO; SCRIVENER, 2022), calcium sulfate being adsorbed to C-S-H until its depletion could be the main factor reducing the availability of gypsum in solution.

The dissolution of calcined clay minerals can also impact sulfate depletion. For instance, Maier et al. (MAIER *et al.*, 2021), studying illite and kaolinite clay minerals in alkaline solutions by inductively coupled plasma optical emission spectroscopy (ICP-OES), concluded that an acceleration of sulfate depletion in blended cements is caused by alumina interactions (from C_3A and calcined clays minerals). In calcined clays, such dissolution is dependent on clay minerals and related to their SSA, reactivity and degree of dehydroxylation, according to Garg and Skibsted (GARG; SKIBSTED, 2019). Using ^{29}Si and ^{27}Al magic angle spinning nuclear magnetic resonance spectroscopy (MAS NMR), they found that in kaolinite, Si and Al dissolution are 4 and 12 times larger, respectively, than in montmorillonite. ^{27}Al MAS NMR data showed highly preferential dissolution of pentahedral aluminum sites (Al^V).

The acceleration of sulfate depletion can also be influenced by adsorption of ions during cement hydration. Such arguments were pointed out by Maier et al. (MAIER *et al.*, 2021) in blended cement concerning kaolinite and illite clay minerals. The authors have proposed that the adsorption processes of SO_4^{2-} ions and/or Ca-SO_4-complexes on the surface of calcined clays impact the rapid sulfate depletion during the hydration process, according to

measurement of the zeta potential of calcined clays at specific ages. Evidence for the affinity of the clay minerals for Ca^{+2} ions was previously presented by Lei and Plank (2014), where kaolinite, montmorillonite, and muscovite showed increased adsorption as a function of Ca^{2+} concentration in solution. However, the calcium sulfate adsorption on the montmorillonite clay surface, such as calcium bentonite, has not yet been evaluated. Thus, the present study evaluates changes in the zeta potential of CK, CM and gypsum in artificial pore solution within 72h.

This research provides new insight into the physicochemical effects of CK and CM on the sulfate balance, early-age hydration and artificial pore solution chemistry of low-carbon cements based on OPC blended with limestone and calcined clay (LC^3).

6 Materials and methods

6.1 Materials

In this study, Portland clinker (PC), limestone (LS) and mineral gypsum (GYP), supplied by a Brazilian cement plant, were used. A natural kaolinite clay (CK) from Pantano Grande (Brazil) and commercial sodium bentonite (montmorillonite-rich clay, CM) from Buschle & Lepper S.A., were studied. Table S1, in the Supplementary Material (SM), shows the technical specification of the Na-bentonite clay provided by the sale company. A commercially available quartz powder was also used as an inert material. Figures S1 and S2, in the SM, show the X-ray diffraction (XRD) and thermogravimetric analysis/differential thermogravimetry (TGA/DTG) data for the materials used here.

The clays were prepared according to the following steps. First, both clays were dried at 100 °C. Then, the clays were sieved (2.4 mm opening sieve) and then calcined in a static furnace at 800 °C for 1 hour (with a heating rate of 10 °C/min) followed by abrupt opening of the muffle at room temperature. Then, both clays were ground in a disc grinding mill to obtain two different particle size distributions (PSD), one coarser ($d_{v,90}$ > 27.29µm) and one finer ($d_{v,90}$ of <27.79µm) than the clinker.

The PSD of the materials was measured by laser granulometry in triplicate with 60 seconds of ultrasound/each repetition and dispersion in isopropanol or water (See SM for a description

of the grinding methodology). The specific surface area of the materials was measured using the BET method (SSA_{BET}), with a heating rate of 20 °C/min with a nitrogen gas atmosphere. The chemical composition was assessed by X-ray fluorescence (XRF) in a sequential X-ray fluorescence spectrometer between 400 and 4000 cm^{-1} wavelengths. All the characterization results are presented in Table 1.

The reactivity of both clays (and both PSD fractions) was assessed using the protocols from the R^3 test (AVET *et al.*, 2016), and the results are presented in Fig. 1. Both coarser clays presented similar heat release after 24 h, indicating similar reactivity. As expected, the reactivity of both clays is increased by the decrease in the PSD. However, it is interesting to note that while the heat released by the CK clay increased by 15 J/g of solid by grinding, the amount of heat released by the CM was less than 5 J/g of solid. This indicated that despite a coarser PSD, both clays present similar reactivity, while at finer PSD, the kaolinite one is more reactive.

Table 1 Materials characterization

Characterization	Portland clinker (PC)	Quartz powder (QP)	Coarser Calcined kaolinite clay ($CK_{coarser}$)	Finer Calcined kaolinite clay (CK_{finer})	Coarser Calcined montmorillonite clay ($CM_{coarser}$)	Finer Calcined montmorillonite clay (CM_{finer})	Limestone (LS)	Gypsum (GYP)
D_{v90} (µm)	27.79	13.01	37.85	25.86	39.83	26.60	37.18	34.83
D_{v50} (µm)	9.01	4.66	14.87	10.15	15.80	10.57	10.24	8.97
D_{v10} (µm)	1.61	0.89	2.86	2.39	2.63	1.89	1.44	1.85
Dvmean	12.67	6.19	18.73	12.86	19.58	13.07	15.91	14.73
Span ($\frac{D_{v90}-D_{v10}}{D_{v50}}$)	2.90	2.60	2.36	2.31	2.35	2.34	3.49	3.67
SSA_{BET} (m^2/g)	2.51	2.71	12.00	13.79	15.35	8.46	1.02	5.11
Oxides compositions by XRF (%)								
SiO_2	19.97	96.98	45.70		61.93		0.23	0.72

Al_2O_3	3.96	2.22	38.20	19.73	0.08	0.21
Fe_2O_3	3.11	-	0.65	5.02	0.05	0.11
CaO	60.43	-	0.31	1.30	55.06	33.27
MgO	7.64	-	-	3.01	0.44	0.59
SO_3	1.21	0.34	-	1.28	0.07	43.48
K_2O	1.39	0.10	0.39	0.45	0.01	0.05
P_2O_5	0.08	-	-	0.09	0.09	-
MnO	0.15	-	-	0.02	0.01	0.03
ZnO	-	0.09	-	-	-	-
SrO	0.04	-	-	0.02	0.23	0.18
Na_2O	0.20	-	-	2.92	0.05	-
TiO_2	0.20	0.06	0.13	0.51	-	0.01
ZrO_2	-	-	-	-	-	-
LOI	1.37	14.62	10.54	3.53	43.61	21.62
%Total	99.8	100	95.92	99.8	99.9	100

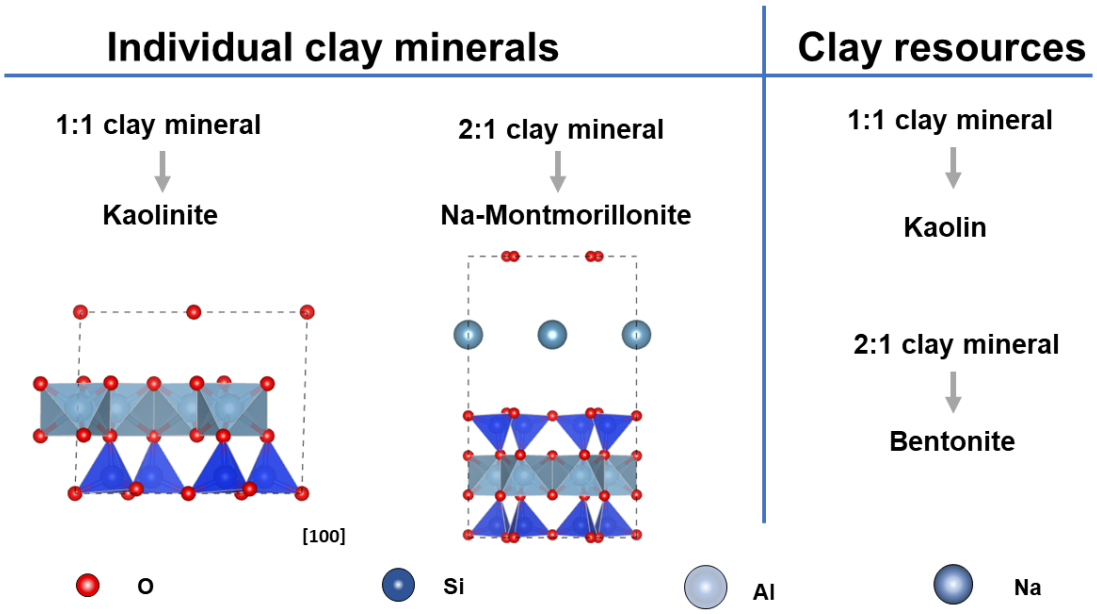

Fig. 1 Structure of the clay(s) (minerals) used in this study: kaolin (kaolinite) and bentonite (montmorillonite), using VESTA software

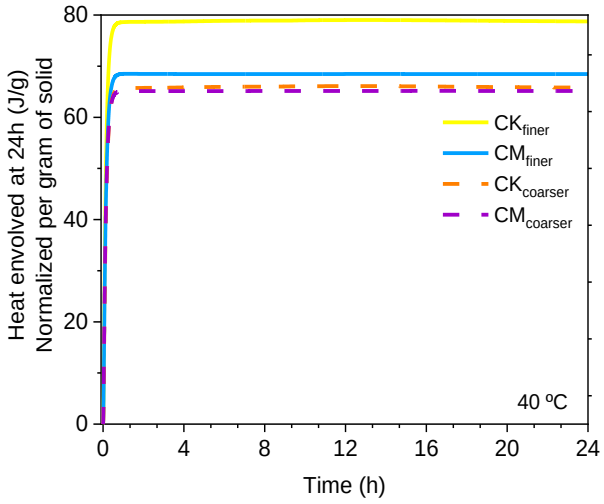

Fig. 2 Reactivity of calcined clays by R³ test

6.2 Mix proportions

The LC³-based blended cements were produced by following to the mix proportions suggested by Antoni et al. (2012), consisting of 50% clinker, 30% calcined clay, 15% limestone, and 5% gypsum by weight (%wt). The contents of calcined clay (or quartz powder in the reference system) and limestone were kept constant across all the cements. Proportions of clinker and gypsum were then adjusted based on 5 levels of SO_{3total} (2.0%, 2.5%, 3.0%, 3.5%, 4% wt.%) under 4.5% SO_{3total} as required by the chemical specifications of Brazilian Portland cement (ABNT, 2018). SO_{3total} values were obtained by applying Equation 1 (ASTM, 2018), where $M_{calcium\ sulfate}$ represents the mass of calcium sulfate (gypsum), M_{cement} represents the mass of cement, $SO_{3\text{-}calcium\ sulfate}$ indicates the mass percentage of SO_3 in calcium sulfate, and $SO_{3\text{-}cement}$ denotes the mass percentage of SO_3 in the cement. The XRF results determined the SO_3 values of each material.

$$SO_{3total} = \frac{M_{calcium\ sulfate}}{M_{calcium\ sulfate} + M_{cement}} x\ SO_{3-calcium\ sulfate} + \frac{M_{cement}}{M_{calcium\ sulfate} + M_{cement}} x\ SO_{3-cement} \quad (1)$$

Table 2 presents the mix proportions used in this study. The 15 mix were evaluated with 5 levels of $SO_{3,total}$ for the cements LC³-QP, LC³-CK and LC³-CM at water:cement (w:c) ratio

of 0.5. The proportion of calcined clay (or quartz powder): limestone was the same for the 3 cements (2:1). The amount of clinker and gypsum was calculated based on $SO_{3,total}$ (Equation 1). The cements nomenclature throughout this study is as follow: *cement type-clay/quartz powder_SO_{3total}* (e.g., LC³-CK_2.5%$\bar{S}$).

Table 2 Mix proportions assessed in this work

Cement	PC	GYP	LS	QP	CK	CM	$SO_{3\ total}$
LC³-QP_2.0%$\bar{S}$	52.11	2.89	15.00	30.00	-	-	2
LC³-QP_2.5%$\bar{S}$	50.93	4.07	15.00	30.00	-	-	2.5
LC³-QP_3.0%$\bar{S}$	49.74	5.26	15.00	30.00	-	-	3
LC³-QP_3.5%$\bar{S}$	48.56	6.44	15.00	30.00	-	-	3.5
LC³-QP_4.5%$\bar{S}$	47.38	7.62	15.00	30.00	-	-	4
LC³-CK_2.0%$\bar{S}$	51.87	3.13	15.00	-	30.00	-	2
LC³-CK_2.5%$\bar{S}$	50.68	4.32	15.00	-	30.00	-	2.5
LC³-CK_3.0%$\bar{S}$	49.50	5.50	15.00	-	30.00	-	3
LC³-CK_3.5%$\bar{S}$	48.32	6.68	15.00	-	30.00	-	3.5
LC³-CK_4.0%$\bar{S}$	47.14	7.86	15.00	-	30.00	-	4
LC³-CM_2.0%$\bar{S}$	52.78	2.22	15.00	-	-	30.00	2
LC³-CM_2.5%$\bar{S}$	51.59	3.41	15.00	-	-	30.00	2.5
LC³-CM_3.0 %$\bar{S}$	50.41	4.59	15.00	-	-	30.00	3
LC³-CM_3.5%$\bar{S}$	49.23	5.77	15.00	-	-	30.00	3.5
LC³-CM_4.0%$\bar{S}$	48,04	6.96	15.00	-	-	30.00	4

6.3 Methods

6.3.1 Experimental program

The experimental methods are organized in Figure 3. Three hypotheses were evaluated to understand better the effects of calcined clay with different mineralogy: the filler effect

(fineness), dissolution under alkaline solution (as in cement hydration), and possible sulfate adsorption on the calcined clays' surface. Techniques such as isothermal calorimetry, compressive strength, ICP-OES and zeta potential measurements were used to validate each of these hypotheses, respectively. In addition, XRD and TGA data were used to assess the phase assemblage and follow the hydration in these mixes.

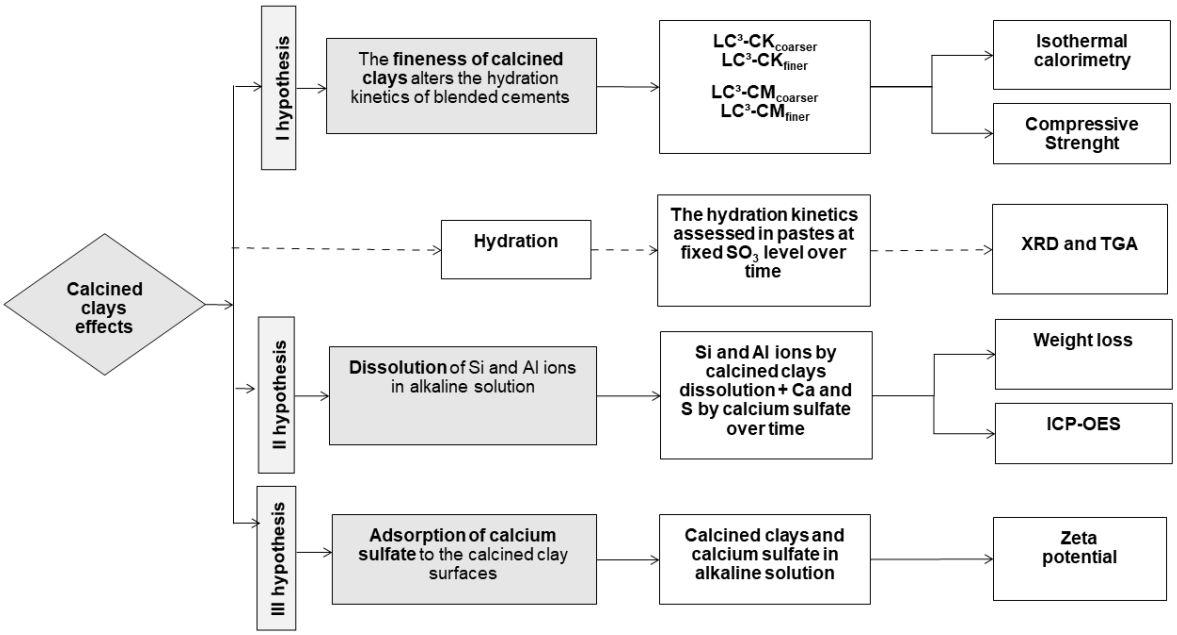

Fig. 3 Schematic representation of experimental program

6.3.2 Test conducted

6.3.2.1 Mixing procedure

The mixing of LC³ pastes were carried out in a vertical mixer. First, 100 g of the LC³ cement were mixed with deionized water, using a water/cement ratio equal to 0.5. The pastes were manually mixed for 30 s, and then mixed for more 70 s at 10,000 rpm mechanical mixer.

6.3.2.2 Isothermal calorimetry

For the isothermal calorimetry test, a TAM Air calorimeter (TA instruments) was used. Approximately 5 grams of the LC³ pastes were added into the calorimeter ampoule, and the heat flow and cumulative heat were recorded up to 72 hours. Deionized water was used as

reference. With this test, conclusion regarding the effect of the calcined clays fineness (CK and CM) on the hydration kinetics of the blended cements were drawn.

6.3.2.3 Compressive strength

For the compressive strength tests, cubic specimens (1 x 1 x 1 cm) were molded. The specimens were cured at room temperature. The compressive strength test was conducted at 3, 7 and 28 days, using a hydraulic press (model EMIC) under constant load (0.2 N/s). The compressive strength results were the mean of 5 samples for each age (in MPa).

6.3.2.4 TGA and XRD

To investigate the development of hydration products in cements with a fixed SO_3 content, X-ray diffraction (XRD) and thermogravimetric analysis (TGA) were carried out at specific time points of 2, 12, 24, 48, and 72 hours. XRD was conducted using a Rigaku Miniflex II with Bragg-Brentano geometry and a CuKα (λ = 1,5418 Å) source, operated at 30 kV and 15 mA. The samples were scanned from 5 to 70° 2θ, with a step of 0.05° 2θ and 1s per step.

TGA was performed using a METTLER TOLEDO (TGA-2) equipment, in which samples of approximately 10 mg were placed in alumina crucibles and pre-heated at 40 ºC for 10 minutes, followed by heating up to 1000 ºC at a rate of 20 ºC/min. The bound water ($BW_{measured}$) was determined by measuring the weight loss (as a percentage) between 40 and 550 ºC. The portlandite content ($Ca(OH)_{2,measured}$) was calculated using Equation 2 and the results were normalized to 100 g of anhydrous cement, based on Equations 3-4 (LOTHENBACH; DURDZI´NSKI; DE WEERDT, 2016).

$$Ca(OH)_{2,measured} = WL_{Ca(OH)_2} \times \frac{m_{Ca(OH)_2}}{m_{H_2O}} \quad (2)$$

$$BW_{rescaled} = \frac{BW_{measured}}{m_{600\,°C}} \quad (3)$$

$$Ca(OH)_{2,rescaled} = \frac{Ca(OH)_{2,measured}}{m_{600\,°C}} \quad (4)$$

The weight loss ($WL_{Ca(OH)_2}$) attributed to the decomposition of portlandite was calculated by integrating the DTG peak located between approximately 400 and 500 °C, using the tangential method (LOTHENBACH; DURDZI´NSKI; DE WEERDT, 2016). The molecular mass of portlandite (74 g/mol) was denoted as $m_{Ca(OH)_2}$, whereas m_{H_2O} (18 g/mol) represented the

molecular mass of water. The weight of the sample at 600 °C (expressed as a percentage) was noted as $m_{600°C}$.

The combined water fraction (*cwf)* was subsequently computed using Equation 5 [22], wherein $Bw_{rescaled}$ is the bound water content rescaled to 100 g of anhydrous cement and Tw represented the total water content in the mix.

$$cwf = \frac{BW_{rescaled}}{TW} \quad (5)$$

6.3.2.5 ICP-OES

The dissolution of the calcined clays was estimated in two different ways. The first one was by means of ICP-OES, where the concentration of silicon (Si) and aluminum (Al) ions from the calcined clays and calcium (Ca) and sulfur (S) from calcium sulfate were measured in MOH solution and pH near Portland cement hydrate (~13.5) as described by Maier et al., (2021), at 2, 12, 24, 48 and 72 hours.

The mixed hydroxide solution (MOH) was based on 50 mmol/l NaOH and 300 mmol/l KOH to a pH close to 13.5 (BEUNTNER *et al.*, 2016) at a solid calcined clays (or calcium sulfate) sample. Such alkaline solution aimed to simulate a cement pore solution pH and isolate the solubility of the calcined clays in the reaction environment as closely as possible to the real pore solution of cements hydrated. Each solution was made based on Scherb et al. (2021) suggest, where 0.25 g of the sample was eluted in 100 ml of MOH. The solution was shaken in dubnoff water bath at 22±1 ºC for 72 hours. The eluted sample was filtered and acidified at each test time to a pH of ~1 to prevent further ion dissolution. Then, 25 µL of the solution is diluted in 25mL of milli-Q water. The solution's elements were compared with the calibration curve of each interested element. Results were measured in ppm.

6.3.2.6 Weight loss (%)

The solid materials retained on the filter after ICP-OES sample preparation were oven-dried to remove any free water. The gypsum was heated at 40°C and the clays at 100°C for 24h. The retained material was carefully removed using a small spatula and weighed on a 0.0001 g precision balance. The difference between the "raw" material (before dissolution) and the dissolved material (after dissolution time) was used to calculate the percentage (%) of soluble

and insoluble material. The % soluble expresses the reactive material that would participate in the cement reactions, in particular, Si and Al ions or Ca and S in the case of calcined clays or gypsum, respectively.

6.3.2.7 Zeta potential

The samples were made by mixing 1g of material in 1L of the alkaline solution (MOH) used for ICP-OES tests, mixed at 200 rpm for 15min. The zeta potential results were calculated from the colloidal current vibration and expressed and in mV.

7 Results

7.1.1 Hypothesis 1: The fineness of calcined clays alters the hydration kinetics of blended cements

In general, all mixes had an induction period of approximately 2h. Overlapping the heat flow silicate peaks, a greater ascendant slope can be qualitatively observed for the LC³-CK mixtures (both coarse and fine) when compared with the LC³-CM mixes (See SM). This increase in intensity of the ascendant slope with the increase of SO_3 content is a consequence of the gypsum additions, which modify the morphology of C-S-H and increase the nucleation density (The influence of sulfate addition on hydration kinetics and C-S-H morphology of C3S and C3S/C3A systemsZUNINO; SCRIVENER, 2022). Moreover, the mineral additions affect this peak via a filler effect either due to the shear conditions of the particles or to the combined fineness of SCMs (calcined clays+limestone) increasing the nucleation of C_3S sites (AVET; SCRIVENER, 2018; BERODIER; SCRIVENER, 2014). Additionally, in systems with limestone, such as LC³, there is a dominant mechanism that can still be attributed to the high affinity of Ca^{2+} to be adsorbed onto clinker surface providing an 'easy' pathway for C-S-H nucleation (BERODIER; SCRIVENER, 2014).

Figure 4 shows the heat flow (left) and cumulative heat flow (right) of the LC^3 pastes with coarser or finer calcined clays, normalized by gram of clinker.

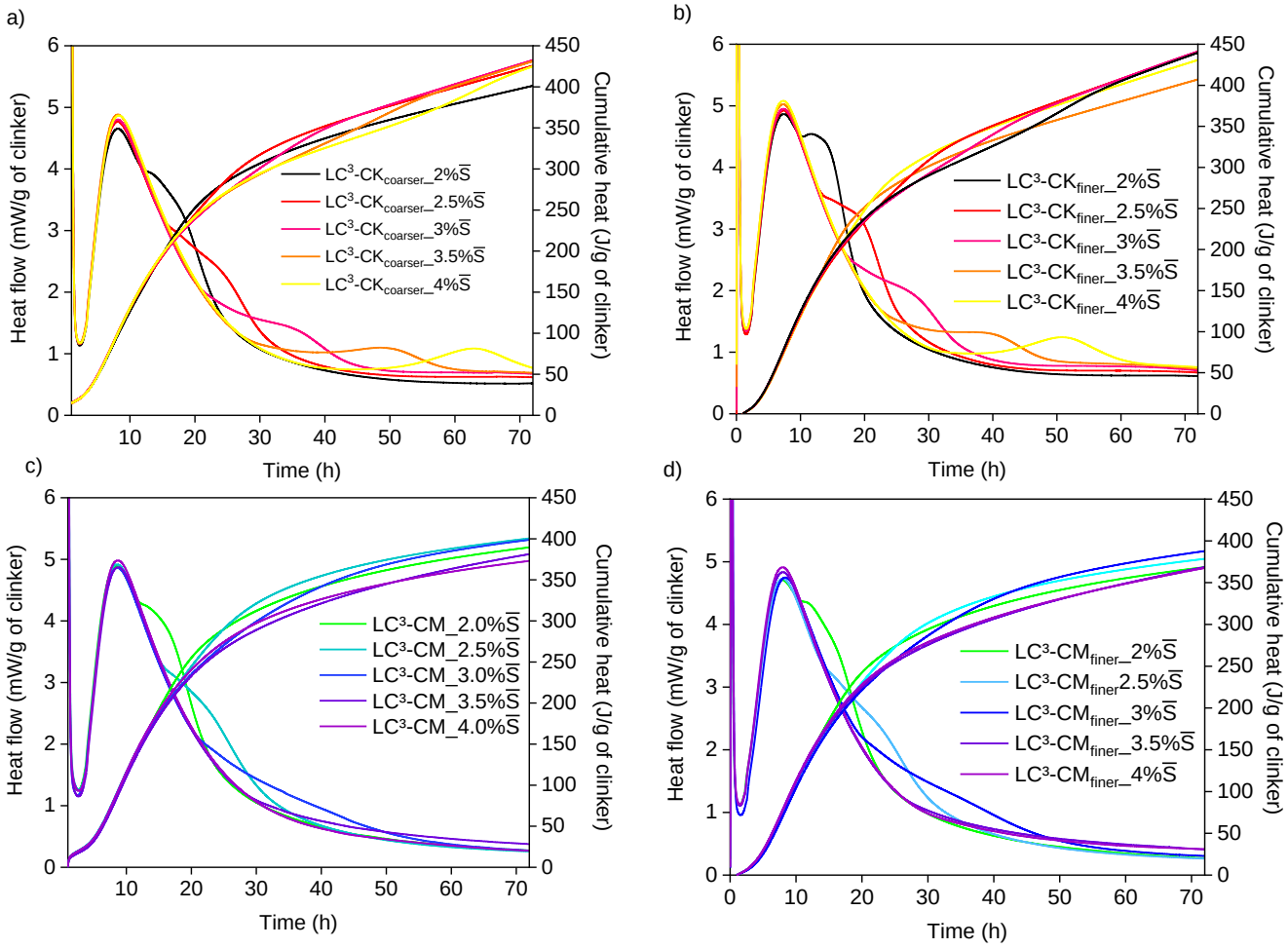

Fig 4 calorimetry results. (a)LC^3-$CK_{coarser}$ (b)LC^3-CK_{finer}, (c) LC^3-$CM_{coarser}$ and (d) LC^3-CM_{finer}. Heat flow (left) and cumulative flow (right) of the LC^3 cement pastes.

That increased nucleation and growth of C-S-H during cement hydration leads to two main effects on the heat flow results: the intensification of the silicate peaks and acceleration of the sulfate depletion, SD. The calcined clay fineness and the SO_3 levels slightly enhanced the first one. As shown in Table 3, in the coarser calcined clays, LC³-$CK_{coarser}$ obtained values of silicate heat flow peaks between 4.65-4.88 mW/g of clinker among the SO_3 contents, while LC³-$CM_{coarser}$ was 4.86-4.98 mW/g of clinker. In the finer calcined clays, LC³-CK_{finer} had values from 5.08-4.97 mW/g of clinker while LC³-CM_{finer} between 4.70-4.91 mW/g of clinker. Note that LC^3-CM_{finer} mixes had the lowest silicate heat flow. Such reduction of reactivity may be consequence of reduced SSA_{BET} due to agglomeration of particles under mechanical

impact, as also observed by previous work with montmorillonite clay (BAKI *et al.*, 2022). Nevertheless, all the peak intensities were within the range observed for LC³-cements with different kaolinite clay contents, normalized per gram of clinker, found in the literature (AVET; SCRIVENER, 2018).

The second effect, the acceleration in SD, occurs when the calcium sulfate is adsorbed by the C-S-H surface up to a "depletion" point, marked by the curve that occurs just after the silicate peak (ZUNINO; SCRIVENER, 2019). Table 3 shows the position of this point occurred at different times for each cement. The coarser calcined clays had SD occurring approximately between 12-45 hours for LC³-$CK_{coarser}$ mixes, and between 12h to more than 72h in the LC³-$CM_{coarser}$. On the other hand, increasing the fineness of both calcined clays led to an acceleration in SD. For instance, LC³-CK_{finer} had SD between 10h-36h, whereas LC³-CM_{finer} had intervals from 10.5 to over 72h. Hence, the results suggested an effect of the calcined clay fineness on the hydration kinetics of LC^3 (in terms of C-S-H nucleation), as indicated by the accelerated SD from early age.

The fineness of the constituent materials of LC³**,** especially calcined clays, must be controlled during grinding to reduce high sulfate demand or rheology problems. This is a problem when co-milling in large ball mills involving materials of different hardness is performed, such as clinker and gypsum. Calcined clays, especially when ground more finely, lead to sub-sulfate in LC³ systems, where the overlap between the silicate and aluminate peaks prevents their distinction and the position of SD. This occurred for Py (PY, 2021) who discussed high efficiency grinding in disc mills. Consequently, those systems with high-fine clays blended with limestone and Portland cement were sub-sulfated with poor rheology. When this happens, it is necessary to use an even larger amount of gypsum in the cement, which can lead to reduced mechanical strength caused by the reduced clinker content at high levels. Also, adding large amounts of gypsum is not the best solution. As previously mentioned, it also produces longer and delayed aluminate peaks, which often does not ensure adequate cement hydration.

Table 3 additional isothermal calorimetry data. *= approximate values

Cement	**1st peak (dissolution of C_3S, precipitation of C-S-H)**	**2nd peak (Dissolution of C_3A and precipitation of ettringite)**

	Heat flow (mW/g of clinker) *	position (h)*	Heat flow (mW/g of clinker) *	position (h)*
LC^3-$CK_{coarser}$_2%$\bar{S}$	4.65	8.23	3.88	12.14
LC^3-CK_{finer}_2%$\bar{S}$	4.87	7.43	4.54	10.38
LC^3-$CK_{coarser}$_2.5%$\bar{S}$	4.77	8.11	2.43	16.14
LC^3-CK_{finer}_2.5%$\bar{S}$	4.92	7.42	3.21	13.63
LC^3-$CK_{coarser}$_3%$\bar{S}$	4.80	8.18	1.40	21.31
LC^3-CK_{finer}_3%$\bar{S}$	4.95	7.34	1.88	17.15
LC^3-$CK_{coarser}$_3.5%$\bar{S}$	4.88	8.14	1.09	37.87
LC^3-CK_{finer}_3.5%$\bar{S}$	5.01	7.33	1.30	22.37
LC^3-$CK_{coarser}$_4%$\bar{S}$	4.87	8.33	*	45.04
LC^3-CK_{finer}_4%$\bar{S}$	5.08	7.31	1.24	36.08
LC^3-$CM_{coarser}$_2%$\bar{S}$	4.89	8.47	4.25	11.97
LC^3-CM_{finer}_2%$\bar{S}$	4.71	7.96	4.35	10.67
LC^3-$CM_{coarser}$_2.5%$\bar{S}$	4.91	8.58	2.63	15.46
LC^3-CM_{finer}_2.5%$\bar{S}$	4.73	8.01	2.28	14.26
LC^3-$CM_{coarser}$_3%$\bar{S}$	4.86	8.67	1.05	20.85
LC^3-CM_{finer}_3%$\bar{S}$	4.76	7.99	1.33	27.75
LC^3-$CM_{coarser}$_3.5%$\bar{S}$	4.87	8.76	0.4	28.84
LC^3-CM_{finer}_3.5%$\bar{S}$	4.83	8.36	*	*
LC^3-$CM_{coarser}$_4%$\bar{S}$	4.98	8.23	*	12.14
LC^3-CM_{finer}_4%$\bar{S}$	4.91	7.43	*	10.38

The SD also marks the onset of the second heat flow peak (aluminate). In this peak, there is a new and fast dissolution of the C_3A while sulfate ions are desorbed from the C-S-H, leading to a second and intensified ettringite precipitation (ANDRADE NETO; DE LA TORRE; KIRCHHEIM, 2021; ZUNINO; SCRIVENER, 2019). Zunino and Scrivener (2019) demonstrate a strong correlation between the formation of ettringite and AFm phase at 24 hours with aluminate peak's intensity (R^2=0.97) from its deconvolution by super-sulfated comparison systems. From such an approach, the LC³ aluminate peak area was also calculated concerning cement type and SO_3 content in coarser and finer LC³-CK and -CM cements, as presented in Figure 5. The point where the trend line intersects the y-axis suggested that the finer the calcined clay the greater its potential formation of ettringite and AFm phases, which would correspond to cements LC³-CK_{finer}>LC³-$CK_{coarser}$>LC³-CM_{finer}>LC³-$CM_{coarser}$.

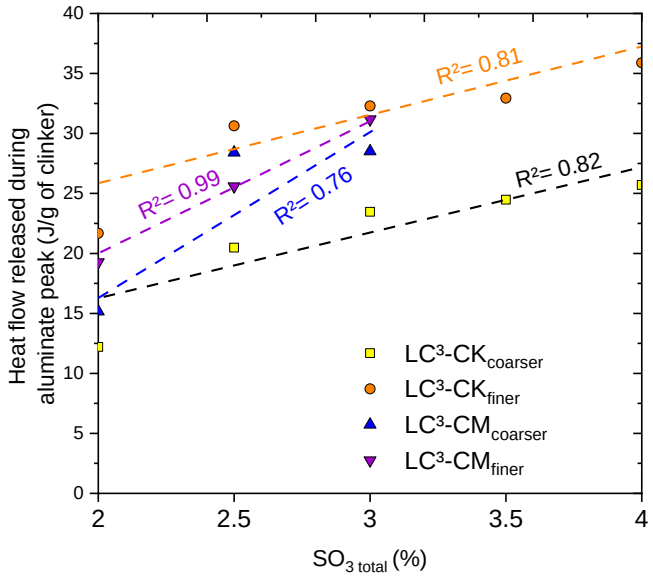

Fig.5 Correlation between heat flow released at 72h with SO_3 levels of LC_3 systems

By comparing all the cements, it was found values of heat flow released during the aluminate peak within the range observed by Zunino and Scrivener (2019) in LC³ systems with calcined kaolinite clays. In general, the higher the total SO_3 content, the larger the area of the aluminate peak, which agrees very well with the statement regarding hydration, i.e., the greater the amount of hydrated products, such as ettringite. LC³-$CK_{coarser}$ reached numbers from ~12.2 to 25.7 J/g of clinker. When the CK was more finely ground, there was, on average an increase of about 44% in the results, reaching values of 21.7-35.9 J/g clinker in LC³-CK_{finer}. Regarding LC_3 with CM, LC³-$CM_{coarser}$ reaches values between 15.1-28.4 J/g of clinker, but when CM was finely ground, there was an increase of 58% in the results reaching values between 19.3-31.2 J/g of clinker in LC³-CM_{finer}. The results confirm that the finer the clays, the higher the intensity of the aluminate peak, as shown by Zunino and Scrivener (2019). Furthermore,

although CK is more reactive than CM, the results between the cements seem similar when analyzing clays of closer fineness, indicating a negligible impact on the chemical composition (mineralogy) of these materials.

The mechanism that dominates the intensity of that aluminate peak (whether physical or chemical) is still under discussion. Zunino and Scrivener (2019) compared a LC^3 with MK 95% (kaolinite content) and SSA_{BET} =13.53m²/g (3% add. of gypsum) against a LC^3 with MK 50% (kaolinite content) and SSA_{BET} = 62.61 m²/g (3% add. of gypsum), concluding that the fineness of calcined clays has more impact on aluminate peak than the mineral composition. However, they compared systems under different SO_{3total} contents and without comparison for clays of the same fineness or kaolinite content. The same predominance of fineness over calcined clay chemistry was found by Py (PY, 2021). The author produced LC^3 cements with two kaolinite clays: HMK (78.25% of kaolinite clay) SSA_{BET} = 34.4 m²/g, and MMK (46.1% of kaolinite clay) SSA_{BET} = 77.5 m²/g. As result, all the mixes with MMK provided sub-sulfated systems even its lower reactivity than HMK clay.

On the other hand, there are some studies where the clays' chemical composition, specifically the kaolinite content, had a higher impact on the sulfate demand of LC^3 (AVET; SCRIVENER, 2018; DA SILVA *et al.*, 2021). Malacarne et al. (MALACARNE *et al.*, 2021), for instance, assessing the impact of low-grade materials on LC^3 hydration, observed that higher kaolinite content, higher intensity of aluminate peak. The authors used two calcined kaolinite clays, one called natural clay (83% of kaolinite clay, NC) SSA_{BET}= 11.8 m²/g, and the other as argillite (35% of kaolinite clay, AR) SSA_{BET} = 24.7 m²/g. Therefore, all the previous studies have indicated that when the SSA_{BET} of calcined clays are close to each other, the chemical composition (in terms of kaolinite content) has more impact on the intensity of the aluminate peak than the fineness; on the other hand, when the comparison is made between clays with very distant SSA_{BET}, the fineness dominates the intensity of this peak, rather than kaolinite content.

The fineness of the calcined clay also impacted the cement pastes' total heat at 72h. In the case of LC^3-CK, the finer the calcined clay, the greater the total heat at 72h. LC^3-$CK_{coarser}$, for instance, had values between 400.1-431 J/g of clinker while LC^3-CK_{finer} between 406.8-440.5 J/g of clinker. On the other hand, LC^3-$CM_{coarser}$ had values between 373.0-398.6 J/g of clinker, whereas LC^3-CM_{finer} were 368.3-387.6/ J of clinker. This suggests that a longer grinding time

reduced the CM reactivity despite the reduction of its PSD, which may occur due to the changes in the structure of the particles.

In several cases, the increase in fineness of the same clay did not significantly impact the compressive strength of LC^3 pastes (P>0.05, n.s.), as shown in Figure 6.

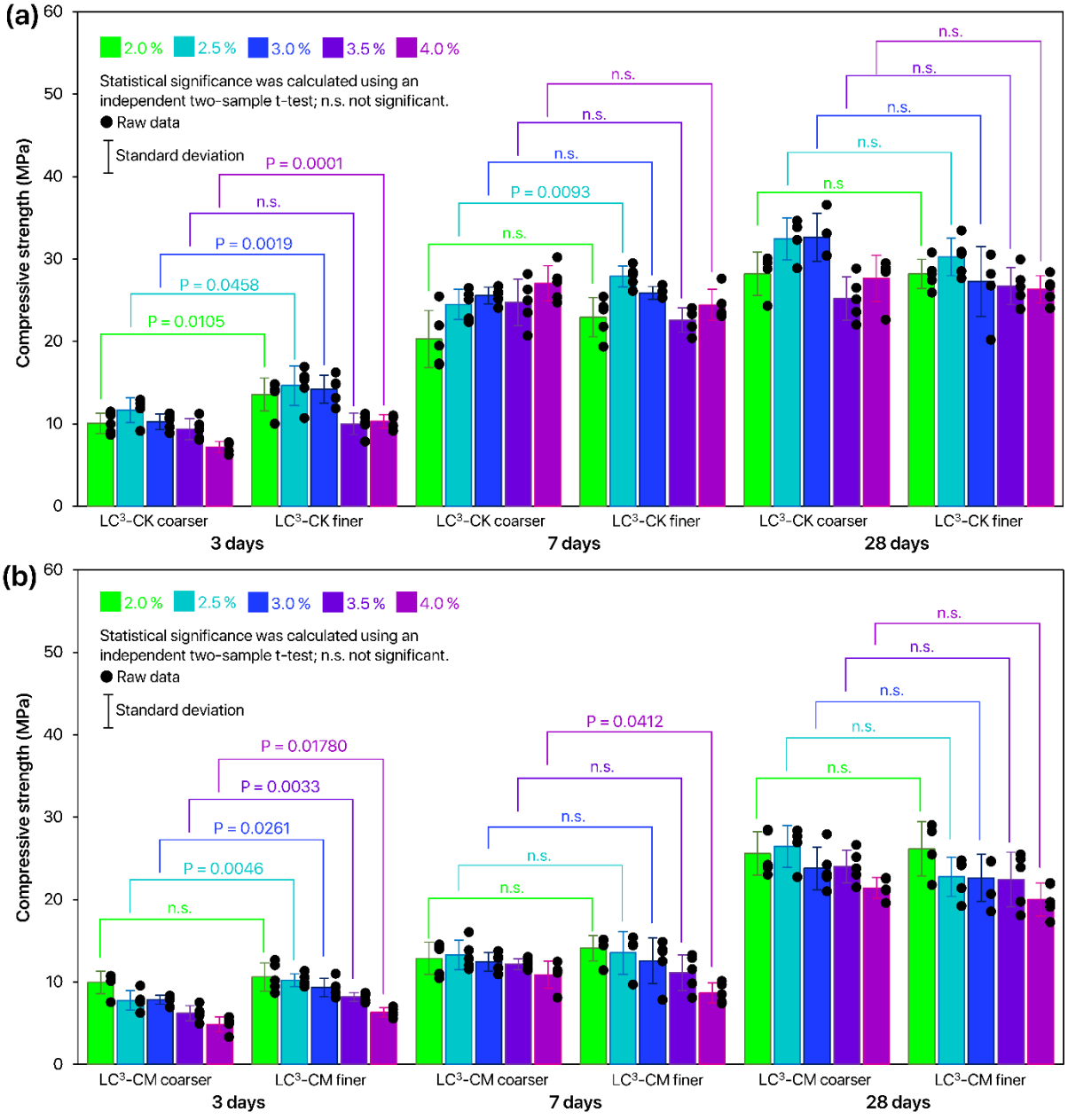

Fig. 6 Impact of calcined clay fineness on the LC^3 compressive strength of pastes with different SO_3 contents.

At 3 days, the increase in fineness increased the compressive strength of almost all SO_3 contents, except for 4% and 2% SO_3 levels for LC-CK and -CM, respectively. The similar strength results between -CK and -CM cements (due to their close finenesses) demonstrate how the physical effect dominates the initial hydration.

At 7 days, there was an increase in strength due to the advancement of the cement hydration reactions, which tended to be more noticeable with LC³-CK than LC³-CM in both finenesses. It is well-known that calcined clays, by pozzolanic reactions, interact with the products of Portland cement reactions, such as portlandite to form C-A-S-H. It is likely that the formation of Hc and Mc phases, which ongoing faster in LC^3-CK contributed to compressive strength results. Also, note that the calcined clay fineness had no significant impact on most mixes, comparing the same SO_3 content, except for 2.5% and 4.5% SO_3 levels of the cements LC^3-CK and - CM, respectively.

The most noticeable behavior (from 7 to 28 days) was the higher strength increase in LC³-CM than in LC³-CK, probably due to the CM pozzolanic reaction and possible porosity refinement in the case of LC³-CK that limited higher compressive strength results. In LC³ systems with high kaolinite content, such as CK with about 90% of kaolinite content, might occur a porosity refinement phenomenon up to a critical point where there was no more space for hydration products to be formed, as observed by Avet and Scrivener (AVET; SCRIVENER, 2018) when studying the impact of kaolinite content in LC³. This porosity refinement may not have occurred with LC³-CM due to its lower SSA BET and lower ion dissolution availability, which will be discussed further below.

7.1.2 Early-age hydration of limestone calcined clays cements

Figure 7 shows the DTG curves of the LC³-CK and LC³-CM pastes at 2, 12, 24, 48 and 72 h. Peaks related to the decomposition of ettringite (at ~ 110 °C), gypsum (at ~ 120 °C), AFm phases (at ~ 150 °C), C-S-H (50 to 600 °C), portlandite (between 400 and 500 °C) and calcium carbonates (between 650 and 800°C) (LOTHENBACH; DURDZI´NSKI; DE WEERDT, 2016) are observed.

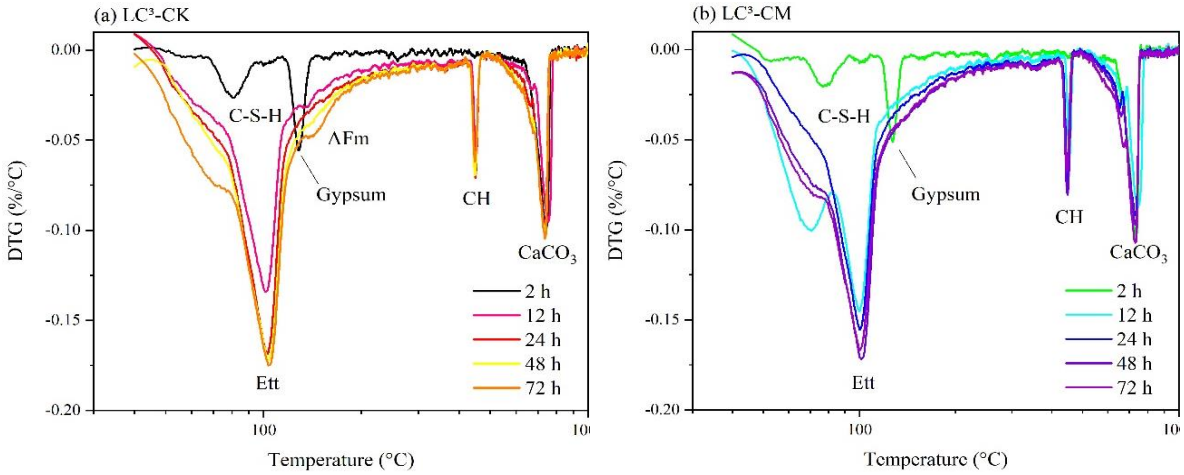

Fig. 7 DTG curves of (a) LC³-CK and (b) LC³-CM pastes at 2, 12, 24, 48 and 72 h.

One can note that at 2h there was still gypsum in both samples, while at 12h there was no evidence of gypsum, indicating that the sulfate depletion already occurred. At 2h, the DTG data for both cements did not show evidence of the presence of portlandite, indicating a limited alite hydration up to this period, which agrees with calorimetry results (both pastes still were in the induction period at 2h), and with previous studies (DE MATOS *et al.*, 2022; JANSEN *et al.*, 2018). From 12h on it was observed ettringite, C-S-H and portlandite DTG peaks for both pastes, as expected. Finally, at 72h was it possible to see AFm peak for the LC³-CK paste, while the LC³-CM did not present a distinguished AFm peak. This evidences that the CK clay promotes an earlier formation of AFm phases when compared to the CM clay, which can be related to the higher reactivity of the CK clay. As observed by De Matos et al. (DE MATOS *et al.*, 2022), when studying calcined kaolinites clays with different amorphous/kaolinite content, the LC³ cements with the clay with 97.62% of ACn (Amorphous and Crystalline non-quantified) content resulted in ~12h earlier hemicarbonate formation than the cements with a clay with 91.11% of ACn. The earlier AFm formation in the LC³ with high reactivity kaolinite clays was also observed by some authors (MAIER *et al.*, 2022; The reaction between metakaolin and limestone and its effect in porosity refinement and mechanical propertiesZUNINO; SCRIVENER, 2021b).

The bound water and portlandite contents of the LC³ pastes are presented in Figure 8. With the progress of the hydration, the bound water content increases, as expected. Comparing both cements, no significant differences in the bound water content were observed (Figure 8a), which agrees with the calorimetry results (see Figure 4, where both cements present similar cumulative heat curves). Regarding the portlandite content (Figure 8b), the pastes showed similar contents up to 12h. However, after 24h, the LC³-CK paste presented lower portlandite contents than the LC³-CM paste. This might indicate a very early pozzolanic activity from the LC³-CK, which agrees with previous studies (DE MATOS *et al.*, 2022; MAIER *et al.*, 2022; The reaction between metakaolin and limestone and its effect in porosity refinement and mechanical propertiesZUNINO; SCRIVENER, 2021b). After 48h, one can note a decrease in

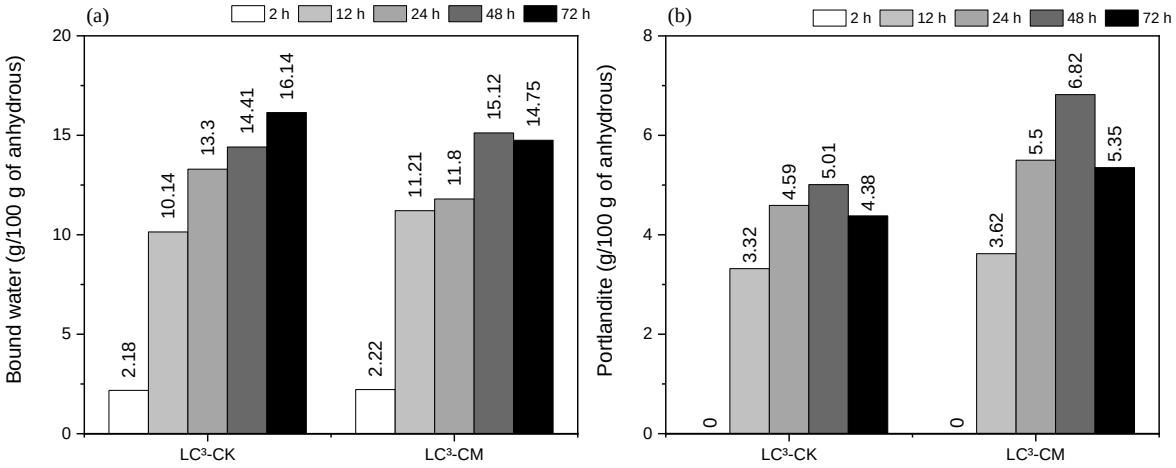

portlandite content in the LC³-CM paste, indicating an early pozzolanic activity of CM clay as well.

Fig. 8 (a) Bound water and (b) Portlandite content of LC³ pastes at different ages.

Figure 9 presents selected ranges of the XRD patterns (7-13 and 16-20 °2θ) of LC³-CK (a,b) and LC³-CM (c,d) pastes at 2, 12, 24, 48 and 72h. The full XRD patterns are presented in Appendix D. For both cements, at 2h gypsum ($CaSO_4.2H_2O$; ICSD 409581) was still present, while no XRD peaks of ettringite ($Ca_6Al_2(SO_4)_3(OH)_{12}\cdot_{26}H_2O$; ICSD 155395) and portlandite ($Ca(OH)_2$; ICSD 202220) were observed. In turn, at 12h, the gypsum XRD peak was not present anymore, indicating that sulfate depletion already occurred for both cements. This agrees with calorimetry and TGA results, as previously discussed. At 12 h, ettringite and portlandite peaks were present and remain for the rest of the time tested. Finally, despite the LC³-CK paste presenting AFm DTG peaks at 72 h, no AFm peaks were observed in the XRD,

probably due to the poorly crystallinity nature of the AFm-type phases (The role of sodium and sulfate sources on the rheology and hydration of C3A polymorphsANDRADE NETO *et al.*, 2022; ECTORS, 2016).

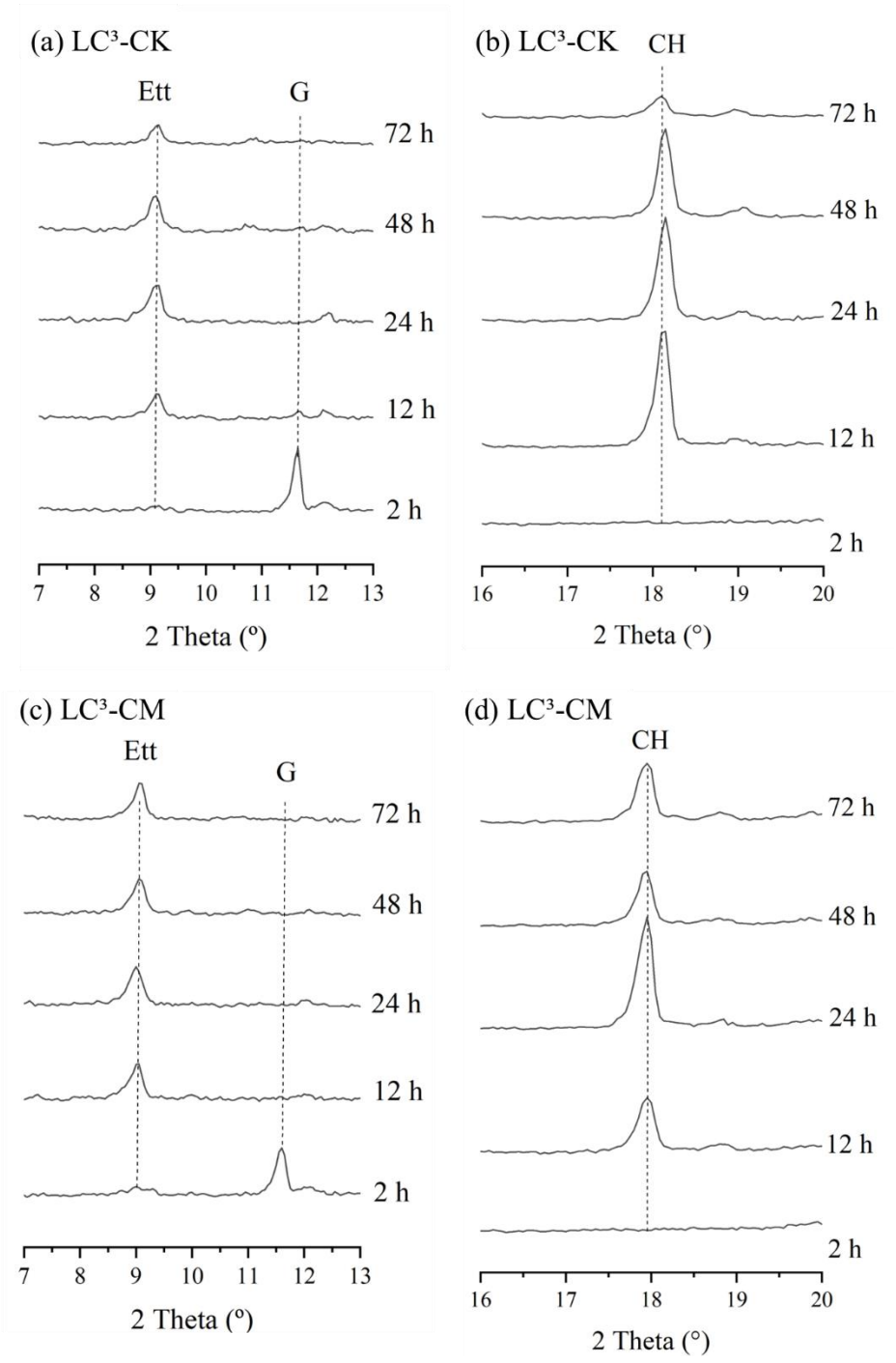

Fig. 9 XRD patterns of LC³-CK (a,b) and LC³-CM (c,d) hydrated pastes. Ett = Ettringite, G = Gypsum and CH = Portlandite.

7.1.3 Hypothesis 2: Calcined clays have a different dissolution of Si and Al ions to interact with calcium sulfate ions

The concentration of ions in the artificial pore solution (pH=13) with CK, CM and GYP as well as their weight loss over time are shown in Figure 10. It is worth noting that the dissolution values may not represent the real values of ions dissolution in the real pore solution during cement hydration, but the technique aims to establish a comparative parameter between the evaluated materials.

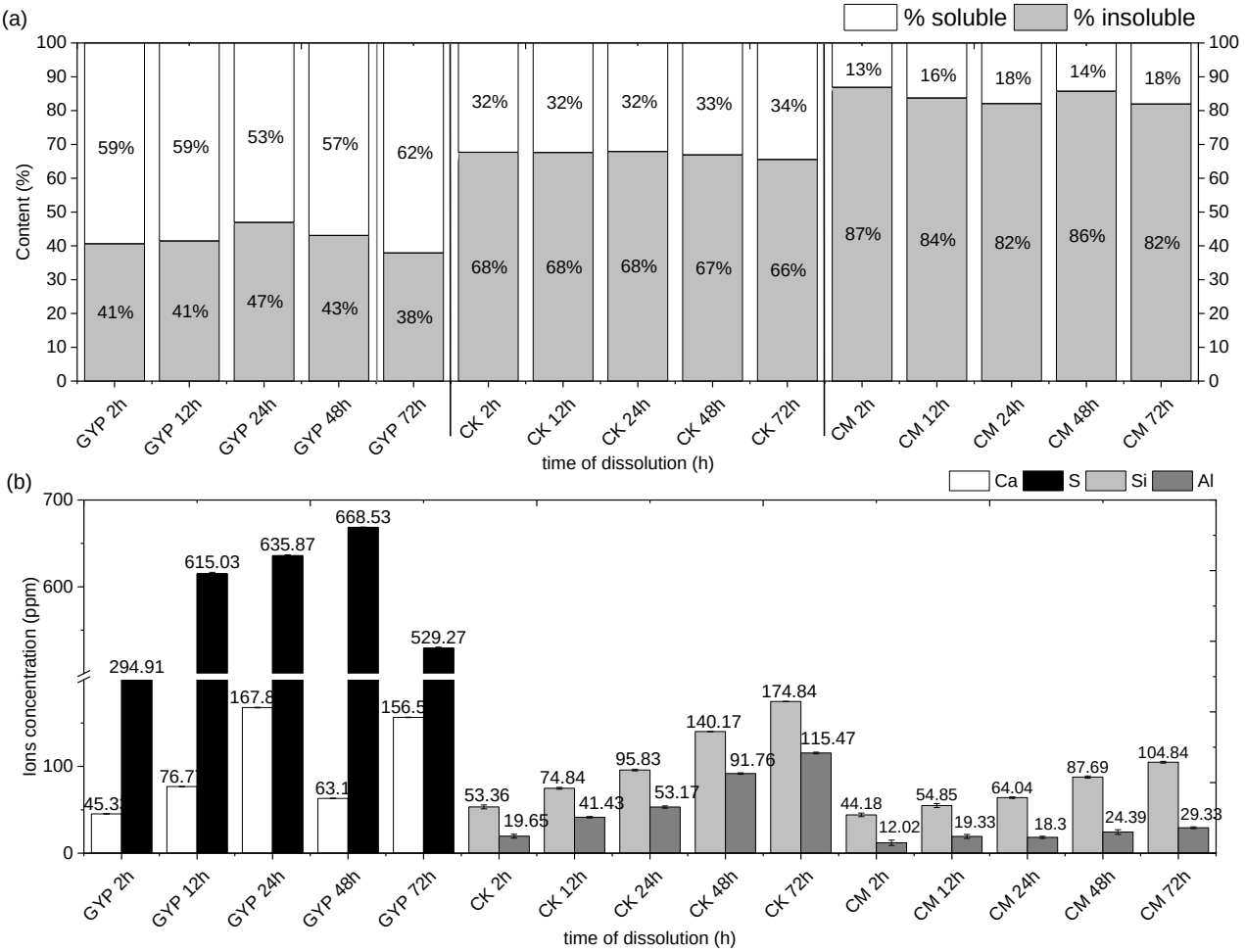

Fig. 10 Kinetics dissolution of GYP, CK_{finer} and CM_{finer} in alkaline solution

The amount of residue (%) filtered over time is shown in figure 32a. Due to its high dissolution under alkaline conditions, GYP showed an amount of soluble material between 59-62%. The calcined clays had a low variation of soluble percentage with time, between 32-34% and 10-16% for the CK and CM clays, respectively. According to Scherb et al. (2020), this proximity between the weighed samples is expected as it assumes that crystalline phases do not dissolve during the test, which measures the soluble part of the samples such as Ca, S, Si or Al ions.

The soluble material, then understood as ICP-OES measured the ions dissolved in the solution. The results shown in Figure 10b reveal a progressive dissolution of Si and Al in both calcined clays over time. CK had values between 53.4-174.84 ppm of Si and 19.65-115.5 ppm of Al. Such dissolution was somewhat lower in CM, the concentration values were between 44.2-104.8 ppm of Si and 12-29.3 ppm of Al. Regarding GYP, there were the highest levels of ions dissolved in the solution. The fast and high dissolution of calcium sulfate during the cement hydration is well-known in the literature (TANG; GARTNER, 1988). The dissolution of S ions was from 3.5 to 10.5 times higher than Ca dissolution in the mineral GYP. Also, a non-linear dissolution of Ca and S ions was observed over time. After an ascendant dissolution of Ca up to 24h, there was a decrease in 48h, while S ions, just happened at 72h. The circumstances that led to these results are unclear but can suggest problems related to the saturation conditions of the solution.

Before calcination, CK is based on 1:1 mineral, with one tetrahedral layer of Si and an octahedral layer of Al, whereas CM is based on 2:1 mineral, as there is an extra Si layer covering the Al layer (BERGAYA; LAGALY, 2013). Despite this, neither Si nor Al ions' dissolution were higher in CM than in CK. Instead, the Si/Al ratios decreased in CK from 2.72 (2h) to 1.51 (72h), demonstrating the greater dissolution of Al ions in the solution. Meanwhile, CM had incongruent results related to Si/Al ratios over time, such as an increased Si/Al at 24h (Si/Al=3.5) after the decrease observed from 12h (Si/Al=3.67) to 12h (Si/Al=2.84) and a decreased at 72h (Si/Al=3.58) after an increased from 24h (Si/Al=3.5) to 48h (Si/Al=3.59).

There are numerous reasons to explain the higher dissolution of kaolinite than montmorillonite, as discussed by Garg and Skibsted (GARG; SKIBSTED, 2019). First, the lower amount of OH^- groups and the double Si layer covering Al layer from both sides greatly inhibit the hydrolysis of montmorillonite clays. Second, after efficiency calcination, calcined kaolinite clays become materials predominantly amorphous with preferential sites of Al for dissolution. ^{27}Al NMR results suggest dissolution of pentahedral coordinated Al sites (Al^{V}) is preferential compared to tetrahedral Al sites (Al^{IV}). Third, the incongruent dissolution and lower reactivity of montmorillonite clays can be explained by forming a passivating layer of Al^{VI} or secondary product on the surface of these clays, as evidenced by the $^{27}Al\{1H\}$ CP/MAS technique. In another study, Yokoyama et al. (YOKOYAMA; KURODA; SATO, 2005) indicated that the dissolution rate of montmorillonite depends on the outer surface rather than the total surface area in alkaline conditions, based on atomic force microscopy (AFM) analysis.

A better understanding of how the dissolution kinetics of calcined clays happen brings insights into their pozzolanic reactivity and behavior in cementitious systems, such as hydration and sulfate demand. Recently, the role of alumina (Al) content and filler effect on the sulfate requirement was discussed by Zunino and Scrivener (Insights on the role of alumina content and the filler effect on the sulfate requirement of PC and blended cements2022). Comparing blended cement with PC and slags (S1 and S8) of different fineness and alumina content, they observed a greater degree of reaction of alite and ettringite formation, simultaneously, a lower content of C_3A and gypsum in cements with lower alumina content (Slag 1 low Al_2O_3), but with one SSA_{BET} twice as high as the other (Slag S8 high Al_2O_3). The authors concluded that the Al content does not dominate the overall sulfate requirement in blended cements. They assumed that C-(A)-S-H formation, stimulated by the filler effect describes this phenomenon, and disagree with authors such as Andrade Neto et al. (ANDRADE NETO; DE LA TORRE; KIRCHHEIM, 2021), who said that Al content governs the rapid sulfate depletion after the silicate peaks. For this purpose, Zunino and Scrivener (Insights on the role of alumina content and the filler effect on the sulfate requirement of PC and blended cements2022) reaffirmed that in the example of Avet and Scrivener (AVET; SCRIVENER, 2018), the silicate peaks are different (height, width, and position) between an LC^3-MK (95% kaolinite) and LC^3-MK (50% kaolinite), indicating different C-(A)-S-H contents, although heat released at the onset of the aluminate peak were similar.

Although, it is plausible the high impact of the C-(A)-S-H formation on the acceleration of the sulfate depletion. It was observed that the chemical impact (dissolution of Al) cannot be considered a factor of minor impact comparing both ternary blended cements (with CK or CM). As observed by calorimetry results all the silicate peaks (among all SO_3 contents) were quite similar (height, width, and position) between CK and CM systems, although their different SSA_{BET}. The main differences were observed in the aluminate peak, where the second precipitation of ettringite intensified because Al ions were released into the pore solution, as the ICP-OES comparison suggests. Also, rapid and high dissolution of gypsum into SO_4^{2-} (higher than Ca^{+2}) more ions were available to interact with Al, for instance, higher in CK than CM.

7.1.4 Hypothesis 3: Calcined clays have a different capacity to adsorb ions from calcium sulfate

Another aspect that may influence the kinetics of hydration and sulfate depletion is the possible adsorption that calcium sulfate ions may have on the surface of the calcined clays. As observed in Figure 11, the zeta potential values of GYP, CK, and CM in an artificial pore solution (pH=13.5) were -12.2, -17.3 and -15.4 mV, respectively.

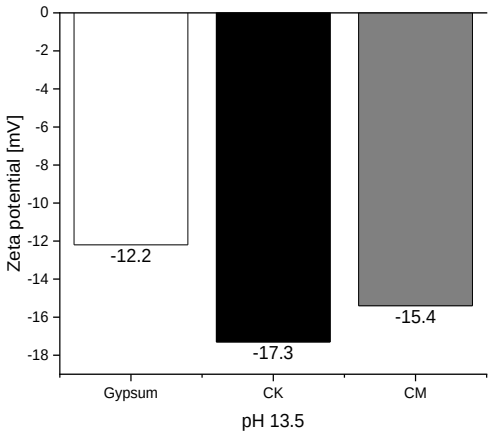

Fig. 11 Zeta potential of GYP, CK_{finer} and CM_{finer} in the artificial pore solution

Throughout the hydration of LC³, there are interactions between the surface of calcined clays and gypsum. However, it is unclear to what extent these interactions can drive the sulfate balance. As known, after the contact of cement with water, clinker phases, such as C_3A, rapidly dissolve to form the first crystals of ettringite in contact with gypsum Myers et al. (2016). Based on zeta potential results, Maier et al. (MAIER *et al.*, 2021) found that the adsorption of SO_4 and/or Ca-SO_4 complexes from gypsum onto calcined clay surface was the main factor inhibiting C_3A hydration in the absence of silicate reactions. However, the impact of the charges provided by calcined clays as the main impact on the sulfate depletion of LC³ is not fully understood.

First, the fact of the calcium sulfate being adsorbed to C-S-H until its depletion point is considered by Zunino and Scrivener (Insights on the role of alumina content and the filler effect on the sulfate requirement of PC and blended cements2022) as the main factor reducing the availability of gypsum in solution, which could explain the fast sulfate depletion in LC³ systems. Calcium sulfate's preferential and higher adsorption on C-(A)-S-H than on the surface of the calcined clays seems acceptable. If we look at the dissolution results (Figure 10), simultaneously, the gypsum released more S ions, which in solution would be sulfur (S)

ions complexes, than Ca cations (in the form of Ca^{+2}), explaining the negative zeta potential results of the GYP.

On the other side are the calcined clays (CK and CM). They release Si cations and Al ions (Al_2O_3) into a pore solution containing alkalis from the clinker. The resulting charge balances in the zeta plane suggest that the calcined clays are negative and, among other ions, will preferably interact with Ca ions, when it happens, the pore solution of systems with clays will become gradually positively charged. Lei and Plank (2014) proved an increasing and positive alteration of zeta potential results as a function of Ca^{+2} additions into alkaline solution with different phyllosilicates such as muscovite, kaolinite and montmorillonite, which would illustrate the affinity of (surface) calcined clay for Ca ions, such as from, gypsum, etc. Also, the ability of the clay surfaces to interact with Ca^{+2} ions was measured by gradually dripping a solution of $CaCl_2.2H_2O$, based on that described by Schmid and Plank (2021). The results indicated that the more negative the zeta potential, the greater the ability of the solution material to interact with Ca^{2+} ions. Thus, such adsorption may happen higher in CK than CM, due to its negative charge of slightly greater magnitude. Given this discussion, it is likely that the adsorption of calcium sulfate ions has less impact than its adsorption on C-(A)-S-H surfaces.

7.2 CONCLUSION

This study investigated the effects of two calcined clays with different mineralogy (kaolinite and montmorillonite) on the hydration of blended cements. The impact of these clays on sulfate depletion kinetics was investigated from the point of view of three hypotheses: 1) impact of fineness, 2) dissolution of Si and Al ions, and 3) possible adsorption of calcium sulfate ions into calcined clay's surface. The main results were:

- **Impact of fineness:** the analyzed fineness of the clays had minor influence on the results of compressive strength and hydration kinetics. Therefore, it was not the mechanism that dominated the accelerated sulfate depletion when comparing CK with CM clays.
- **Dissolution of S and Al ions:** the chemical effect that clays have on the sulfate balance is the main explanation found when comparing clays of close fineness but different mineralogy. The higher dissolution of ions (especially Al) from the CK increases the

intensity of the aluminate peaks and accelerates the sulfate depletion by competing ions to form ettringite.

- **Adsorption of calcium sulfate ions into calcined clay's surface:** The negative zeta potential values of the calcined clays in solution demonstrate their affinity for interaction with Ca^{2+} ions (either from gypsum or from clinker), but the results cannot confirm it as the main mechanism driving the sulfate balance of the LC^3. The adsorption of sulfate ions on C-S-H seems to be the most plausible explanation.

These results provide new insight into the mechanisms involved in the sulfate balancing of LC^3s, comparing kaolinite with montmorillonite clays. Here we demonstrated that the chemical effect of the clays has the most significant impact on achieving the correct sulfate balance, and that alternative clays to metakaolin, such as bentonites (rich in montmorillonites) can overcome this problem.

References

ABNT. **NBR 16697: Cimento Portland-Requisitos**. [*S. l.: s. n.*], 2018. Disponível em: www.abnt.org.br. .

ANDRADE NETO, José S. *et al.* Hydration of C3S and Al-doped C3S in the presence of gypsum. **Cement and Concrete Research**, [*s. l.*], v. 152, p. 106686, 2022.

ANDRADE NETO, José S. *et al.* The role of sodium and sulfate sources on the rheology and hydration of C3A polymorphs. **Cement and Concrete Research**, [*s. l.*], v. 151, 2022.

ANDRADE NETO, José da Silva; DE LA TORRE, Angeles G.; KIRCHHEIM, Ana Paula. Effects of sulfates on the hydration of Portland cement – A review. **Construction and Building Materials**, [*s. l.*], v. 279, 2021.

ANTONI, M. *et al.* Cement substitution by a combination of metakaolin and limestone. **Cement and Concrete Research**, [*s. l.*], v. 42, n. 12, p. 1579–1589, 2012.

ASTM. **C1608-12, Standard Test Method for Chemical Shrinkage of Hydraulic Cement Paste, ASTM International, West Conshohocken, PA, 2012, www.astm.org**. [*S. l.: s. n.*], 2012.

ASTM. C563:18 - Standard Guide for Approximation of Optimum SO3 in Hydraulic Cement 1. [*s. l.*], 2018. Disponível em: www.astm.org,.

AVET, François *et al.* Development of a new rapid, relevant and reliable (R3) test method to evaluate the pozzolanic reactivity of calcined kaolinitic clays. **Cement and Concrete Research**, [*s. l.*], v. 85, p. 1–11, 2016.

AVET, François; BOEHM-COURJAULT, Emmanuelle; SCRIVENER, Karen. Investigation of C-A-S-H composition, morphology and density in Limestone Calcined Clay Cement (LC 3). **Cement and Concrete Research**, [*s. l.*], v. 115, p. 70–79, 2019. Disponível em: https://doi.org/10.1016/j.cemconres.2018.10.011. Acesso em: 9 ago. 2021.

AVET, François; SCRIVENER, Karen. Effect of temperature on the water content of C-A-S-H in plain Portland and blended cements. **Cement and Concrete Research**, [*s. l.*], v. 136, 2020. Disponível em: www.elsevier.com/locate/cemconres. Acesso em: 2 jul. 2021.

AVET, François; SCRIVENER, Karen. Investigation of the calcined kaolinite content on the hydration of Limestone Calcined Clay Cement (LC3). **Cement and Concrete Research**, [*s. l.*], v. 107, p. 124–135, 2018.

BAKI, Vahiddin Alperen *et al.* The impact of mechanochemical activation on the physicochemical properties and pozzolanic reactivity of kaolinite, muscovite and montmorillonite. **Cement and Concrete Research**, [*s. l.*], v. 162, 2022.

BERGAYA, F.; LAGALY, G. General Introduction: Clays, Clay Minerals, and Clay Science. **Developments in Clay Science**, [*s. l.*], v. 5, p. 1–19, 2013.

BERODIER, E.; SCRIVENER, K. Understanding the filler effect on the nucleation and growth of C-S-H. **Journal of the American Ceramic Society**, [*s. l.*], v. 97, n. 12, p. 3764–3773, 2014.

BEUNTNER, Nancy *et al.* **Solubility and kinetics of calcined clay: study of interaction by pore solution**. [*S. l.: s. n.*], 2016. Disponível em: https://www.researchgate.net/publication/309426709. .

BULLARD, Jeffrey W. *et al.* Mechanisms of cement hydration. **Cement and Concrete Research**, [*s. l.*], v. 41, n. 12, p. 1208–1223, 2011.

CANBEK, Oğulcan *et al.* A quantitative approach to determining sulfate balance for LC3. **CEMENT**, [*s. l.*], v. 12, p. 100063, 2023. Disponível em: https://linkinghub.elsevier.com/retrieve/pii/S2666549223000099. Acesso em: 6 mar. 2023.

CEMENTIR HOLDING. **The Cement of the Future Is now Here: Cementir Launches**

FUTURECEM^{TM} With up to 30 Percent Lower Carbon Emissions | Cementir Holding N.V. [*S. l.*], 2020. Disponível em: https://www.cementirholding.com/en/media/whats-new/cement-future-now-here-cementir-launches-futurecemtm-30-percent-lower-carbon. Acesso em: 10 jun. 2021.

DA SILVA, Micael Rubens Cardoso *et al.* Valorization of kaolin mining waste from the Amazon region (Brazil) for the low-carbon cement production. **Case Studies in Construction Materials**, [*s. l.*], v. 15, p. e00756, 2021.

DE LA VARGA, Igor *et al.* Evaluating the hydration of high volume fly ash mixtures using chemically inert fillers. **Construction and Building Materials**, [*s. l.*], v. 161, p. 221–228, 2018.

DE MATOS, P.R. *et al.* Effect of superplasticizer addition time and metakaolin source on the early-age hydration of limestone calcined clay cement (LC3). **Materials and Structures - Under Revision (2022)**, [*s. l.*], 2022.

ECTORS, D. **Advances in the analysis of cementitious reactions and hydrate phases-Fortschritte in der Analyse von zementären Reaktionen und Hydratphasen**. 2016. [*s. l.*], 2016. Disponível em: https://opus4.kobv.de/opus4-fau/frontdoor/index/index/docId/7174.

EN 197-1. **EN 197-1 Cement-Part 1: Composition, specifications and conformity criteria for common cements**. [*S. l.: s. n.*], 2018. Disponível em: www.mbsmw.org. Acesso em: 5 jul. 2021.

FERNANDEZ, Rodrigo; MARTIRENA, Fernando; SCRIVENER, Karen L. The origin of the pozzolanic activity of calcined clay minerals: A comparison between kaolinite, illite and montmorillonite. **Cement and concrete research**, [*s. l.*], v. 41, p. 113–122, 2011. Disponível em: http://ees.elsevier.com/CEMCON/default.asp. Acesso em: 31 jul. 2021.

FLEGAR, Matea *et al.* Overview of clay as supplementarycementitious material. **SIMPOZIJ DOKTORSKOG STUDIJA GRAĐEVINARSTVA**, [*s. l.*], 2019. Disponível em: https://doi.org/10.5592/CO/PhDSym.2019.14. Acesso em: 10 jun. 2021.

GARG, Nishant. **STRUCTURE, REACTIVITY, AND DISSOLUTION OF CALCINED CLAYS BY SOLID-STATE NMR**. 2015. - Aarhus University, Denmark , 2015.

GARG, Nishant; SKIBSTED, Jørgen. Dissolution kinetics of calcined kaolinite and montmorillonite in alkaline conditions: Evidence for reactive Al(V) sites. **Journal of the**

American Ceramic Society, [*s. l.*], v. 102, n. 12, p. 7720–7734, 2019. Disponível em: https://ceramics.onlinelibrary.wiley.com/doi/full/10.1111/jace.16663. Acesso em: 11 jul. 2021.

GEIKER, METTE. Characterisation of development of cement hydration using chemical shrinkage. *In*: SCRIVENER, Karen; SNELLINS, Ruben; LOTHENBACH, Barbara (org.). **A Practical Guide to Microstructural Analysis of Cementitious Materials** . 1. ed. [*S. l.*]: CCR Press, 2016. v. 1, p. 75–106.

HE, Changling; OSBAECK, Bjarne; MAKOVICKY, Emil. Pozzolanic reactions of six principal clay minerals: Activation, reactivity assessments and technological effects. **Cement and Concrete Research**, [*s. l.*], v. 25, n. 8, p. 1691–1702, 1995.

IEA. **International Energy Agency, Iea. Technology Roadmap - Low-Carbon Transition in the Cement Industry**. [*S. l.: s. n.*], 2018. Disponível em: www.wbcsdcement.org. Acesso em: 10 jun. 2021.

ITO, Akihiko; WAGAI, Rota. Global distribution of clay-size minerals on land surface for biogeochemical and climatological studies. **Scientific Data**, [*s. l.*], v. 4, n. 1, p. 1–11, 2017. Disponível em: www.nature.com/sdata/. Acesso em: 10 jun. 2021.

JANSEN, D. *et al.* The early hydration of OPC investigated by in-situ XRD, heat flow calorimetry, pore water analysis and 1H NMR: Learning about adsorbed ions from a complete mass balance approach. **Cement and Concrete Research**, [*s. l.*], v. 109, p. 230–242, 2018.

JOHN, Vanderley M. *et al.* **Rethinking cement standards: Opportunities for a better future**. [*S. l.*]: Elsevier Ltd, 2019.

JUENGER, Maria C.G.; SNELLINGS, Ruben; BERNAL, Susan A. **Supplementary cementitious materials: New sources, characterization, and performance insights**. [*S. l.*]: Elsevier Ltd, 2019.

KURDOWSKI, Wieslaw. **Cement and Concrete Chemistry**. 1. ed. Dordrecht: Springer Netherlands, 2014. v. 1

LEI, L; PLANK, J. A study on the impact of different clay minerals on the dispersing force of conventional and modified vinyl ether based polycarboxylate superplasticizers. [*s. l.*], 2014. Disponível em: http://dx.doi.org/10.1016/j.cemconres.2014.02.009. Acesso em: 12

ago. 2022.

LOTHENBACH, B.; DURDZI´NSKI, P. T.; DE WEERDT, K. Thermogravimetric analysis. *In*: SCRIVENER, K.; SNELLINGS, R.; LOTHENBACH, B. (org.). **A Practical Guide to Microstructural Analysis of Cementitious Materials**. [*S. l.*]: CCR Press, 2016. v. 1st ed., p. 177–212.

LU, Z. C. *et al.* Characterization data of reference cement CEM III/A 42.5N used for priority program DFG SPP 2005 “Opus Fluidum Futurum – Rheology of reactive, multiscale, multiphase construction materials”. **Data in Brief**, [*s. l.*], v. 30, p. 105524, 2020.

MA, Yihan *et al.* **Research progress on polycarboxylate based superplasticizers with tolerance to clays - A review**. [*S. l.*]: Elsevier Ltd, 2020.

MAIER, Matthias *et al.* Hydration of cubic tricalcium aluminate in the presence of calcined clays. **Journal of the American Ceramic Society**, [*s. l.*], v. 104, n. 7, p. 3619–3631, 2021.

MAIER, Matthias *et al.* Particle characteristics of calcined clays and limestone and their impact on early hydration and sulfate demand of blended cement. **Cement and Concrete Research**, [*s. l.*], v. 154, p. 106736, 2022. Disponível em: https://linkinghub.elsevier.com/retrieve/pii/S0008884622000278.

MALACARNE, C. *et al.* Influence of low-grade materials as clinker substitute on the rheological behavior, hydration and mechanical performance of ternary cements. **Case Studies in Construction Materials**, [*s. l.*], v. 15, p. e00776, 2021.

MANDALIA, Tushar; BERGAYA, Faïza. Organo clay mineral–melted polyolefin nanocomposites Effect of surfactant/CEC ratio. **Journal of Physics and Chemistry of Solids**, [*s. l.*], v. 67, n. 4, p. 836–845, 2006.

MOHAMMED, Siline; SAFIULLAH, Omary. Optimization of the SO3 content of an Algerian Portland cement: Study on the effect of various amounts of gypsum on cement properties. **Construction and Building Materials**, [*s. l.*], v. 165, p. 362–370, 2018. Disponível em: https://doi.org/10.1016/j.conbuildmat.2017.12.218. Acesso em: 30 jul. 2021.

MURRAY, Haydn H. Chapter 6 Bentonite Applications. *In*: DEVELOPMENTS IN CLAY SCIENCE. [*S. l.: s. n.*], 2006. v. 2, p. 111–130.

MYERS, Rupert J *et al.* Role of Adsorption Phenomena in Cubic Tricalcium Aluminate Dissolution. [*s. l.*], 2016. Disponível em: https://pubs.acs.org/sharingguidelines. Acesso em:

15 out. 2021.

NIEMUTH, Mark D.; BARCELO, Laurent; WEISS, Jason. Effect of Fly Ash on Optimum Sulfate Levels Measured Using Heat and Strength at Early Ages. **Advances in Civil Engineering Materials**, [*s. l.*], v. 1, n. 1, p. 1–18, 2012. Disponível em: http://www.astm.org/DIGITAL_LIBRARY/JOURNALS/ACEM/PAGES/ACEM20120012.htm. Acesso em: 12 ago. 2021.

PY, Lucas Goldenberg. **Balanceamento de sulfatos e hidratação de cimentos ternários à base de calcários e argilas calcinadas**. 2021. - Universidade Federal do Rio Grande do Sul, Porto Alegre, 2021.

QUENNOZ, Alexandra; SCRIVENER, Karen L. Interactions between alite and C3A-gypsum hydrations in model cements. **Cement and Concrete Research**, [*s. l.*], v. 44, p. 46–54, 2013.

SCHERB, Sebastian *et al.* Reaction kinetics during early hydration of calcined phyllosilicates in clinker-free model systems. **Cement and Concrete Research**, [*s. l.*], v. 143, p. 106382, 2021.

SCHERB, Sebastian *et al.* Reactivity of metakaolin in alkaline environment: Correlation of results from dissolution experiments with XRD quantifications. **Materials**, [*s. l.*], v. 13, n. 10, 2020.

SCHMID, Marlene; PLANK, Johann. Interaction of individual meta clays with polycarboxylate (PCE) superplasticizers in cement investigated via dispersion, zeta potential and sorption measurements. **Applied Clay Science**, [*s. l.*], v. 207, p. 106092, 2021.

SCHÖLER, Axel *et al.* Hydration of quaternary Portland cement blends containing blast-furnace slag, siliceous fly ash and limestone powder. **Cement and Concrete Composites**, [*s. l.*], v. 55, p. 374–382, 2015.

SCRIVENER *et al.* Impacting factors and properties of limestone calcined clay cements (LC 3) . **Green Materials**, [*s. l.*], v. 7, n. 1, p. 3–14, 2019.

SCRIVENER, K. *et al.* Advances in understanding cement hydration mechanisms. **Cement and Concrete Research**, [*s. l.*], v. 124, p. 105823, 2019.

SHI, Zhenguo *et al.* Sulfate resistance of calcined clay-Limestone-Portland cements. **Cement and Concrete Research**, [*s. l.*], v. 116, p. 238–251, 2019. Disponível em:

https://doi.org/10.1016/j.cemconres.2018.11.003.

SKIBSTED, Jørgen; SNELLINGS, Ruben. **Reactivity of supplementary cementitious materials (SCMs) in cement blends**. [*S. l.*]: Elsevier Ltd, 2019.

SUN, Huaqiang *et al.* Optimization of gypsum and slag contents in blended cement containing slag. **Cement and Concrete Composites**, [*s. l.*], v. 112, 2020.

TANG, Fulvio J.; GARTNER, Ellis M. Influence of sulphate source on Portland cement hydration. **Advances in Cement Research**, [*s. l.*], v. 1, n. 2, p. 67–74, 1988.

TAYLOR-LANGE, Sarah C. *et al.* Calcined kaolinite-bentonite clay blends as supplementary cementitious materials. **Applied Clay Science**, [*s. l.*], v. 108, p. 84–93, 2015.

WADSÖ, L. *et al.* Calorimetry. *In*: SCRIEVENER, Karen; SNELLINGS, Ruben; LOTHENBACH, Barbara (org.). **A Practical Guide to Microstructural Analysis of Cementitious Materials**. 1. ed. [*S. l.*]: CCR Press, 2016. v. 1, p. 37–74.

WEI, Jianqiang; GENCTURK, Bora. Hydration of ternary Portland cement blends containing metakaolin and sodium bentonite. **Cement and Concrete Research**, [*s. l.*], v. 123, 2019.

YOKOYAMA, Shingo; KURODA, Masato; SATO, Tsutomu. Atomic force microscopy study of montmorillonite dissolution under highly alkaline conditions. **Clays and Clay Minerals 2005 53:2**, [*s. l.*], v. 53, n. 2, p. 147–154, 2005. Disponível em: https://link.springer.com/article/10.1346/CCMN.2005.0530204. Acesso em: 3 ago. 2021.

ZUNINO, Franco; SCRIVENER, Karen. Insights on the role of alumina content and the filler effect on the sulfate requirement of PC and blended cements. **Cement and Concrete Research**, [*s. l.*], v. 160, p. 106929, 2022. Disponível em: https://linkinghub.elsevier.com/retrieve/pii/S0008884622002216.

ZUNINO, Franco; SCRIVENER, Karen. Microstructural developments of limestone calcined clay cement (LC3) pastes after long-term (3 years) hydration. **Cement and Concrete Research**, [*s. l.*], v. 153, p. 106693, 2022.

ZUNINO, Franco; SCRIVENER, Karen. The influence of sulfate addition on hydration kinetics and C-S-H morphology of C3S and C3S/C3A systems. **Cement and Concrete Research**, [*s. l.*], v. 160, p. 106930, 2022. Disponível em: https://linkinghub.elsevier.com/retrieve/pii/S0008884622002228.

ZUNINO, Franco; SCRIVENER, Karen. The influence of the filler effect on the sulfate requirement of blended cements. **Cement and Concrete Research**, [*s. l.*], v. 126, 2019. Disponível em: www.elsevier.com/locate/cemconres. Acesso em: 2 jul. 2021.

ZUNINO, Franco; SCRIVENER, Karen. The reaction between metakaolin and limestone and its effect in porosity refinement and mechanical properties. **Cement and Concrete Research**, [*s. l.*], v. 140, p. 106307, 2021a.

ZUNINO, Franco; SCRIVENER, Karen. The reaction between metakaolin and limestone and its effect in porosity refinement and mechanical properties. **Cement and Concrete Research**, [*s. l.*], v. 140, 2021b.

SUPPLEMENTARY MATERIAL

APPENDIX A – Thermal Analysis of the raw materials

This appendix presents partial results from thermal analysis (TGA/DTG) of the materials.

Figure A1 - This appendix presents thermal analysis (TGA/DTG) of raw materials. A) clinker. B) gypsum. C) Limestone. D) kaolinite clay e) montmorillonite clay.

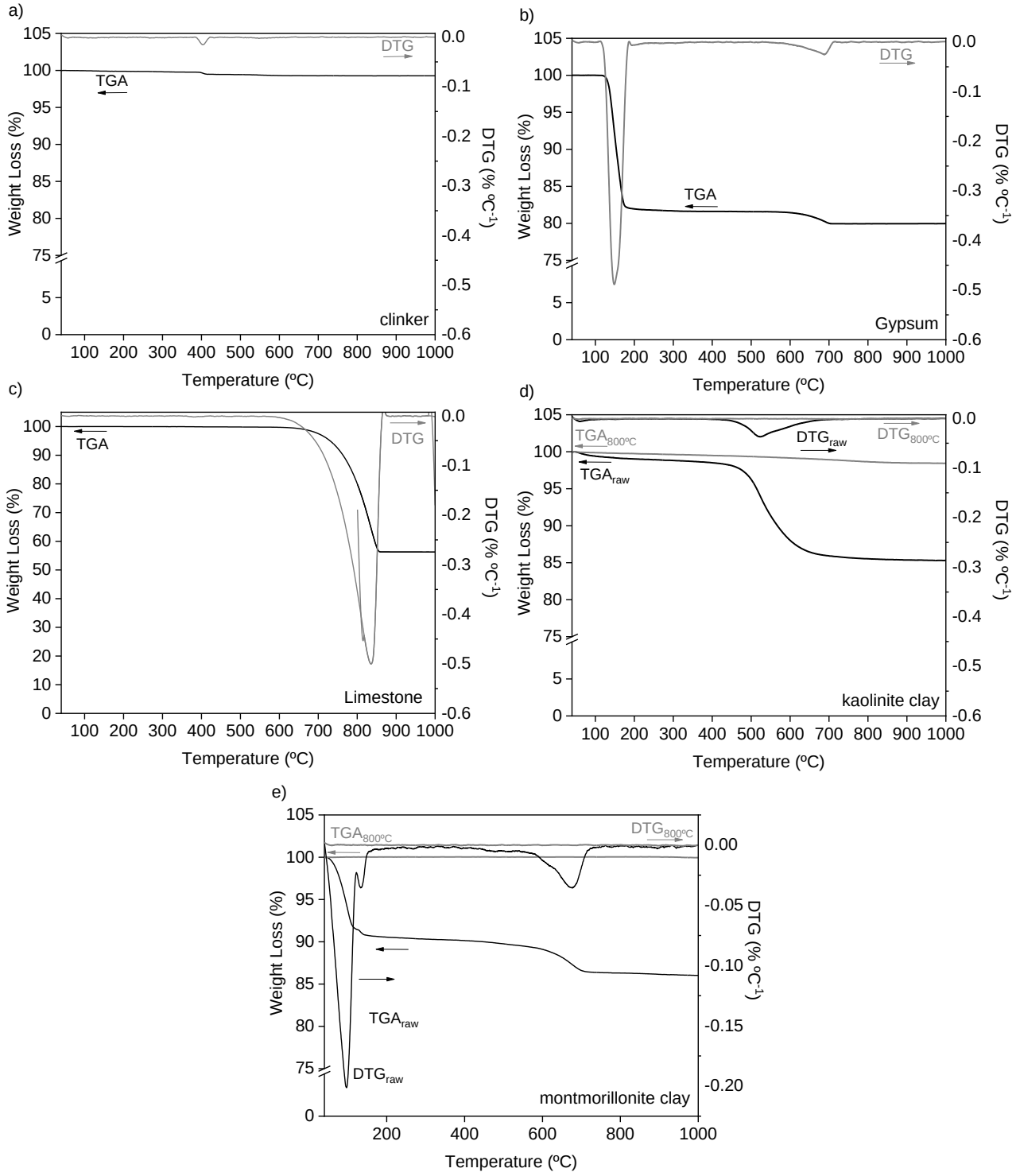

Source: Author (2022)

APPENDIX B – Particle Size distribution of the clays

This appendix presents the particle size distribution of the clays. Table B1 – grinding test at different times in CM. Table B2 – checking agglomeration.

Table B1 – PSD and SSA_{BET} of calcined montmorillonite at 800ºC (CM), under different times of grinding

PSD	CM_NoGrinding	CM_10min	CM_20min	CM_30min	CM_40min	CM_50min
D_{v90} (µm)	75.46	67.29	59.08	54.69	43.51	39.83
D_{v50} (µm)	33.49	28.89	24.45	21.75	17.34	15.80
D_{v10} (µm)	9.15	7.30	4.49	3.70	2.88	2.63
$D_{v\,mean}$ (µm)	40.19	34.97	29.75	26.92	21.38	19.58
Span $\frac{D_{v90} - D_{v10}}{D_{v50}}$	1.98	2.08	2.23	2.34	2.34	2.35
SSA_{BET} (m^2/g)	54.05	-	-	-	-	15.35

PSD	CM_60min	CM_90min	CM_120min	CM_150min
D_{v90} (µm)	33.50	27.06	27.32	26.60
D_{v50} (µm)	12.45	10.07	9.81	10.57
D_{v10} (µm)	2.27	1.91	1.80	1.89
$D_{v\,mean}$ (µm)	16.03	12.95	12.86	13.07
Span $\frac{D_{v90} - D_{v10}}{D_{v50}}$	2.51	2.50	2.60	2.34
SSA_{BET} (m^2/g)	-	-	-	8.46

Table B1 – PSD and SSA_{BET} of CK at 800ºC, under different times of grinding

PSD	CK_NoGrinding	CK_15min
D_{v90} (µm)	37.85	25.86
D_{v50} (µm)	14.87	10.15
D_{v10} (µm)	2.86	2.39
$D_{v\,mean}$ (µm)	18.73	12.86
Span $\frac{D_{v90} - D_{v10}}{D_{v50}}$	2.36	2.31
SSA_{BET} (m^2/g)	12.00	13.79

APPENDIX C – Additional data taken from isothermal calorimetry results

Isothermal calorimetry data

To allow an easy understanding of the hydration kinetics, important points identified from the calorimetry curves are shown in Table S.1-3. These are the time until reaching the maximum heat flow during the main hydration peak (first peak), the point of sulfate depletion, and the total cumulative heat after 72 hours of testing.

Table S.1: additional information obtained from isothermal calorimetry (times)

Cement	Time of higher value of first peak (h)	Sulfate depletion (h)	Total heat after 72 h (J/g cement)
		Phase 1	
LC³-QP_2%$\bar{S}$	9.49	13.25	381.14
LC³-QP_2.5%$\bar{S}$	9.67	17.27	391.70
LC³-QP_3%$\bar{S}$	9.68	22.35	396.26
LC³-QP_3.5%$\bar{S}$	10.11	*	373.26
LC³-QP_4%$\bar{S}$	9.95	*	358.67
LC³-CK_2%$\bar{S}$	8.23	12.14	401.33
LC³-CK_2.5%$\bar{S}$	8.11	16.14	425.80
LC³-CK_3%$\bar{S}$	8.18	21.31	432.62
LC³-CK_3.5%$\bar{S}$	8.14	37.87	431.21
LC³-CK_4%$\bar{S}$	8.33	45.04	424.97
LC³-CM_2%$\bar{S}$	8.47	11.97	389.61
LC³-CM_2.5%$\bar{S}$	8.58	15.46	400.48
LC³-CM_3%$\bar{S}$	8.67	20.85	398.76
LC³-CM_3.5%$\bar{S}$	8.76	28.84	381.35
LC³-CM_4%$\bar{S}$	8.71	*	373.09

Table S.2: additional information obtained from isothermal calorimetry (heat released)

Cement	1st peak (dissolution of C_3S, precipitation of C-S-H	2nd Dissolution of C_3A and precipitation of etringite	3 nd peak AFm phases
		mW/ g cement	
		Phase 1	
LC³-QP_2%$\bar{S}$	4.79	4.27	*
LC³-QP_2.5%$\bar{S}$	4.78	3.21	*
LC³-QP_3%$\bar{S}$	4.83	2.15	*
LC³-QP_3.5%$\bar{S}$	4.75	*	*

LC³-QP_4%$\bar{S}$	4.83	*	*
LC³-CK_2%$\bar{S}$	4.65	3.98	*
LC³-CK_2.5%$\bar{S}$	4.77	3.06	*
LC³-CK_3%$\bar{S}$	4.80	2.09	*
LC³-CK_3.5%$\bar{S}$	4.88	1.03	*
LC³-CK_4%$\bar{S}$	4.87	0.74	*
LC³-CM_2%$\bar{S}$	4.89	4.32	*
LC³-CM_2.5%$\bar{S}$	4.91	3.29	*
LC³-CM_3%$\bar{S}$	4.86	2.13	*
LC³-CM_3.5%$\bar{S}$	4.87	1.15	*
LC³-CM_4%$\bar{S}$	4.98	*	*

* Not observed

Table S.3: additional information obtained from isothermal calorimetry (heat released)

Cement	**Time of higher value of first peak (h)**	**Position of the Sulfate depletion (h)**	**Total heat after 72 h (J/g cement)**
	Phase 2		
LC³-CK$_{coarser}$_2%$\bar{S}$	8.23	12.14	401.33
LC³-CK$_{finer}$_2%$\bar{S}$	7.43	10.38	407.15
LC³-CK$_{coarser}$_2.5%$\bar{S}$	8.11	16.14	425.80
LC³-CK$_{finer}$_2.5%$\bar{S}$	7.42	13.63	430.80
LC³-CK$_{coarser}$_3%$\bar{S}$	8.18	21.31	432.62
LC³-CK$_{finer}$_3%$\bar{S}$	7.34	17.15	440.02
LC³-CK$_{coarser}$_3.5%$\bar{S}$	8.14	37.87	431.21
LC³-CK$_{finer}$_3.5%$\bar{S}$	7.33	22.37	441.21
LC³-CK$_{coarser}$_4%$\bar{S}$	8.33	45.04	424.97
LC³-CK$_{finer}$_4%$\bar{S}$	7.31	36.08	439.68
LC³-CM$_{coarser}$_2%$\bar{S}$	8.47	11.97	389.61
LC³-CM$_{finer}$_2%$\bar{S}$	7.96	10.67	368.57
LC³-CM$_{coarser}$_2.5%$\bar{S}$	8.58	15.46	400.48
LC³-CM$_{finer}$_2.5%$\bar{S}$	8.01	14.26	378.53
LC³-CM$_{coarser}$_3%$\bar{S}$	8.67	20.85	398.76
LC³-CM$_{finer}$_3%$\bar{S}$	7.99	27.75	387.79
LC³-CM$_{coarser}$_3.5%$\bar{S}$	8.76	28.84	381.35
LC³-CM$_{finer}$_3.5%$\bar{S}$	8.36	*	368.59

LC^3-$CM_{coarser}$_4%$\bar{S}$	8.71	*	373.09
LC^3-CM_{finer}_4%$\bar{S}$	7.98	*	367.62

Table S.4: additional information obtained from isothermal calorimetry (heat released)

Cement	**1st peak (dissolution of C_3S, precipitation of C-S-H**	**2nd Dissolution of C_3A and precipitation of etringite**	**Aluminate peak area**
	mW/ g cement		
		Phase 2	
LC^3-$CK_{coarser}$_2%$\bar{S}$	4.65	3.88	*
LC^3-CK_{finer}_2%$\bar{S}$	4.87	4.54	
LC^3-$CK_{coarser}$_2.5%$\bar{S}$	4.77	2.43	*
LC^3-CK_{finer}_2.5%$\bar{S}$	4.92	3.21	
LC^3-$CK_{coarser}$_3%$\bar{S}$	4.80	1.40	*
LC^3-CK_{finer}_3%$\bar{S}$	4.95	1.88	
LC^3-$CK_{coarser}$_3.5%$\bar{S}$	4.88	1.09	*
LC^3-CK_{finer}_3.5%$\bar{S}$	5.01	1.30	
LC^3-$CK_{coarser}$_4%$\bar{S}$	4.87	*	*
LC^3-CK_{finer}_4%$\bar{S}$	5.08	1.24	
LC^3-$CM_{coarser}$_2%$\bar{S}$	4.89	4.25	*
LC^3-CM_{finer}_2%$\bar{S}$	4.71	4.35	
LC^3-$CM_{coarser}$_2.5%$\bar{S}$	4.91	2.63	*
LC^3-CM_{finer}_2.5%$\bar{S}$	4.73	2.28	
LC^3-$CM_{coarser}$_3%$\bar{S}$	4.86	1.05	*
LC^3-CM_{finer}_3%$\bar{S}$	4.76	1.33	
LC^3-$CM_{coarser}$_3.5%$\bar{S}$	4.87	0.4	*
LC^3-CM_{finer}_3.5%$\bar{S}$	4.83	*	
LC^3-$CM_{coarser}$_4%$\bar{S}$	4.98	*	*
LC^3-CM_{finer}_4%$\bar{S}$	4.91	*	

APPENDIX D – XRD results

The appendix shows the additional results of the XRD analysis. Figure D.1 full XRD patterns of the pastes. Figure D.2 – XRD of the raw materials. Gypsum (G) ($CaSO_4.2H_2O$; ICSD 409581) ettringite (Ett) ($Ca_6Al_2(SO_4)_3(OH)_{12}\cdot_{26}H_2O$; ICSD 155395) and portlandite (CH) (Ca (OH) $_2$; ICSD 202220). Calcite (Cc) ($CaCO_3$; ICSD 73446), Alite M3 (A) (C_3S M3; ICSD 94742). Belite β (B) (C_2S β; ICSD 81906).

Figure – full XRD patterns of the LC³-Ck and LC³-CM within 72 hours.

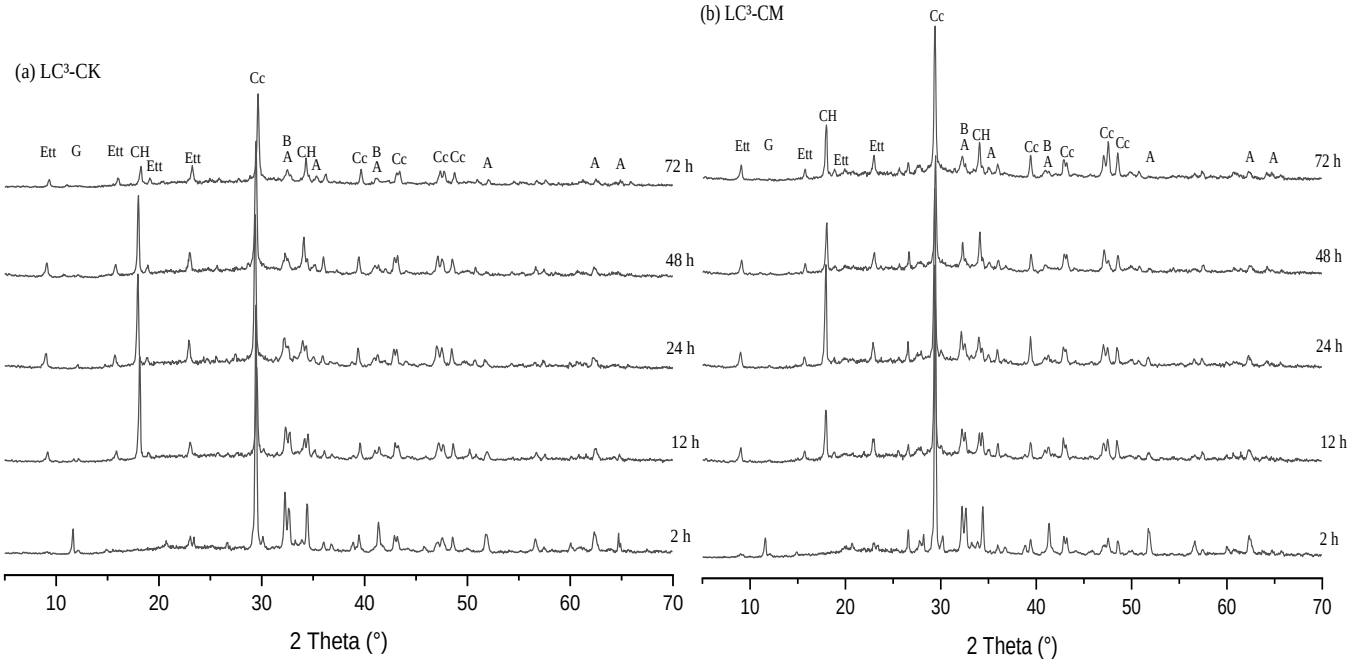

Source: Author (2022)

Settings of XRD of the raw materials performed by the cement industry: Diffractometer system=EMPYREAN. Goniometer=Theta/Theta; Minimum step size 2Theta:0.0001; Minimum step size Omega:0.0001. Sample stage=Reflection-transmission spinner 3.0; Minimum step size Phi:0.1

Measurement type: Single scan: Used wavelength; Intended wavelength type: Kα1 (Å): 1.540598; Kα2 (Å): 1.544426 Kα2/Kα1 intensity ratio: 0.50 Kα (Å): 1.541874 Kβ (Å): 1.392250; Incident beam path - Radius (mm): 240.0. X-ray tube. Scan axis: Gonio; Scan range (°): 4.9998 - 80.0000 [Start position (°): 5.0064 - End position (°): 79.9934] Step size (°): 0.0131. No. of points: 5712. Scan mode: Continuous Phi (°): 51.5 Counting time (s): 99.195.

In the clinker (Fig. D.2a) was identified mainly peaks of Alite M3 (A) (C_3S M3; ICSD 94742). Belite β (B) (C_2S β; ICSD 81906), cubic C_3A (C_3Acub; ICSD #1841), C_4AF (Ca_2FeAlO_5; ICSD #9197), periclase (MgO; ICSD #104844), free lime (CaO; ICSD #75785; 0.04%) and arcanite (K_2SO_4 ICSD 01-070-1488). In Gypsum (Fig. D.2b) was identified gypsum ($Ca_2SO_4\cdot2H_2O$; PDF 01-074-1433), Anhydrite (Ca_2SO_4; PDF 01-072-0916), quartz (SiO_2; PDF 01-085-0335) and dolomite ($Ca_3Mg_3C_6O_{18}$, COD 96-900-3525). Limestone shows peaks of calcite (CaCO3; PDF 01-083-0578) (Figure D.2c). Kaolinite clay has peaks of kaolinite minera ($Al_2Si_2O_5(OH)_4$; PDF 01-078-2109), muscovite ($KAl_2(Si_3Al)O_{10}(OH)_2$; PDF 01-074-1392), and quartz (SiO_2; PDF 01-083-0539). Montmorillonite have peaks of Montmorillonite mineral ($Si_{7.80}Al_{1.72}Li_{0.16}Fe_{0.20}Mg_{0.28}O_{20}$, COD 96-901-0959).,

Quartz (SiO_2, 01-086-1560) and muscovite ($KAl_2O_{10}(OH,F)_2$; COD 96-900-5474) (Figure D.2d). While quartz only quartz mineral (SiO2; PDF 01-085-0335) Figure D.2e).

Figure D.2 – XRD of the raw materials

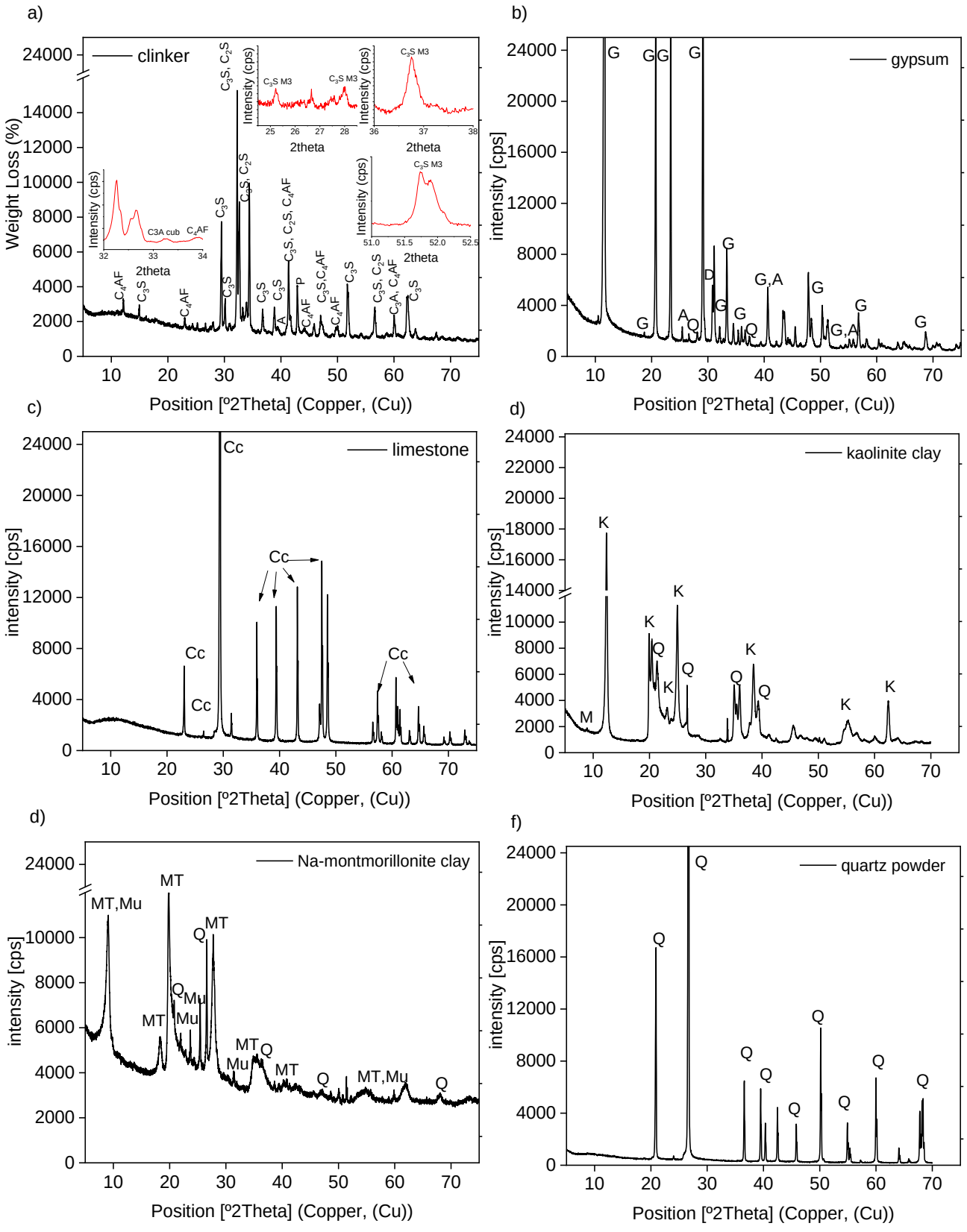

ANNEX A – Technical specifications of bentonite provided by the sale company

This annex presents technical specifications of the Na-montmorillonite raw (MT) clay.

Table A1.1- item description. Table A.2 Na-montmorillonite raw (MT).

Table A.1 – Item description

Clays nomenclature	**Batch**	**Description**
Natural sodium bentonite (MT)	11439	Table A.1

Table A.2 – Physical-chemical characteristics (MT)

Determination	**Min.[a]**	**Max.[a]**	**Results[b]**
Moisture content (%)	9.0	13.0	13.0
Swelling (ml)	30.0	40.0	34.0
200 mesh sieve	0.0	15.0	14.2
Adsorption of methylene blue (ml/0.5g)	50.0	65.0	54.0
Adsorption of methylene blue (ml) (550 °C)	35.0	50.0	45.0
Green Compressive Strength (N/cm²)	11.0	15.0	14.1
Wet tensile strength (N/cm²)	0.28	0.32	0.29

Source: [a](ABIFA, 1991) [b] Buschle & lepper S/A